CAPITAL UNIVERSITY OF SCIENCE AND TECHNOLOGY, ISLAMABAD

Flow Analysis of Hybrid Casson Nanofluid Containing Motile Micro-Organism Subjected to Cattaneo-Christov Double Diffusion

by

Taqmeem Bibi

A thesis submitted in partial fulfillment for the degree of Master of Philosophy

in the

Faculty of Computing
Department of Mathematics

2024

*I dedicate my dissertation work to my **family** and dignified **teachers**. A special feeling of gratitude to my loving parents who have supported me in my studies.*

CERTIFICATE OF APPROVAL

Flow Analysis of Hybrid Casson Nanofluid Containing Motile Micro-Organism Subjected to Cattaneo-Christov Double Diffusion

by

Taqmeem Bibi

(MMT221002)

THESIS EXAMINING COMMITTEE

(a)	External Examiner	Dr. Ahmed Zeeshan	IIU, Islamabad
(b)	Internal Examiner	Dr. Muhammad Sabeel Khan	CUST, Islamabad
(c)	Supervisor	Dr. Muhammad Sagheer	CUST, Islamabad

Dr. Muhammad Sagheer
Thesis Supervisor
January, 2024

Dr. Muhammad Sagheer
Head
Dept. of Mathematics
January, 2024

Dr. M. Abdul Qadir
Dean
Faculty of Computing
January, 2024

Author's Declaration

I, **Taqmeem Bibi**, hereby state that my M.Phil thesis titled "**Flow Analysis of Hybrid Casson Nanofluid Containing Motile Micro-Organism Subjected to Cattaneo-Christov Double Diffusion**" is my own work and has not been submitted previously by me for taking any degree from Capital University of Science and Technology, Islamabad or anywhere else in the country/abroad.

At any time if my statement is found to be incorrect even after my graduation, the University has the right to withdraw my M.Phil Degree.

(Taqmeem Bibi)
Registration No: MMT221002

Plagiarism Undertaking

I solely declare that research work presented in this thesis titled "**Flow Analysis of Hybrid Casson Nanofluid Containing Motile Micro-Organism Subjected to Cattaneo-Christov Double Diffusion**" is solely my research work with no significant contribution from any other person. Small contribution/help wherever taken has been dully acknowledged and that complete thesis has been written by me.

I understand the zero tolerance policy of the HEC and Capital University of Science and Technology towards plagiarism. Therefore, I as an author of the above titled thesis declare that no portion of my thesis has been plagiarized and any material used as reference is properly referred/cited.

I undertake that if I am found guilty of any formal plagiarism in the above titled thesis even after award of MPhil Degree, the University reserves the right to withdraw/revoke my MPhil degree and that HEC and the University have the right to publish my name on the HEC/University website on which names of students are placed who submitted plagiarized work.

(Taqmeem Bibi)
Registration No: MMT221002

Acknowledgement

I got no words to articulate my cordial sense of gratitude to **Almighty Allah** who is the most merciful and most beneficent to his creation.

I also express my gratitude to the last prophet of **Almighty Allah, Prophet Muhammad (PBUH)** the supreme reformer of the world and knowledge for human being.

I would like to be thankful to all those who provided support and encouraged me during this work.

I would like to be grateful to my thesis supervisor **Dr. Muhammad Sagheer**, the Head of the Department of Mathematics, for guiding and encouraging towards writing this thesis. It would have remained incomplete without his endeavours. Due to his efforts I was able to write and complete this dissertation.

I would like to pay great tribute to my **parents**, for their prayers, moral support, encouragment and appreciation.

Last but not the least, I want to express my gratitude to my **friends** who helped me throughout in my MPhil degree.

(Taqmeem Bibi)

Abstract

The purpose of this research is to examine in depth, the flow of $(TiO_2 + Ag)/EO$ hybrid nanofluid along a stretching sheet. Cattaneo-Christov double diffusion model has been incorporated along with the inclusion of motile gyrotactic microorganisms. The resistance to the flow and measure of heat transfer rate have been analyzed subjected to some crucial effects like Darcy-Forchheimer medium, magnetic field, thermal radiation and activation energy. The nonlinear ordinary differential equations extracted from the partial differential equations governing the aforementioned flow, through the similarity transformations and are solved using the shooting approach in the computational framework of MATLAB. The drag force, heat and mass transfer rate are calculated numerically. Plots and tables are used to show the numerical results. From the conclusion of the current work, it is important to mention that the Forchheimer parameter and the bio-convection Peclet number respectively animate to scale down the fluid velocity and density distribution of motile gyrotactic microorganisms.

Contents

List of Figures

List of Tables

Abbreviations

CC	Cattaneo-Christov
HNF	Hybrid Nanofluid
IVPs	Initial value problems
MHD	Magnetohydrodynamics
NF	Nanofluid
ODEs	Ordinary differential equations
PDEs	Partial differential equations
RK	Runge-Kutta

Symbols

T_∞	Ambient temperature of the nanofluid
C_∞	Ambient concentration of the hybrid nanofluid
k^*	Absorption coefficient
E_0	Activation energy
Bi	Biot number
C_w	Concentration of nanoparticles at the stretching surface
C	Concentration
β	Casson parameter
ρ	Density
ρ_f	Density of the fluid
ρ_{nf}	Density of the nanofluid
Nn_x	Density of motile micro-organisms
D_f	Darcian drag force
ρ_{hnf}	Density of the hybrid nanofluid
ρ_f	Density of the pure fluid
f	Dimensionless velocity
θ	Dimensionless temperature
ϕ	Dimensionless concentration
G	Dimensionless motile density
σ	Electrical conductivity
Ec	Eckert number
σ_{hnf}	Electrical conductivity of the hybrid nanofluid
σ_f	Electrical conductivity of the base fluid (Engine Oil)

$(\rho C_p)_{hnf}$	Heat capacitance of hybrid nanofluid
$(\rho C_p)_f$	Heat capacitance of base fluid
ν	Kinematic viscosity
ν_f	Kinematic viscosity of the base fluid
Nu_x	Local Nusselt number
Sh_x	Local Sherwood number
Re_x	Local Reynolds number
B_0	Magnetic field strength
M	Magnetic parameter
Ω	Microorganism Parameter
Nu	Nusselt number
Φ	Nanoparticle volume fraction
Pr	Prandtl number
P_0	Porosity parameter
Pe	Peclet number
q_r	Radiative heat flux
Re	Reynolds number
σ^*	Stefan Boltzmann constant
	Stream function
ξ	Similarity variable
C_f	Skin friction coefficient
Sh	Sherwood number
n	Shape factor
S_0	Suction/injection parameter
Sc	Schmidt number
K	Thermal conductivity
α	Thermal diffisuitivity
T_w	Temperature of the wall
T	Temperature
η	Thermal relaxation time parameter
Nr	Thermal radiation parameter

K_{hnf}	Thermal conductivity of the hybrid nanofluid
K_{nf}	Thermal conductivity of the nanofluid
K_f	Thermal conductivity of the base fluid
μ_f	Viscosity of the fluid
μ_{nf}	Viscosity of the nanofluid
Λ	Velocity slip parameter
μ_{hnf}	Viscosity of the hybrid nanofluid
μ_f	Viscosity of the base fluid
u	x-component of fluid velocity
v	y-component of fluid velocity

Subscripts

hnf	Hybrid nanofluid
nf	Nanofluid
p	Particle

Chapter 1

Introduction

Hybrid nanofluids are a class of nanofluids that are manufactured by combining different nanoparticles with a base fluid. Hybrid nanofluids take advantage of the synergistic effects resulting from combining different nanoparticles to further enhance these properties. In comparison to the conventional fluids, hybrid nanofluids are expected to transfer heat more effeciently. The hybrid nanofluids have a wide range of potential applications due to their improved properties. Some important applications of hybrid nanofluids include heat transfer enhancement, solar thermal systems, electronics cooling, automotive cooling systems, energy storage systems, aerospace technology, biomedical applications such as hyperthermia therapy for cancer treatment, food processing such as pasteurization and sterilization, ensuring food safety and quality and oil and gas industry such as refining processes, improving efficiency and reducing energy consumption.

Hussain et al. [1] examine findings on the flow of a $Cu - Al_2O_3/H_2O$ nanofluid within a blocked cavity. They employed Finite Element Method (FEM) for numerical solutions, focusing on understanding the behaviour of few physical factors on the heat transfer properties of hybrid nanofluids. The study by Mollamahdi [2] delves into forced convection fluid flow and heat transfer within a porous channel featuring walls that can either expand or contract. This channel is filled with an $Al_2O_3 - Cu/H_2O$ micropolar hybrid nanofluid, and a magnetic field is present.

To address the governing equations analytically, the least square method is utilized. The study investigates the impact of significant parameters, including the Reynolds number, Hartmann number, micro-rotation factor, and nanoparticle volume fraction, on velocity and temperature profiles. The findings reveal that as the Reynolds number rises, the values of temperature and micro-rotation profiles decrease. Additionally, it is observed that an increase in the Hartmann number leads to an increase in the Nusselt number.

The scientific community has conducted both analytical and numerical investigations into flows involving hybrid nanofluids. Karabanova et al. [3] explored a novel hybrid nanofluid, Ammonia-SrCl2, and analyzed the simultaneous impacts of mass and heat transfer in the system. Nawaz et al. [4] provided a compelling numerical analysis to investigate the effect of dust particles on the thermal properties of hybrid nanoparticles. They demonstrated that the fluid speed decreased along with a reduction in skin friction, attributed to the impact of the magnetic interaction parameter. The researchers utilized a numerical technique to conduct the simulations. Further relevant research on the practical applications of hybrid nanoparticle flow can be found in references [5–9].

The boundary layer flow of a Casson fluid under the effect of magnetohydrodynamics (MHD) through shrinking sheet is examined by Nadeem et al. [10], where Adomian Decomposition Method (ADM) is used to obtaine analytical solution. Mukhopadhyay et al. [11] explored the unsteady two-dimensional ($2D$) Casson fluid model over a stretching sheet. The transformed equations are solved numerically using the shooting method. As the unsteadiness parameter increases, the fluid velocity as well as the temperature profile experienced a notable decrease. Khalid et al. [12] investigated an unsteady MHD free convection flow of a Casson fluid past an oscillating vertical plate through a permeable medium by using the Laplace transform technique. Kataria and Patel [13] opted the Laplace transform for finding the solution of an MHD flow of a Casson fluid past an oscillating vertical plate embedded in a porous medium. The Casson parameter is reported to exhibit an inverse relationship with the yield stress of the fluid. Fazle Mabood

and Das [14] delineated the characteristics of melting heat transfer in the context of magnetohydrodynamic Casson fluid flow within a porous medium. The model proposed in this study is utilized to simulate the viscoelastic behavior of the fluid within the porous regime using the Runge-Kutta Fehlberg-45 method. It was observed that with the enhancing values of M and Ω, the velocity profile declined but the temperature profile behaved the other way round. The objective of Goud et al. [15] investigated the impact of heat source on the magnetohydrodynamic Casson fluid flow over a vertical fluctuating porous plate. The transformed non-dimensional ordinary differential equations governing the velocity and temperature were solved using the Galerkin element technique. The study conducted by Jamshed et al. [16] delves into the analysis of the Casson nanofluid, specifically focusing on its thermal transport and entropy. On the transformed set of ODEs, a numerical technique, namely the Keller box method, was employed to obtain the self-similar solution. The findings indicate that an increase in both Reynolds number and effective Brinkman numbers leads to an augmentation of overall entropy within the system.

The phenomenon of heat transformation is exceedingly significant across a multitude of industrial and engineering domains, encompassing microelectronics, fuel cells, and transportation. To address this need, Fourier [17] laid the foundational groundwork in 1882, by initially articulating the heat conduction law, providing a basis for understanding the mechanism of heat transportation. In 1948, Cattaneo [18] introduced a modification to Fourier's [17] heat conduction law by incorporating a relaxation time parameter. This modification aimed to refine the understanding of heat conduction processes. Later on, Christov [19] further refined the theories of Fourier and Cattaneo by introducing Oldroyd's convective derivative. This enhancement led to the development of a new model known as the Cattaneo-Christov model for heat flux, which has implications in understanding heat conduction in a more comprehensive and accurate manner. The model proposed by Mustafa [20] was based on a modification of the classical Fourier's law, incorporating the intriguing aspect of thermal relaxation time. The solution was obtained in series form using a powerful homotopy analysis method (HAM).

Jamshed and Aziz [21] presented the study of entropy generation and heat transfer rate of a thermal system containing hybrid nanofluid. In this analysis the governing equations are solved by Keller Box method. Farooq et al. [22] analyzed a novel scenario involving the implementation of the Cattaneo-Christov heat theory in conjunction with the melting phenomenon, specifically focusing on utilizing transformer oil as a base fluid. The shooting scheme was employed to assess the numerical results of different physical variables. The radial velocity exhibited an increase as the volume fraction of nanoparticles increased. Concurrently, the radial velocity field demonstrated an enhancement with an increase in the porosity parameter. Moreover, the temperature profile exhibited a decrease with higher values of the thermal reduction parameter. Alsaedi et al. [23] discussed the MHD flow through stretching cylinder. The formulation was based on the fluxes using the Cattaneo-Christov relation. The solutions were developed using the optimal homotopy analysis approach (OHAM). The entropy rate was seen to increase with an increase in the Brinkman number. An opposite trend was noted for the entropy rate concerning magnetic and temperature difference variables. A decrease in concentration was noted against the random motion parameter, while an increase in temperature was noted to occurr for the thermophoresis variable. Numerous other scholars have also made significant contributions to investigate this model in various contexts, as cited in the referenced articles [24–27].

Acharya et al. [28] investigated the influence of Hall current on the radiative transport of a $Cu - TiO_2/H_2O$ nanofluid over a rotating disc. They conducted a numerical study utilizing the shooting method to obtain similarity solutions. The results indicated that temperature profiles in the hybrid nanofluid were higher compared to those in traditional nanofluids. Maskeen et al. [29] explored numerical solutions concerning the influence of heat transfer and flow properties in the context of $Cu - Al_2O_3/H_2O$ hybrid nanofluid flow over an expanding cylinder. Their model integrated linear thermal radiation and Lorentz magnetic forces. The study showcased that this hybrid nanofluid exhibited greater efficacy in heat transfer processes compared to the nanofluids. Rehman et al. [30] made an effort to provide a numerical solution for the tangent hyperbolic fluid model in the context

of both cylindrical and flat stretching surfaces. A computational algorithm was employed to facilitate the solution process. The findings indicated that the temperature profile exhibited an increasing trend with respect to the thermal radiation parameter. Conversely, opposite trends were observed for positive values of the thermal stratification parameter. Bilal et al. [31] reported the impact of thermal radiation on an incompressible thermo-convective flow of a micropolar fluid over a permeable extensible sheet with energy and mass transfer. Numerical solutions for the problem were obtained using the Parametric Continuation Method (PCM). An interesting observation was made regarding the influence of the permeability parameter, which was found to increase the micro-rotation profile. In various contexts, a multitude of other researchers have also made substantial contributions to the investigation of model incorporating the thermal radiation, as mentioned in articles [32–34].

Shankaralingappa et al. [35] discussed the impacts of Darcy-Forchheimer and Cattaneo-Christov model in dusty tangent hyperbolic fluid. The model problem was defined by highly nonlinear partial differential equations, derived using suitable formulations. Further characterization of Darcy Forchheimer flows can be found in the referenced articles [36–40]. Ahmad et al. [41–43] successfully obtained results for nanofluid flow through a permeable medium involving gyrotactic microorganisms.

Harfash [44] investigated the problem of double-diffusive convection in a reacting fluid considering a magnetic field effect-based internal heat source. The numerical approach utilized the finite element method to obtain the numerical results. The presented numerical results encompassed scenarios with fixed-fixed and free-free boundary conditions. Bilal et al. [45] discussed the flow pattern within the boundary layer under the influence of a magnetic field. The nonlinear differential system resulting from this consideration was solved using the shooting scheme. The investigation involved analyzing the influence of various variables on the velocity and temperature fields.

The present study is focused on the Casson fluid model incorporating double diffusion based Cattaneo-Christov approach along with the thermal radiation and

magnetic field, all over a stretching surface through a porous medium. The literature survey reveals that no model has so far been proposed addressing the heat and mass transfer phenomenon along with the presence of motile gyrotactic micro-organisms, activation energy and Darcy-Forchheimer medium. This article involves different aspects of fluid dynamics, nanofluid behavior, microbiology and mathematical modeling.

1.1 Thesis Contributions

In this thesis, we provide a review and extended study of [46]. The target of this survey is on numerical analysis of Cattaneo-Christov double diffusion with additional Casson effect, magnetic effect and thermal radiation effect. The flow model is a system of PDEs that have been transformed into ODEs using the similarity transformations and then solved by the shooting method. Utilizing MATLAB, the numerically acquired findings are computed. The influence of significant parameters on velocity distribution $f'(\xi)$, temperature distribution $\theta(\xi)$, concentration distribution $\phi(\xi)$, motile distribution $G(\xi)$, skin friction coefficient Cf, local Nusselt number Nu_x, local Sherwood number Sh_x and density of motile micro-organisms Nn_x have been discussed through the plots and tables.

1.2 Layout of Thesis

The following is a brief summary of the thesis's content.

Chapter 2:
This chapter provides a list of fundamental definitions and covers some terminologies that facilitate to uderstand the concepts discussed in subsequent chapters.

Chapter 3:
This chapter provides a detailed review of the work reported by Ahmad et al [46]. Numerical technique, shooting method, is used to obtain the solutions of the flow

model. Graphs and plots express the impact of different physical parameters on the velocity, temperature, concentration and motile profiles.

Chapter 4:

This chapter extends the flow model discussed in chapter 3, by including Casson fluid and the impacts of Cattaneo-Christov double diffusion, magnetic field and thermal radiation. The shooting methodology is used to generate the numerical solutions of the governing flow model.

Chapter 5:

This chapter summaries overall the thesis final findings.

References used in the thesis are mentioned in **Biblography**.

Chapter 2

Preliminaries

This chapter contains some basic definitions and governing laws, which will be helpful in the subsequent chapters.

2.1 Some Fundamental Terminologies

Definition 2.1.1 (Fluid)

"A substance exists in three primary phases: solid, liquid, and gas. (At very high temperatures, it also exists as plasma.) A substance in the liquid or gas phase is referred to as a fluid." [48]

The differentiation between a solid and a fluid relies on the substance's capacity to withstand an applied shear (or tangential) stress attempting to alter its shape. A solid can withstand applied shear stress by undergoing deformation, while a fluid consistently undergoes deformation under even the slightest influence of shear stress. In solids, stress is directly related to strain, whereas in fluids, stress is directly related to strain rate. In the case of a constant shear force, a solid eventually ceases deformation at a specific strain angle, whereas a fluid continues to deform indefinitely and approaches a specific strain rate.

Definition 2.1.2 (Fluid Dynamics)

"The study of fluid if the pressure forces are considered for the fluids in motion, is called fluid dynamics." [49]

Definition 2.1.3 (Fluid Mechanics)

"The fluid mechanics is defined as the science that deals with the behavior of fluids at rest or in motion, and the interaction of fluids with solids or other fluids at the boundaries." [48]

Definition 2.1.4 (Fluid Statics)

"The study of fluids at rest is called fluid statics." [49]

Definition 2.1.5 (Viscosity)

"Viscosity is defined as the property of a fluid which offers resistance to the movement of one layer of fluid over another adjacent layer. Mathematically,

$$\mu = \frac{\tau}{\frac{\partial u}{\partial y}},$$

where μ is viscosity coefficient, τ is shear stress and $\frac{\partial u}{\partial y}$ represents the velocity gradient." [49]

The SI units of viscosity is $kgm^{-1}s^{-1}$.

Definition 2.1.6 (Density)

"Density is defined as the mass per unit volume, that is,

$$\rho = \frac{m}{v},$$

where m and v are the mass and volume of the substance, respectively." [49]

The SI units of density is kgm^3.

Definition 2.1.7 (Kinematic Viscosity)

"It is defined as the ratio between the dynamic viscosity and density of fluid. It

is denoted by symbol ν. Mathematically,

$$\nu = \frac{\mu}{\rho},$$

The SI units of kinematic viscosity ν is m^2/sec." [49]

Definition 2.1.8 (Nanofluid)

"Nanofluids are engineered by suspending nanoparticles with average size below 100 nm in traditional heat transfer fluids such as water, oil and ethylene glycol. A very small amount of guest nanoparticles, when dispersed uniformly and suspended stably in host fluids, can provide dramatic improvements in the thermal properties of host fluids." [50]

Definition 2.1.9 (Hybrid Nanofluid)

"Hybrid nanofluid is a very new type of nanofluids that contains two or more various nanoparticles. The use of hybrid nanofluids is aimed at simultaneously using the physical and chemical properoties of two or more different types of nanoparticles, for improving the base fluid properties." [51]

Definition 2.1.10 (Magnetohydrodynamics)

"Magnetohydrodynamics (MHD) is concerned with the flow of electrically conducting fluids in the presence of magnetic fields, either externally applied or generated within the fluid by inductive action." [52]

Definition 2.1.10 (Boundary Layer)

"Viscous effects are particularly important near the solid surfaces, where the strong interaction of the molecules of the fluid with molecules of the solid causes the relative velocity between the fluid and the solid to become almost exactly zero for a stationary surface. Therefore, the fluid velocity in the region near the wall must reduce to zero. This is called no slip condition. In that condition there is no relative motion between the fluid and the solid surface at their point of contact. It follows that the flow velocity varies with distance from the wall; from zero at the

wall to its full value at some distance away, so that significant velocity gradients are established close to the wall. In most cases this region is thin (compared to the typical body dimension), and it is called a boundary layer." [53]

2.2 Types of Flow

In this section, different types of fluid flows have been described which are experienced in different scenarios while investigating the motion of a fluid.

Definition 2.2.1 (Compressible Flow)

"Compressible flow is that type of flow in which the density of the fluid changes from point to point or in other words the density (ρ) is not constant for the fluid. Mathematically,

$$\rho \neq k,$$

where k is constant." [49]

Air is considered as compressible, which means that you can compress the air and add a little bit more air.

Definition 2.2.2 (Incompressible Flow)

"Incompressible flow is that type of flow in which the density is constant for the fluid flow. Liquids are generally incompressible while gases are compressible, Mathematically,

$$\rho = k,$$

where k is constant." [49]

Gallon of milk can be put into a differently shaped gallon-sized container, but you would not be able to squeeze that entire gallon of milk into half gallon-sized container.

Definition 2.2.3 (Rotational Flow)

"Rotational flow is that type of flow in which the fluid particles while flowing along stream-lines, also rotate about their own axis." [49]

Definition 2.2.4 (Irrotational Flow)

"Irrotational flow is that type of flow in which the fluid particles while flowing along stream-lines, do not rotate about their own axis." [49]

Definition 2.2.5 (Laminar Flow)

"Laminar flow is defined as that type of flow in which the fluid particles move along well-defined paths or stream lines and all the stream-lines are straight and parallel." [49]

Definition 2.2.6 (Turbulent Flow)

"Turbulent flow is that type of flow in which the fluid particles move in a zig-zag way." [49]

Definition 2.2.7 (Steady Flow)

"Steady flow is defined as that type of flow in which the fluid characteristics like velocity, pressure, density, etc., at a point do not change with time. Thus for steady flow, Mathematically, we have

$$\frac{\partial Q}{\partial t} = 0,$$

where Q is any fluid property." [49]

Definition 2.2.8 (Unsteady Flow)

"Unsteady flow is defined as that type of flow in which the fluid characteristics like velocity, pressure, density, etc., at a point do change with time. Thus for Unsteady flow, Mathematically, we have,

$$\frac{\partial Q}{\partial t} \neq 0,$$

where Q is any fluid property." [49]

Definition 2.2.9 (Viscous Flow)

"Flows in which the frictional effects are significant are called viscous flows." [48]

Definition 2.2.10 (Internal Flow)

"Flows completely bounded by a solid surfaces are called internal or duct flows." [48]

Definition 2.2.11 (External Flow)

"Flows over bodies immersed in an unbounded fluid are said to be an external flows." [48]

2.3 Types of Fluids

In this section, different types of flows have been discussed which we normally come across in real-life and industrial scenarios.

Definition 2.3.1 (Ideal Fluids)

"A fluid, which is incompressible and has no viscosity, is known as an ideal fluid. Ideal fluid is only an imaginary fluid as all the fluids, which exist, have some viscosity." [49]

Definition 2.3.2 (Real Fluids)

"A fluid, which possesses viscosity, is known as a real fluid. In actual practice, all the fluids are real fluids." [49]

Examples of such fluids are water, diesel and honey.

Definition 2.3.3 (Newtonian Fluids)

"A real fluid, in which the shear stress is directly proportional to the rate of shear strain (or velocity gradient), is known as a Newtonian fluid." [49]

Examples of such fluids are water, oil and alcohol.

Definition 2.3.4 (Non-Newtonian Fluids)

"A real fluid in which the shear stress is not directly proportional to the rate of shear strain (or velocity gradient), is known as a non-Newtonian fluid." [49]

Some examples of non-Newtonian fluids are toothpaste, shampoo, and honey etc.

2.4 Modes of Heat Transfer and Mass Transfer

In this section, the formal definition of heat transfer and its different types are included:

Definition 2.4.1 (Heat Transfer)

"Heat transfer is a branch of engineering that deals with the transfer of thermal energy from one point to another within a medium or from one medium to another due to the occurrence of a temperature difference. Heat transfer may take place in one or more of its three basic forms: conduction, convection, and radiation." [54]

Definition 2.4.2 (Conduction)

"The transfer of heat within a medium due to a diffusion process is called conduction. The Fourier heat conduction law states that the heat flow is proportional to the temperature gradient." [54]
Due to conduction, during the ironing process, heat is transferred from the iron to the fabric. Likewise chocolate candy in a hand will eventually melt as heat is conducted from hand to the chocolate.

Definition 2.4.3 (Convection)

"Convection heat transfer is usually defined as energy transport affected by the motion of a fluid. The convection heat transfer between two dissimilar media is governed by Newton's law of cooling. It states that the rate of heat flow is proportional to the difference of the temperatures of the two media. The proportionality coefficient is called the convection heat transfer coefficient." [54]
Examples of this type of heat transfer are heating water on the stove and air Conditioner.

Definition 2.4.4 (Thermal Radiation)

"Thermal radiation is defined as radiant (electromagnetic) energy emitted by a medium and is due solely to the temperature of the medium." [54]

Examples of thermal radiation include microwaves from an oven, X-rays from X-ray tubes and ultraviolet radiation from the sun, etc.

2.5 Dimensionless Numbers

Some important dimensionless numbers will be discussed in this section which will subsequently be used in the next chapters.

Definition 2.5.1 (Eckert Number)

"It expresses the ratio of kinetic energy to the thermal energy change. Mathematically, it can be written as

$$Ec = \frac{w_\infty^2}{C_p \delta T},$$

where w_∞ is the fluid flow velocity far from body, C_p is the specific heat capacity of fluid and δT denote the temperature difference." [55]

Definition 2.5.2 (Prandtl Number)

"The Prandtl number is the ratio of momentum to heat diffusivities. Mathematically, it can be defined as

$$Pr = \frac{\mu C_p}{k},$$

where μ represents the dynamic viscosity, C_p denotes the specific heat and k stands for thermal conductivity." [56]

Definition 2.5.3 (Skin Friction)

"The skin friction coefficient can be defined as

$$C_f = \frac{2\tau_0}{\rho u_w^2},$$

where τ_∞ denotes the wall shear stress, ρ is the density and the velocity of free fluid flow is denoted by w_∞." [55]

Definition 2.5.3 (Schmidt Number)

"It is the ratio between kinematic viscosity ν and molecular diffusion D. It is denoted by Sc and mathematically we can write it as:

$$Sc = \frac{\nu}{D},$$

where ν is the kinematic viscosity and D is the mass diffusivity." [54]

Definition 2.5.4 (Nusselt Number)

"It is a dimensionless number, first introduced by a German engineer Ernst Kraft Wilhelm Nusselt. Mathematically,

$$Nu = \frac{\alpha L}{k},$$

where α represents the heat transfer coefficient, L denotes the characteristic length and k is the thermal conductivity. It expresses the ratio of the total heat transfer in a system to the heat transfer by conduction." [55]

Definition 2.5.5 (Biot Number)

"This number expresses the ratio of the heat flow transferred by convection on a body surface to the heat flow transferred by conduction in a body. Mathematically,

$$B_i = \alpha(2\pi f \lambda c Q)^{-1/2},$$

where α is the heat transfer coefficient, f is the frequency, c is the specific heat capacity, Q is the density and λ is thermal conductivity." [55]

Definition 2.5.6 (Reynolds Number)

"It is defined as the ratio of inertial forces to viscous forces. Mathematically,

$$Re = \frac{\rho U L}{\nu},$$

where ρ denotes the density of the fluid, U the characteristic flow velocity, μ is the fluid viscosity, and L is a characteristic dimension of the flow region." [54]

Definition 2.5.7 (Sherwood Number)

"The Sherwood number was first introduced by an American chemical engineer, Thomas Kilgore Sherwood and it is defined as

$$Sh = \frac{BL}{D},$$

where B is the mass transfer coefficient, L denotes the characteristic length and D stands for molecular diffusivity. It expresses the ratio of the heat transfer to the molecular diffusion. It characterizes the mass transfer intensity at the interface of phases." [55]

2.6 Governing Laws

Definition 2.6.1 (Continuity Equation)

"The principle of conservation of mass can be stated as the time rate of change of mass in a fixed volume is equal to the net rate of flow of mass across the surface. The mathematical statement of the principle results in the following equation, known as the continuity (of mass) equation.

$$\frac{\partial \rho}{\partial t} + \nabla.(\rho \mathbf{v}) = 0,$$

where t is time, ρ is density of fluid and $\mathbf{v}$ is the fluid velocity and ∇ the nabla or del operator. By introducing the material derivative $\frac{D}{Dt}$,

$$\frac{D}{Dt} = \frac{\partial}{\partial t} + \mathbf{v}.\nabla.$$

The above continuity equation can be expressed in the alternate non-conservation form, as

$$\frac{\partial \rho}{\partial t} + \mathbf{v}.\nabla\rho + \rho\nabla.\mathbf{v} = 0.$$

For steady-state conditions, the continuity equation becomes

$$\nabla.(\rho \mathbf{v}),$$

when the density changes following a fluid particle are negligible, the continuum is termed incompressible and we have $\frac{D\rho}{Dt} = 0$. The continuity equation then becomes

$$\nabla.\mathbf{v} = 0,$$

which is often referred to as the incompressibility condition or incompressibility constraint." [54]

Definition 2.6.2 (Momentum Equation)

"The momentum equation states that the time rate of change of linear momentum of a given set of particles is equal to the vector sum of all the external forces acting on the particles of the set, provided Newton's Third Law of action and reaction governs the internal forces." Mathematically, it can be written as:

$$\frac{\partial}{\partial t}(\rho \mathbf{u}) + \nabla.[(\rho \mathbf{u})\mathbf{u}] = \nabla.\mathbf{T} + \rho g. \text{ [54]}$$

Definition 2.6.3 (Energy Equation)

"The law of conservation of energy (or the first law of thermodynamics) states that the time rate of change of the total energy is equal to the sum of the rate of work done by applied forces and change of heat content per unit time.

$$\frac{\partial \rho}{\partial t} e + \nabla.\rho \mathbf{v} e = -\nabla.\mathbf{q} + Q + \Phi,$$

where Φ is the dissipation function, e is the internal energy q is the heat flux vector and Q is internel heat generation." [54]

2.7 Shooting Method

This section is devoted to the illustration of the shooting method, which is a numerical scheme for the computation of the solution of a boundary value problem. To explain the working procedure of the shooting method, consider the following

boundary value problem:

$$\left.\begin{aligned} f''(x) &= f(x)f'(x) + 2f^2(x) \\ f(0) &= 0, \qquad f(H) = G. \end{aligned}\right\} \tag{2.1}$$

Introduce the following notations to reduce the order of the above boundary value problem.

$$\left.\begin{aligned} f &= z_1 \\ f' &= z_1' = z_2, \\ f'' &= z_2'. \end{aligned}\right\} \tag{2.2}$$

As a result, (2.1) is transformed into the following system of first order ODEs.

$$z_1' = z_2, \qquad z_1(0) = 0, \tag{2.3}$$

$$z_2' = z_1 z_2 + 2z_1^2, \qquad z_2(0) = s. \tag{2.4}$$

where s is the missing initial condition which will be guessed.

The above IVP will be numerically solved by the RK-4 method. The missing condition s is to be chosen such that.

$$z_1(H, s) = G. \tag{2.5}$$

For convenience, now onward $z_1(H, s)$ will be denoted by $z_1(s)$.

Let us further denote $z_1(s) - G$ by $\phi(s)$, so that

$$\phi(s) = 0. \tag{2.6}$$

The above equation can be solved by using any appropriate root-finding technique , e.g., Newton's method which has the following iterative formula:

$$t_{n+1} = t_n - \frac{\phi(t_n)}{\left(\frac{\partial \phi(t)}{\partial t}\right)_{t=t_n}},$$

or

$$t_{n+1} = t_n - \frac{z_1(t_n) - G}{\left(\frac{\partial z_1(t)}{\partial t}\right)_{t=t_n}}. \tag{2.7}$$

To find $\frac{\partial z_1(t)}{\partial t}$, we introduce the following new notations:

$$\frac{\partial z_1}{\partial t} = z_3, \quad \frac{\partial z_2}{\partial t} = z_4. \tag{2.8}$$

By using these notations Newton's iterative scheme, will get the form:

$$t_{n+1} = t_n - \frac{z_1(t_n) - G}{z_3(t_n)}. \tag{2.9}$$

Now differentiating the ODEs (2.3) and (2.4) w.r.t s, we get another system of ODEs, as follows:

$$z_3' = z_4, \qquad z_3(0) = 0, \tag{2.10}$$

$$z_4' = z_3 z_2 + z_1 z_4 + 4 z_1 z_3, \qquad z_4(0) = 1. \tag{2.11}$$

Finally, we have the following IVP:

$$\begin{aligned} z_1' &= z_2, & z_1(0) &= 0, \\ z_2' &= z_1 z_2 + 2 z_1^2, & z_2(0) &= t, \\ z_3' &= z_4, & z_3(0) &= 0, \\ z_4' &= z_3 z_2 + z_1 z_4 + 4 z_1 z_3, & z_4(0) &= 1. \end{aligned}$$

The above IVP will be solved numerically by using any appropriate method, e.g., the RK-4 method.

The stopping criteria is set as,

$$\mid z_1(t) - G \mid < \epsilon,$$

where $\epsilon > 0$ is an sufficiently small positive number.

Chapter 3

Novel Thermal Aspects of Hybrid Nanofluid Flow Comprising of Manganese Zinc Ferrite, Nickel Zinc Ferrite and Motile Micro-organisms

3.1 Introduction

In this chapter, we will perform a numerical analysis of the flow and thermal aspects of hybrid nanofluids comprising of the nanoparticles $MnZnFe_2O_4$ and $NiZnFe_2O_4$ and the base fluid water in the presence of motile microorganisms. This chapter contains a detailed review of the article published by Ahmed et al. [46]. The numerical solution for this model was computed by the finite difference method. In the present chapter, a numerical solution of this work is reproduced by using the shooting method. Water-based hybrid nanofluid flow is considered over a stretching sheet. Motile gyrotactic microorganisms are involved in the flow with the understanding that motion of these microbes is due to the bioconvection

phenomenon. The Darcy-Forchheimer medium and the effect of activation energy have also been taken into account.

3.2 Mathematical Modeling

Consider the flow of hybrid nanofluid over a stretching sheet. Motile gyrotactic microorganisms are involved in the flow and motion of these microbes is due to the bioconvection phenomenon. The stretching velocity of sheet is taken as $U_w(x)$. The Cartesian dimensional coordinates are assumed with x-axis along the porous surface, and y-axis normal to it, as depicted in figure 3.1. Hybrid nanofluids are manufactured by adding $MnZnFe_2O_4$ (manganese zinc ferrite) and $NiZnFe_2O_4$ (nickel zinc ferrite) of volume frictions Φ_1 and Φ_2 respectively in the pure water (H_2O) of volume friction Φ. The nanoparticle volume concentration of the resulting hybrid nanofluid is defined as $\Phi_{hnf} = \Phi_1 + \Phi_2$. The stretching velocity has been taken as:

$$U_w(x, 0) = cx. \tag{3.1}$$

The governing mathematical model proposed by Ahmad et al. [46] for the hybrid nanofluids has been given below in equations (3.2)- (3.6).

Mass conservation equation:

$$\frac{\partial u}{\partial x} + \frac{\partial v}{\partial y} = 0. \tag{3.2}$$

Momentum equation:

$$u\frac{\partial u}{\partial x} + v\frac{\partial u}{\partial y} = \nu_{hnf}\frac{\partial^2 u}{\partial y^2} - \frac{\mu_{hnf}}{\rho_{hnf}k^*}u - \frac{C_b}{\rho_{hnf}\sqrt{k^*}}u^2. \tag{3.3}$$

Energy equation:

$$u\frac{\partial T}{\partial x} + v\frac{\partial T}{\partial y} = \frac{\kappa_{hnf}}{(\rho C_p)_{hnf}}\frac{\partial^2 T}{\partial y^2}. \tag{3.4}$$

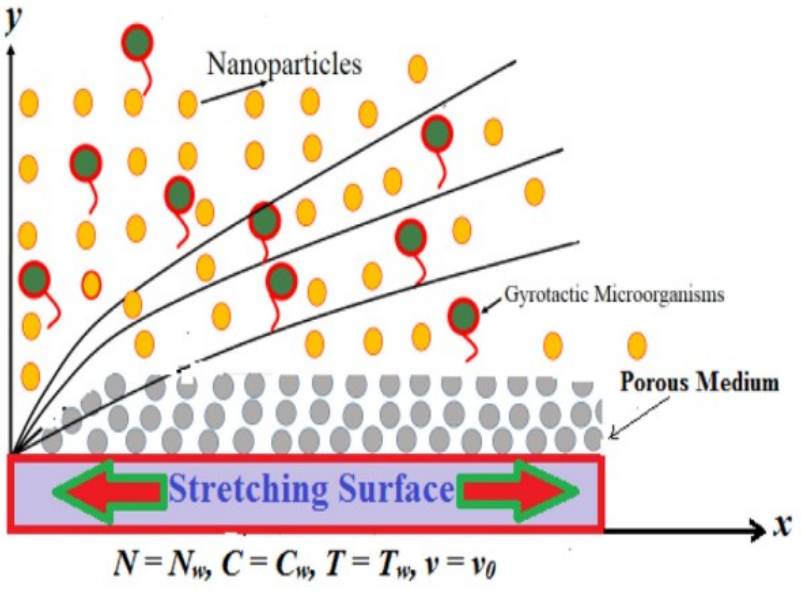

FIGURE 3.1: Geometry of the problem.

Concentration equation:

$$u\frac{\partial C}{\partial x}+v\frac{\partial C}{\partial y}=D_B\frac{\partial^2 C}{\partial y^2}-K_r^2(C-C_\infty)\left(\frac{T}{T_\infty}\right)^{m_1}exp\left(\frac{-E^*}{k^*T}\right). \tag{3.5}$$

Motile equation:

$$v\frac{\partial N}{\partial x}+u\frac{\partial N}{\partial y}+\frac{1}{C_w-C_\infty}\frac{\partial(N\frac{\partial C}{\partial y})}{\partial y}bW_c=D_n\frac{\partial^2 N}{\partial y^2}. \tag{3.6}$$

Boundary condition:

The associated BCs have been taken as:

$$\left.\begin{aligned}&u(x,0)=U_w(x)=cx,\ v(x,0)=-v_0,\ T(x,0)=T_w,\ C(x,0)=C_w,\\&N(x,0)=N_w \quad at \quad y=0,\\&u\to 0,\ \ T\to T_\infty, C\to C_\infty, N\to N_\infty \ \ as \ \ y\to\infty.\end{aligned}\right\} \tag{3.7}$$

Here, u and v are horizontal and vertical velocities respectively. Furthermore μ_{hnf}, ρ_{hnf}, K_{hnf}, $(\rho Cp)_{hnf}$, and K_r are viscosity, density, thermal conductivity, specific heat capacity and rate constant of chemical reaction of hybrid nanofluid respectively.

3.3 Non-Dimensionalization

In this section, the mathematical model mentioned in (3.2)-(3.7) will be non-dimensionalized.

3.3.1 Similarity Transformation

For the conversion of the mathematical model in the form of partial differential equations (3.2)-(3.7) into the ODEs, the following similarity transformation has been introduced:

$$\left.\begin{aligned} &\xi(x,y)=\sqrt{\frac{c}{\nu_f}}y, \quad \psi(x,y)=\sqrt{\nu_f c}xf(\xi), \quad \theta(\xi)=\frac{T-T_\infty}{T_w-T_\infty},\\ &G(\xi)=\frac{N-N_\infty}{N_w-N_\infty}, \quad \phi_(\xi)=\frac{C-C_\infty}{C_w-C_\infty}. \end{aligned}\right\} \tag{3.8}$$

where ψ denotes the stream function.

3.3.2 Some Useful Notations

Thermo-physical properties of hybrid nanofluid are presented in Table 3.1.

TABLE 3.1: Thermo-physical properties of hybrid naonofluid

Feature	**Hybrid Nanofluid** ***($MnZnFe_2O_4$-$NiZnFe_2O_4$/H_2O)***
Viscosity (μ)	$\mu_{hnf}=\mu_f(1-\Phi_1)^{-2.5}(1-\Phi_2)^{-2.5}$
Density (ρ)	$\rho_{hnf}=(1-\Phi_2)\big((1-\Phi_1)\rho_f+\Phi_1\rho_{p_1}\big)+\Phi_2\rho_{p_2}$
Heat Capacity (ρC_p)	$\frac{(\rho C_p)_{hnf}}{(\rho C_p)_f}=(1-\Phi_2)\big((1-\Phi_1)(\rho C_p)_f+\Phi_1\frac{(\rho C_p)_{p_1}}{(\rho C_p)_f}\big)+\Phi_2\frac{(\rho C_p)_{p_2}}{(\rho C_p)_f}$
Thermal conductivity (K)	$\frac{K_{hnf}}{K_{bf}}=\frac{K_{p_2}+(n-1)K_{bf}-(n-1)\Phi_2(K_{bf}-K_{p_2})}{p_2+(n-1)K_{bf}+\Phi_2(k_{bf}-K_{p_2})}$, $\frac{K_{bf}}{K_f}=\frac{K_{p_1}+(n-1)K_f-(n-1)\Phi_1(K_f-K_{p_1})}{K_{p_1}+(n-1)K_f+\Phi_1(K_f-K_{p_1})}$
Electrical conductivity (σ)	$\frac{\sigma_{hnf}}{\sigma_bf}=\frac{\sigma_{p_2}(1+2\Phi_2)+2\sigma_{bf}(1-\Phi_2)}{\sigma_{p_2}(1-\Phi_2)+\sigma_{bf}(2+\Phi_2)}$, $\frac{\sigma_{bf}}{\sigma_f}=\frac{\sigma_{p_1}(1+2\Phi_2)+2\sigma_f(1-\Phi_1)}{\sigma_{p_1}(1-\Phi_1)+\sigma_f(2+\Phi_1)}$

For convenience, the following notations have been introduced which will be later used in the conversion of the dimensional model (3.2)-(3.7) to its dimensionless form.

$$P_a = (1-\Phi_1)^{2.5}(1-\Phi_2)^{2.5},$$

$$\Delta_1 = P_a\left[(1-\Phi_2)\left\{(1-\Phi_1)+\Phi_1\frac{\rho_{p_1}}{\rho_f}\right\}+\Phi_2\frac{\rho_{p_2}}{\rho_f}\right],$$

$$\Delta_2 = \frac{K_{hnf}}{K_f},$$

$$\Delta_3 = \left[(1-\Phi_2)\left\{(1-\Phi_1)+\Phi_1\frac{(\rho C_p)_{p_1}}{(\rho C_p)_f}\right\}+\Phi_2\frac{(\rho C_p)_{p_2}}{(\rho C_p)_f}\right],$$

$$\Delta_4 = \frac{P_a}{\rho_f},$$

$$\Delta_5 = \frac{\sigma_{hnf}}{\sigma_f}.$$

TABLE 3.2: Different dimensionless parameters of the governing model.

Symbols	**Name**	**Appearance**
S_0	Suction parameter	$S_0 = \frac{\nu}{\sqrt{c\nu_f}}$
P_0	Porosity parameter	$P_0 = \frac{\nu_f}{k^* c}$
D_f	Darcy Forchheimer parameter	$D_f = \frac{C_b}{\sqrt{k^*}}x$
Pr	Prandtl number	$Pr = \frac{K_f}{\mu_f (C_p)_f}$
S_c	Schmidt number	$S_c = \frac{\nu_f}{D_B}$
σ	Chemical reaction rate constant	$\sigma = \frac{K_r^2}{c}$
E_0	Activation energy	$E_0 = \frac{E^*}{K^* T_\infty}$
Pe	Peclet number	$Pe = \frac{W_c b}{D_n}$
Ω	Micro-organisms parameter	$\Omega = \frac{N_\infty}{N_w - N_\infty}$

3.3.3 Conversion of Partial Derivatives to the Ordinary Derivatives

The following derivatives are required to non-dimensionalize the dimensional model:

$$\begin{aligned}\frac{\partial \xi}{\partial x} &= \frac{\partial}{\partial x}\left(\sqrt{\frac{c}{\nu_f}}y\right)\\ &= 0. \end{aligned} \tag{3.9}$$

$$\begin{aligned}\frac{\partial \xi}{\partial y} &= \frac{\partial}{\partial y}\left(\sqrt{\frac{c}{\nu_f}}y\right)\\ &= \sqrt{\frac{c}{\nu_f}}. \end{aligned} \tag{3.10}$$

$$\begin{aligned} u &= \frac{\partial \psi}{\partial y}\\ &= \frac{\partial}{\partial y}\left(\sqrt{\nu_f c}xf(\xi)\right)\\ &= \sqrt{\nu_f c}xf'(\xi)\frac{\partial \xi}{\partial y}\\ &= \sqrt{\nu_f c}\sqrt{\frac{c}{\nu_f}}f'\\ &= cxf'. \end{aligned} \tag{3.11}$$

$$\begin{aligned}\frac{\partial u}{\partial x} &= \frac{\partial}{\partial x}\left(cxf'(\xi)\right)\\ &= cf'(\xi). \end{aligned} \tag{3.12}$$

$$\begin{aligned} v &= -\frac{\partial \psi}{\partial x}\\ &= -\frac{\partial}{\partial x}\left(\sqrt{\nu_f c}xf(\xi)\right)\\ &= -\sqrt{\nu_f c}f(\xi). \end{aligned} \tag{3.13}$$

$$\begin{aligned}\frac{\partial v}{\partial y} &= \frac{\partial}{\partial y}\left(-\sqrt{c\nu_f}f(\xi)\right)\\ &= -cf'(\xi). \end{aligned} \tag{3.14}$$

$$\frac{\partial u}{\partial y} = \frac{\partial}{\partial y}\left(cxf'(\xi)\right)$$

$$= cx\frac{\partial}{\partial y}f'(\xi)$$

$$= cx\frac{\partial}{\partial y}f'\left(\sqrt{\frac{c}{\nu_f}}y\right)$$

$$= \frac{c^{3/2}x}{\sqrt{\nu_f}}f''(\xi). \tag{3.15}$$

$$\frac{\partial^2 u}{\partial y^2} = \frac{\partial}{\partial y}\left(\frac{c^{3/2}x}{\sqrt{\nu_f}}f''(\xi)\right)$$

$$= \frac{c^{3/2}x}{\sqrt{\nu_f}}\frac{\partial}{\partial y}\left(f''(\xi)\right)$$

$$= \frac{c^2 x}{\nu_f}f'''(\xi). \tag{3.16}$$

$$\theta(\xi) = \frac{T - T_\infty}{T_w - T_\infty}.$$

$$\Rightarrow \quad T = \theta(\xi)(T_w - T_\infty) + T_\infty.$$

$$\Rightarrow \frac{\partial T}{\partial x} = \frac{\partial}{\partial x}\big(T_\infty + (T_w - T_\infty)\theta(\xi)\big)$$

$$= \frac{\partial T_\infty}{\partial x} + (T_w - T_\infty)\frac{\partial \theta(\xi)}{\partial x} = 0. \tag{3.17}$$

$$\frac{\partial T}{\partial y} = \frac{\partial}{\partial y}\big(T_\infty + (T_w - T_\infty)\theta(\xi)\big)$$

$$= (T_w - T_\infty)\frac{\partial \theta(\xi)}{\partial y}$$

$$= (T_w - T_\infty)\sqrt{\frac{c}{\nu_f}}\theta'(\xi). \tag{3.18}$$

$$\frac{\partial^2 T}{\partial y^2} = \frac{\partial}{\partial y}\Big((T_w - T_\infty)\sqrt{\frac{c}{\nu_f}}\theta'(\xi)\Big)$$

$$= (T_w - T_\infty)\left(\sqrt{\frac{c}{\nu_f}}\right)^2\theta''(\xi)$$

$$= (T_w - T_\infty)\frac{c}{\nu_f}\theta''(\xi). \tag{3.19}$$

$$\phi(\xi) = \frac{C - C_\infty}{C_w - C_\infty}.$$

$$\Rightarrow \qquad C = (C_w - C_\infty)\phi(\xi) + C_\infty.$$

$$\Rightarrow \quad \frac{\partial C}{\partial x} = \frac{\partial}{\partial x}\big((C_w - C_\infty)\phi(\xi) + C_\infty\big)$$

$$= (C_w - C_\infty)\frac{\partial \phi(\xi)}{\partial x} = 0. \tag{3.20}$$

$$\frac{\partial C}{\partial y} = \frac{\partial}{\partial y}\big((C_w - C_\infty)\phi(\xi) + C_\infty\big)$$

$$= (C_w - C_\infty)\frac{\partial \phi(\xi)}{\partial y}$$

$$= (C_w - C_\infty)\left(\sqrt{\frac{c}{\nu_f}}\right)\phi'(\xi). \tag{3.21}$$

$$\frac{\partial^2 C}{\partial y^2} = \frac{\partial}{\partial y}\left((C_w - C_\infty)\sqrt{\frac{c}{\nu_f}}\phi'(\xi)\right)$$

$$= (C_w - C_\infty)\sqrt{\frac{c}{\nu_f}}\frac{\partial \phi'(\xi)}{\partial y}$$

$$= (C_w - C_\infty)\left(\sqrt{\frac{c}{\nu_f}}\right)^2\phi''(\xi)$$

$$= (C_w - C_\infty)\frac{c}{\nu_f}\phi''(\xi). \tag{3.22}$$

$$G(\xi) = \frac{N - N_\infty}{N_w - N_\infty}.$$

$$\Rightarrow \quad N = N_\infty + (N_w - N_\infty)G(\xi).$$

$$\Rightarrow \quad \frac{\partial N}{\partial x} = \frac{\partial}{\partial x}\big(N_\infty + (N_w - N_\infty)G(\xi)\big)$$

$$= (N_w - N_\infty)\frac{\partial}{\partial x}G(\xi) = 0. \tag{3.23}$$

$$\frac{\partial N}{\partial y} = \frac{\partial}{\partial y}\big(N_\infty + (N_w - N_\infty)G(\xi)\big)$$

$$= (N_w - N_\infty)\frac{\partial G(\xi)}{\partial y}$$

$$= (N_w - N_\infty)\sqrt{\frac{c}{\nu_f}}G'(\xi). \tag{3.24}$$

$$\frac{\partial^2 N}{\partial y^2} = \frac{\partial}{\partial y}\left((N_w - N_\infty)\sqrt{\frac{c}{\nu_f}}G'(\xi)\right)$$

$$= (N_w - N_\infty)\sqrt{\frac{c}{\nu_f}}\frac{\partial G'(\xi)}{\partial y}$$

$$= (N_w - N_\infty)\left(\sqrt{\frac{c}{\nu_f}}\right)^2 G''(\xi)$$

$$= (N_w - N_\infty)\frac{c}{\nu_f}G''(\xi). \tag{3.25}$$

From (3.21), we have

$$\frac{\partial C}{\partial y} = (C_w - C_\infty)\sqrt{\frac{c}{\nu_f}}\phi'(\xi).$$

$$\Rightarrow \quad N\frac{\partial C}{\partial y} = \big(N_\infty+(N_w-N_\infty)G(\xi)\big)\left((C_w-C_\infty)\sqrt{\frac{c}{\nu_f}}\phi'(\xi)\right).$$

$$\Rightarrow \quad \frac{\partial C}{\partial y}\left(N\frac{\partial C}{\partial y}\right) = \frac{\partial C}{\partial y}\left(\big(N_\infty+(N_w-N_\infty)G(\xi)\big)\left((C_w-C_\infty)\sqrt{\frac{c}{\nu_f}}\phi'(\xi)\right)\right).$$

$$\Rightarrow \quad \frac{\partial C}{\partial y}\left(N\frac{\partial C}{\partial y}\right) = \big(N_\infty + (N_w - N_\infty)G(\xi)\big)\frac{\partial}{\partial y}\left((C_w - C_\infty)\sqrt{\frac{c}{\nu_f}}\phi'(\xi)\right)$$
$$+ \left((C_w - C_\infty)\sqrt{\frac{c}{\nu_f}}\phi'(\xi)\right)\frac{\partial}{\partial y}\left(N_\infty + (N_w - N_\infty)G(\xi)\right).$$

$$\Rightarrow \quad \frac{\partial C}{\partial y}\left(N\frac{\partial C}{\partial y}\right) = \big(N_\infty + (N_w - N_\infty)G(\xi)\big)\left((C_w - C_\infty)\left(\sqrt{\frac{c}{\nu_f}}\right)^2\phi''(\xi)\right)$$
$$+ \left((C_w - C_\infty)\sqrt{\frac{c}{\nu_f}}\phi'(\xi)\right)\left((N_w - N_\infty)\sqrt{\frac{c}{\nu_f}}G'(\xi)\right).$$
$$= \left(N_\infty\frac{c}{\nu_f}(C_w - C_\infty)\phi''(\xi) + \frac{c}{\nu_f}(N_w - N_\infty)(C_w - C_\infty)\right.$$
$$\left. G(\xi)(\phi''(\xi) + \frac{c}{\nu_f}(C_w - C_\infty)(N_w - N_\infty)\phi'(\xi)G'(\xi)\right).$$
$$= \left(\Omega(N_w - N_\infty)\frac{c}{\nu_f}(C_w - C_\infty)\phi''(\xi) + \frac{c}{\nu_f}(N_w - N_\infty)\right.$$
$$\left.(C_w - C_\infty)G(\xi)(\phi''(\xi) + \frac{c}{\nu_f}(C_w - C_\infty)(N_w - N_\infty)\phi'(\xi)G'(\xi)\right).$$
$$= \frac{c}{\nu_f}(C_w - C_\infty)(N_w - N_\infty)\big(\Omega\phi''(\xi) + G(\xi)\phi''(\xi) + \phi'(\xi)G'(\xi)\big).$$
$$= \frac{c}{\nu_f}(C_w-C_\infty)(N_w-N_\infty)\big(\phi''(\Omega+G(\xi))+\phi'(\xi)G'(\xi)\big). \tag{3.26}$$

3.3.4 Identical Satisfaction of Continuity Equation

By using equations (3.12) and (3.14) in (3.2), we get

$$cf'(\xi) - cf'(\xi) = 0.$$

Thus, equation (3.2) is identically satisfied.

3.3.5 Dimensionless Form of Momentum Equation

The dimensionless form of the momentum equation (3.3) can be obtained by using equations (3.11)-(3.13), (3.15) and (3.16) as follows:

$$\begin{aligned}
&\big(cxf'(\xi)\big)\big(cf'(\xi)\big) - \big(\sqrt{c\nu_f}f(\xi)\big)\left(\frac{c^{3/2}x}{\sqrt{\nu_f}}f''(\xi)\right) \\
&\quad = \frac{\mu_{hnf}}{\rho_{hnf}}\left(\frac{c^2x}{\nu_f}f'''(\xi)\right) - \frac{\mu_{hnf}}{\rho_{hnf}k^*}\big(cxf'(\xi)\big) - \frac{C_b}{\rho_{hnf}\sqrt{k^*}}\big(c^2x^2f'^2(\xi)\big).
\end{aligned}$$

$$\begin{aligned}
\Rightarrow\quad & c^2xf'^2(\xi) - c^2xf(\xi)f''(\xi) \\
&\quad = \frac{\mu_{hnf}}{\rho_{hnf}}\left(\frac{c^2x}{\nu_f}f'''(\xi)\right) - \frac{\mu_{hnf}}{\rho_{hnf}k^*}\big(cxf'(\xi)\big) - \frac{C_b}{\rho_{hnf}\sqrt{k^*}}\big(c^2x^2f'^2(\xi)\big).
\end{aligned}$$

$$\Rightarrow\quad c^2x\big(f'^2 - ff''\big) = c^2x\left(\frac{\mu_{hnf}}{\rho_{hnf}\nu_f}f''' - \frac{\mu_{hnf}}{\rho_{hnf}k^*c}f' - \frac{C_b}{\rho_{hnf}\sqrt{k^*}}xf'^2\right).$$

$$\Rightarrow\quad \big(f'^2 - ff''\big) = \frac{\mu_{hnf}}{\rho_{hnf}\nu_f}f''' - \frac{\mu_{hnf}}{\rho_{hnf}k^*c}f' - \frac{C_b}{\rho_{hnf}\sqrt{k^*}}xf'^2.$$

$$\Rightarrow\quad \frac{\mu_{hnf}}{\rho_{hnf}\nu_f}f''' = (f'^2 - ff'') + \frac{\mu_{hnf}}{\rho_{hnf}k^*c}f' + \frac{C_b}{\rho_{hnf}\sqrt{k^*}}xf'^2.$$

$$\Rightarrow\quad f''' = \frac{\rho_{hnf}\nu_f}{\mu_{hnf}}\left((f'^2 - ff'') + \frac{\mu_{hnf}}{\rho_{hnf}k^*c}f' + \frac{C_b}{\rho_{hnf}\sqrt{k^*}}xf'^2\right).$$

$$\Rightarrow\quad f''' = \frac{\rho_{hnf}\nu_f}{\mu_{hnf}}(f'^2 - ff'') + \frac{\nu_f}{k^*c}f' + \frac{\nu_f}{\mu_{hnf}}D_ff'^2.$$

Using $\nu = \frac{\mu}{\rho}$ and Table 3.1,

$$\nu_f \frac{\rho_{hnf}}{\mu_{hnf}} = \frac{\mu_f}{\rho_f}\left(\frac{(1-\Phi_2)((1-\Phi_1\rho_f+\Phi_1\rho_{p_1})+\Phi_2\rho_{p_2})}{\mu_f(1-\Phi_1)^{-2.5}(1-\Phi_2)^{-2.5}}\right)$$
$$= Pa\left((1-\Phi_2)(1-\Phi_1+\Phi_1\frac{\rho_{p_1}}{\rho_f})\right)+\Phi_2\frac{\rho_{p_2}}{\rho_f} = \Delta_1.$$

As a result, the above equation gets the following form:

$$f''' = \Delta_1(f'^2 - ff'') + P_0 f' + \frac{\nu_f}{\mu_{hnf}} D_f f'^2.$$

Now

$$\frac{\nu_f}{\mu_{hnf}} = \frac{\mu_f}{\rho_f}\left(\frac{1}{\mu_f(1-\Phi_1)^{-2.5}(1-\Phi_2)^{-2.5}}\right) = \frac{P_a}{\rho_f} = \Delta_4.$$

Therefore, the dimensionless form of the momentum equation gets the form:

$$f''' = \Delta_1(f'^2 - ff'') + P_0 f' + \Delta_4 D_f f'^2. \tag{3.27}$$

3.3.6 Dimensionless Form of Energy Equation

The dimensionless form of (3.4) can be achieved by substituting equations (3.11), (3.13) and (3.17) - (3.19) as follows:

$$u.0 + (-\sqrt{c\nu_f}f)(T_w - T_\infty)\sqrt{\frac{c}{\nu_f}}\theta' = \frac{K_{hnf}}{(\rho C_p)_{hnf}}\left((T_w - T_\infty)\frac{c}{\nu_f}\theta''\right).$$

$$\Rightarrow \quad -cf(T_w - T_\infty)\theta' = \frac{K_{hnf}}{(\rho C_p)_{hnf}}\left((T_w - T_\infty)\frac{c}{\nu_f}\theta''\right).$$

$$\Rightarrow \quad -f\theta' = \frac{K_{hnf}}{(\rho C_p)_{hnf}}\frac{1}{\nu_f}\theta''. \tag{3.28}$$

Since

$$\frac{K_{hnf}}{(\rho C_p)_{hnf}}\nu_f = \frac{K_{hnf}}{(\frac{\mu_f}{\rho_f})\left((1-\Phi_2)((1-\Phi_1)(\rho C_p)_f + \Phi_1(\rho C_p)_{p_1}) + \Phi_2(\rho C_p)_{p_2}\right)}$$

$$= \frac{K_{hnf}}{(\frac{\mu_f}{\rho_f})\frac{(\rho C_p)_f}{(\rho C_p)_f}\Big((1-\Phi_2)((1-\Phi_1)(\rho C_p)_f + \Phi_1(\rho C_p)_{p_1}) + \Phi_2(\rho C_p)_{p_2}\Big)}$$

$$= \frac{K_{hnf}}{(\frac{\mu_f}{\rho_f})(\rho C_p)_f\Big((1-\Phi_2)((1-\Phi_1) + \Phi_1\frac{(\rho C_p)_{p_1}}{(\rho C_p)_f} + \Phi_2\frac{(\rho C_p)_{p_2}}{(\rho C_p)_f}\Big)}$$

$$= \frac{K_{hnf}}{\mu_f(C_{p_f})\Delta_3}$$

therefore equation (3.28) becomes:

$$-f\theta' = \frac{K_{hnf}}{\mu_f(C_p)_f\Delta_3}\theta''.$$

$$\Rightarrow \quad -\Delta_3 f\theta' = \frac{K_{hnf}}{K_f}\frac{K_f}{\mu_f(C_p)_f}\theta''.$$

$$\Rightarrow \quad -\Delta_3 f\theta' = \frac{\Delta_2}{Pr}\theta''.$$

Finally, the dimensionless form of the energy equation (3.4), is as follows:

$$\frac{1}{Pr}\Delta_2\theta'' + \Delta_3 f\theta' = 0. \tag{3.29}$$

3.3.7 Dimensionless Form of Concentration Equation

The concentration equation (3.5) can be reduced into the dimensionless form by using equations (3.11), (3.13) (3.20) - (3.22) as follows:

$$u.0 + (-\sqrt{c\nu_f}f)(C_w - C_\infty)\sqrt{\frac{c}{\nu_f}}\phi'$$
$$= D_B(\frac{c}{\nu_f})(C_w - C_\infty)\phi''(\xi) - K_r^2(C - C_\infty)\left(\frac{T}{T_\infty}\right)^{m_1} exp\left(\frac{-E^*}{k^*T}\right).$$

$$\Rightarrow \quad -c(C_w - C_\infty)f\phi' = c\frac{D_B}{\nu_f}(C_w - C_\infty)\phi''$$
$$- K_r^2(C_w - C_\infty)\left(\frac{T}{T_\infty}\right)^{m_1} exp\left(\frac{-E^*}{K^*(T_\infty + (T_w - T_\infty))\theta}\right)\phi.$$

$$\Rightarrow \quad -f\phi' = \frac{1}{S_c}\phi'' - \frac{K_r^2}{c}\left(\frac{T}{T_\infty}\right)^{m_1} exp\left(\frac{-E^*}{K^*T_\infty + K^*(T_w - T_\infty)\theta}\right)\phi.$$

$$\Rightarrow \quad -f\phi' = \frac{1}{S_c}\phi'' - \frac{K_r^2}{c}\left(\frac{T}{T_\infty}\right)^{m_1} exp\left(\frac{\frac{-E^*}{K^*T_\infty}}{1+\frac{T_w-T_\infty}{T_\infty}\theta}\right)\phi.$$

$$\Rightarrow \quad -f\phi' = \frac{1}{S_c}\phi'' - \frac{K_r^2}{c}\left(\frac{T}{T_\infty}\right)^{m_1} exp\left(\frac{-E_0}{1+\delta\theta}\right)\phi.$$

$$\Rightarrow \quad -f\phi' = \frac{1}{S_c}\phi'' - \sigma\big(1+\delta\theta\big)^{m_1} exp\left(\frac{-E_0}{1+\delta\theta}\right)\phi.$$

Therefore, the dimensionless concentration equation (3.5), is as follows:

$$\frac{1}{S_c}\phi'' + f\phi' - \sigma\big(1+\delta\theta\big)^{m_1} exp\left(\frac{-E_0}{1+\delta\theta}\right)\phi = 0. \tag{3.30}$$

3.3.8 Dimensionless Form of Motile Equation

The dimensionless form of equation (3.6) can be obtained by using equations (3.11), (3.13) and (3.23) - (3.26), as follows:

$$(-\sqrt{c\nu_f}f)(N_w - N_\infty)\sqrt{\frac{c}{\nu_f}}G'(\xi) + \frac{1}{C_w - C_\infty}\frac{c}{\nu_f}(C_w - C_\infty)(N_w - N_\infty)$$
$$\Big(\phi''(\Omega + G(\xi)) + \phi' G'(\xi)\Big)bW_c = D_n(N_w - N_\infty)\frac{c}{\nu_f}G''(\xi).$$

$$\Rightarrow \quad -c(N_w - N_\infty)fG'(\xi) + \frac{c}{\nu_f}(N_w - N_\infty)\big(\phi''(\xi)(\Omega + G(\xi)) + \phi'(\xi)G'(\xi)\big)bW_c$$
$$= D_n(N_w - N_\infty)\frac{c}{\nu_f}G''(\xi).$$

$$\Rightarrow \quad -fG'(\xi) + \frac{1}{\nu_f}\big(\phi''(\xi)(\Omega + G(\xi) + \phi'(\xi)G'(\xi)\big)bW_c = \frac{D_n}{\nu_f}G''(\xi).$$

$$\Rightarrow \quad G''(\xi) = \frac{\nu_f}{D_n}\left(-fG'(\xi) + \frac{1}{\nu_f}\big(\phi''(\xi)(\Omega + G(\xi)) + \phi'(\xi)G'(\xi)\big)bW_c\right).$$

$$\Rightarrow \quad G''(\xi) = -\frac{\nu_f}{D_n}fG'(\xi) + \frac{1}{D_n}\big(\phi''(\xi)(\Omega + G(\xi)) + \phi'(\xi)G'(\xi)\big)bW_c.$$

$$\Rightarrow \quad G''(\xi) = -S_c fG'(\xi) + Pe\big(\phi''(\xi)(\Omega + G(\xi)) + \phi'(\xi)G'(\xi)\big).$$

Therefore, the dimensionless form of the concentration equation (3.6) gets the form:

$$G'' = Pe\big(\phi''(\Omega + G) + \phi' G'\big) - S_c fG'. \tag{3.31}$$

3.3.9 Dimensionless Form of Boundary Condition

The related BCs are converted into the dimensionless form by the following calculation:

- $v(x,0) = -v_0, \quad at \quad y = 0.$

  $\Rightarrow \quad v_0 = -\sqrt{c\nu_f} f(\xi), \quad at \quad y = 0.$

  $\Rightarrow \quad f(\xi) = \dfrac{v_0}{\sqrt{c\nu_f}}, \quad at \quad \xi = 0.$

  $\Rightarrow \quad f(0) = \dfrac{v_0}{\sqrt{c\nu_f}}$

  $\Rightarrow \quad f(0) = S_0.$

- $u(x,0) = cx, \quad at \quad y = 0.$

  $\Rightarrow \quad cx = cxf'(\xi), \quad at \quad \xi = 0.$

  $\Rightarrow \quad f'(\xi) = \dfrac{cx}{cx}, \quad at \quad \xi = 0.$

  $\Rightarrow \quad f'(0) = 1.$

- $T(x,0) = T_w, \quad at \quad y = 0.$

  $\Rightarrow \quad T_w = T_\infty + (T_w - T_\infty)\theta(\xi), \quad at \quad y = 0.$

  $\Rightarrow \quad \theta(\xi) = \dfrac{T_w - T_\infty}{T_w - T_\infty}, \quad at \quad y = 0.$

  $\Rightarrow \quad \theta(\xi) = 1, \quad at \quad \xi = 0.$

  $\Rightarrow \quad \theta(0) = 1.$

- $C(x,0) = C_w, \quad at \quad y = 0.$

  $\Rightarrow \quad C(x,0) = C_\infty + (C_w - C_\infty)\phi(\xi), \quad at \quad \xi = 0.$

  $\Rightarrow \quad \phi(\xi) = \dfrac{C_w - C_\infty}{C_w - C_\infty}, \quad at \quad \xi = 0.$

  $\Rightarrow \quad \phi(\xi) = 1, \quad at \quad \xi = 0.$

$\Rightarrow \quad \phi(0) = 1.$

- $N(x,0) = N_w, \qquad at \quad y = 0.$

$\Rightarrow \quad N(x,0) = N_\infty + (N_w - N_\infty)G(\xi), \qquad at \quad \xi = 0.$

$\Rightarrow \quad G(\xi) = \dfrac{N_w - N_\infty}{N_w - N_\infty}, \qquad at \quad \xi = 0.$

$\Rightarrow \quad G(\xi) = 1, \qquad at \quad \xi = 0.$

$\Rightarrow \quad G(0) = 1.$

- $u \longrightarrow 0, \qquad as \quad y \longrightarrow \infty.$

$\Rightarrow \quad f'(\xi) \longrightarrow 0, \qquad as \quad \xi \longrightarrow \infty.$

- $T \to T_\infty, \qquad as \quad y \longrightarrow \infty.$

$\Rightarrow \quad \theta(\xi) \to 0, \qquad as \quad \xi \longrightarrow \infty.$

- $C \to C_\infty, \qquad as \quad y \longrightarrow \infty.$

$\Rightarrow \quad \phi(\xi) \to 0, \qquad as \quad \xi \longrightarrow \infty.$

- $N \to N_\infty, \qquad as \quad y \longrightarrow \infty.$

$\Rightarrow \quad G(\xi) \to 0, \qquad as \quad \xi \longrightarrow \infty.$

Finally,

$$\left.\begin{array}{l} f = S_0, \quad f' = 1, \quad \theta = 1, \quad G = 1, \quad \phi = 1 \quad as \quad \xi \to 0. \\ f' \to 0, \quad \theta \to 0, \quad G \to 0, \quad \phi \to 0, \quad as \quad \xi \to \infty. \end{array}\right\} \tag{3.32}$$

3.4 Physical Quantities of Interest

This section provides an introduction to the dimensional physical quantities and their conversion to the dimensionless form.

Skin Friction:

$$C_{f_x} = \frac{\tau_w}{\rho_f U_w^2},$$

where

$$\tau_w = \mu_{hnf}\left(\frac{\partial u}{\partial y}\right)_{y=0}.$$

Therefore

$$\begin{aligned} C_{f_x} &= \frac{\mu_{hnf} c^{3/2} x}{\rho_f c^2 x^2 \sqrt{\nu_f}} f''(0) \qquad \text{(using (3.15))} \\ &= \frac{\mu_{hnf}\nu_f}{\mu_f \sqrt{c} x \sqrt{\nu_f}} f''(0) \\ &= \frac{\mu_{hnf}}{\mu_f}\sqrt{\frac{\nu_f}{c}} x f''(0) \\ &= \frac{1}{Re_x^{\frac{1}{2}}(1-\Phi_1)^{2.5}(1-\Phi_2)^{2.5}} f''(0) \\ \Rightarrow \quad Re_x^{\frac{1}{2}} C_{f_x} &= \frac{1}{(1-\Phi_1)^{2.5}(1-\Phi_2)^{2.5}} f''(0). \end{aligned}$$

Here $Re_x^{1/2}$ denotes the Reynolds number.

Nusselt Number:

$$Nu_x = -\frac{x q_m}{K_f(T_w - T_\infty)}$$

where

$$q_m = K_{hnf}\left(\frac{\partial T}{\partial y}\right)_{y=0}.$$

$$\begin{aligned} Therefore \quad Nu_x &= -\frac{x K_{hnf}(T_w - T_\infty)\sqrt{\frac{c}{\nu_f}}\theta'(0)}{K_f(T_w - T_\infty)} \qquad \text{(using (3.18))} \\ Nu_x &= -\frac{K_{hnf}}{K_f}\sqrt{\frac{c}{\nu_f}} x \theta'(0) \\ \Rightarrow \quad Re_x^{-\frac{1}{2}} Nu_x &= -\frac{K_{hnf}}{K_f}\theta'(0). \end{aligned}$$

Sherwood Number:

$$Sh_x = -\frac{xq_m}{D_B(C_w - C_\infty)}$$

where

$$q_m = -D_B\left(\frac{\partial C}{\partial y}\right)_{y=0}.$$

Therefore

$$Sh_x = -\frac{xD_B(C_w - C_\infty)\sqrt{\frac{c}{\nu_f}}\phi'(0)}{D_B(C_w - C_\infty)} \qquad \text{(using (3.21))}$$

$$Sh_x = -\sqrt{\frac{c}{\nu_f}}x\phi'(0)$$

$$\Rightarrow \quad Re_x^{-\frac{1}{2}}Sh_x = -\phi'(0).$$

Density of Motile Micro-organism:

$$Nn_x = -\frac{xq_m}{D_n(N_w - N_\infty)}$$

where

$$q_m = -D_n\left(\frac{\partial N}{\partial y}\right)_{y=0}.$$

Therefore

$$Nn_x = -\frac{xD_n(N_w - N_\infty)\sqrt{\frac{c}{\nu_f}}}{D_n(N_w - N_\infty)}G'(0) \qquad \text{(using (3.24))}$$

$$Nn_x = -\sqrt{\frac{c}{\nu_f}}xG'(0)$$

$$\Rightarrow \; `Re_x^{-\frac{1}{2}}Nn_x = -G'(0).$$

3.5 Solution Methodology

The ordinary differential equation (3.27) has been solved numerically by using the shooting technique. The following notations have been taken into consideration:

$$f = G_1, \qquad f' = G_1' = G_2, \qquad f'' = G_1'' = G_2' = G_3.$$

The momentum equation is then transformed into the system of first-order ODEs shown below:

$$\left.\begin{aligned} G_1' &= G_2, & G_1(0) &= S_0, \\ G_2' &= G_3, & G_2(0) &= 1, \\ G_3' &= \Delta_1\left(G_2^2 - G_1 G_3\right) + P_0 G_2 + \Delta_4 D_f G_2^2, & G_3(0) &= p. \end{aligned}\right\} \tag{3.33}$$

The above IVP will be numerically solved by the Runge-Kutta method of oder 4. The domain of the problem is considered to be bounded i.e. $[0,\ \xi_\infty]$, where ξ_∞ is a positive real number, for which the variation in the solution is ignorable after $\xi = \xi_\infty$. The missing condition p is to be chosen such that.

$$G_2(\xi_\infty, p) = 0.$$

Newton's method will be used to find p. This method has the following iterative scheme.

$$p_{n+1} = p_n - \frac{G_2(\xi_\infty, p_n)}{\left(\frac{\partial}{\partial p} G_2(\xi_\infty, p)\right)_{p=p_n}}.$$

We, further introduce the following notations:

$$\frac{\partial G_1}{\partial p} = G_4, \qquad \frac{\partial G_2}{\partial p} = G_5, \qquad \frac{\partial G_3}{\partial p} = G_6.$$

As a result of these new notations, the Newton's iterative scheme gets the form:

$$p_{n+1} = p_n - \frac{G_2(\xi_\infty, p_n)}{G_5(\xi_\infty, p_n)}.$$

Now, differentiating the system of first order ODEs (**??**) with respect to p, we get another system of ODEs as follows:

$$\left.\begin{aligned} G_4' &= G_5, & G_4(0) &= 0, \\ G_5' &= G_6, & G_5(0) &= 0, \\ G_6' &= \Delta_1\big(2G_2G_5 - G_1G_6 - G_3G_4\big) + P_0G_5 & & \\ &\quad + 2\Delta_4 D_f G_2 G_5, & G_6(0) &= 1. \end{aligned}\right\} \tag{3.34}$$

The stopping criteria for the Newton's technique is set as:

$$\mid G_2(\xi_\infty, p) \mid < \epsilon,$$

where $\epsilon > 0$ is a sufficiently small number. From now onward, ϵ has been considered as 10^{-10}.

The ordinary differential equation (3.29) will be approximated by using the shooting technique and assuming f as a known function. For this, we utilize the following notions:

$$\theta = H_1, \qquad \theta' = H_1' = H_2.$$

The energy equation (3.29) is then transformed into the system of first-order ODEs shown below.

$$\left.\begin{aligned} H_1' &= H_2, & H_1(0) &= 1, \\ H_2' &= -Pr\frac{\Delta_3}{\Delta_2}G_1H_2, & H_2(0) &= q. \end{aligned}\right\} \tag{3.35}$$

The above IVP will be numerically solved by Runge-Kutta method of oder 4. The missing condition q is to be chosen such that.

$$H_1(\xi_\infty, q) < \epsilon.$$

The above equation can be solved by using Newton's method with the following iterative formula:

$$q_{n+1} = q_n - \frac{H_1(\xi_\infty, q_n)}{\left(\frac{\partial}{\partial q} H_1(\xi_\infty, q)\right)_{q=q_n}}.$$

We, further introduce the following notations:

$$\frac{\partial H_1}{\partial q} = H_3, \qquad \frac{\partial H_2}{\partial q} = H_4.$$

As a result of these new notations, the Newton's iterative scheme gets the form:

$$q_{n+1} = q_n - \frac{H_1(\xi_\infty, q_n)}{H_3(\xi_\infty, q_n)}.$$

Now, differentiating the (3.35) w.r.t q, we get another system of ODEs, as follows:

$$\left.\begin{aligned} H_3' &= H_4, & H_3(0) &= 0, \\ H_4' &= -Pr\frac{\Delta_3}{\Delta_2} G_1 H_4, & H_4(0) &= 1. \end{aligned}\right\} \quad (3.36)$$

The stopping criteria for the Newton's method is set as:

$$\mid H_1(\xi_\infty, q) \mid = 0.$$

Now, the ordinary differential equations (3.30) and (3.31) has been solved numerically by using the shooting technique, f and θ will be taken as the known functions. The following notation have been taken:

$$\phi = T_1, \qquad \phi' = T_1' = T_2, \qquad G = T_3, \qquad G' = T_3' = T_4.$$

The equations (3.30) and (3.31) are then transformed into the system of first-order ODEs shown below:

$$\left.\begin{aligned}
&T_1' = T_2, && T_1(0) = 1.\\
&T_2' = Sc\left(\sigma\big(1+\delta\theta\big)^{m_1} exp\left(\frac{-E_0}{1+\delta\theta}\right)T_1 - G_1T_2\right), && T_2(0) = d.\\
&T_3' = T_4, && T_3(0) = 1.\\
&T_4' = Pe\left(Sc\left(\sigma\big(1+\delta\theta\big)^{m_1} exp\left(\frac{-E_0}{1+\delta\theta}\right)T_1 - G_1T_2\right)(\Omega+T_3) + T_2T_4\right)\\
&\quad - ScG_1T_3, && T_4(0) = s.
\end{aligned}\right\} \quad (3.37)$$

The above IVP will be numerically solved by the Runge-Kutta method of order 4. The domain of the problem is considered to be bounded i.e. $[0,\ \xi_\infty]$, where ξ_∞ is a positive real number, for which the variation in the solution is ignorable after $\xi = \xi_\infty$. The missing conditions d and s are to be chosen such that:

$$T_1(\xi_\infty, d) = 0,\ T_3(\xi_\infty, s) = 0.$$

Newton's method will be used to find d and s. This method has the following iterative scheme:

$$\begin{bmatrix} d \\ s \end{bmatrix}_{(n+1)} = \begin{bmatrix} d \\ s \end{bmatrix}_{(n)} - \begin{bmatrix} \frac{\partial T_1}{\partial d} & \frac{\partial T_1}{\partial s} \\ \frac{\partial T_3}{\partial d} & \frac{\partial T_3}{\partial s} \end{bmatrix}^{-1}_{(n)} \begin{bmatrix} T_1 \\ T_3 \end{bmatrix}_{(n)}$$

Furthermore, the following notations will be useful for computing the entries of the Jacobian matrix.

$$\begin{aligned}
&\frac{\partial T_1}{\partial d} = T_5, && \frac{\partial T_2}{\partial d} = T_6, && \frac{\partial T_3}{\partial d} = T_7, && \frac{\partial T_4}{\partial d} = T_8,\\
&\frac{\partial T_1}{\partial s} = T_9, && \frac{\partial T_2}{\partial s} = T_{10}, && \frac{\partial T_3}{\partial s} = T_{11}, && \frac{\partial T_4}{\partial s} = T_{12}.
\end{aligned}$$

Newton's iterative scheme will change its form, after utilizing the above mentioned notations, as follows:

$$\begin{bmatrix} d \\ s \end{bmatrix}_{(n+1)} = \begin{bmatrix} d \\ s \end{bmatrix}_{(n)} - \begin{bmatrix} T_5 & T_9 \\ T_7 & T_{11} \end{bmatrix}^{-1}_{(n)} \begin{bmatrix} T_1 \\ T_3 \end{bmatrix}_{(n)}.$$

Now differentiating (3.37) w.r.t d and s, we get another system of ODEs as follows:

$$\left.\begin{aligned}
&T_5' = T_6, && T_5(0) = 0.\\
&T_6' = Sc\left(\sigma\left(1+\delta\theta\right)^{m_1} exp\left(\frac{-E_0}{1+\delta\theta}\right)T_5 - G_1 T_6\right), && T_6(0) = 1.\\
&T_7' = T_8, && T_7(0) = 0.\\
&T_8' = Pe\left(Sc\left(\sigma\left(1+\delta\theta\right)^{m_1} exp\left(\frac{-E_0}{1+\delta\theta}\right)T_1 - G_1 T_2\right)T_7\right.\\
&\quad + (\Omega + T_3)\left(Sc\left(\sigma\left(1+\delta\theta\right)^{m_1} exp\left(\frac{-E_0}{1+\delta\theta}\right)T_5 - G_1 T_6\right)\right.\\
&\quad \left.\left. + T_2 T_8 + T_6 T_4\right)\right) - ScG_1 T_7, && T_8(0) = 0.\\
&T_9' = T_{10}, && T_9(0) = 0.\\
&T_{10}' = Sc\left(\sigma\left(1+\delta\theta\right)^{m_1} exp\left(\frac{-E_0}{1+\delta\theta}\right)T_9 - G_1 T_{10}\right), && T_{10}(0) = 0.\\
&T_{11}' = T_{12}, && T_{11}(0) = 0.\\
&T_{12}' = Pe\left(Sc\left(\sigma\left(1+\delta\theta\right)^{m_1} exp\left(\frac{-E_0}{1+\delta\theta}\right)T_1 - G_1 T_2\right)T_{11}\right.\\
&\quad + (\Omega + T_3)\left(Sc\left(\sigma\left(1+\delta\theta\right)^{m_1} exp\left(\frac{-E_0}{1+\delta\theta}\right)T_9 - G_1 T_{10}\right)\right.\\
&\quad \left.\left. + T_2 T_{12} + T_{10} T_4\right)\right) - ScG_1 T_{11}, && T_{12}(0) = 1.
\end{aligned}\right\} \quad (3.38)$$

The stopping criteria for the Newton's method is set as:

$$max\left\{\mid T_1(\xi_\infty, d)\mid, \mid T_3(\xi_\infty, s)\mid\right\} < \epsilon.$$

3.6 Results Interpretation

The main focus of this section is to investigate the influence of various factors, including the porosity parameter (P_0), Darcy inertial parameter (D_f), Prandtl number (Pr), Schmidt number (S_c), chemical reaction rate constant (σ), activation energy parameter (E_0), Peclet number (Pe), suction parameter (S_0) and

bioconvection parameter (Ω) on the variable profiles of the problem. These factors play a crucial role in interpreting the fields of velocity $f'(\xi)$, temperature $\theta(\xi)$, concentration $\phi(\xi)$, and motile profile $G(\xi)$. Moreover, through the adjustment of dimensionless parameter values, the impact of these parameters on physical quantities, such as skin friction Nusselt number, Sherwood number and density of motile microorganism is investigated and presented in tabular format.

The velocity, temperature, concentration and motile profiles plots offer clear indications about how the system behaves as the physical parameters fluctuate. Through observing the trends in these profiles, a more comprehensive understanding of the system's physical characteristics can be observed. The graphical representations help to understand how variations in various physical parameters effect different profiles.

3.6.1 Discussion of Computational results

In Table 3.3, T_{f_1} and T_{f_2} are the intervals for the choice of missing condition p while computing the of skin friction coefficient for nanofluid and hybrid nanofluid respectively. It is observed that for the computation of Nusselt number, there is great flexibility in the choice of the missing initial condition. Table 3.4 presents the results of the skin friction coefficient for the $NiZnFe_2O_4/H_2O$ nanofluid and $NiZnFe_2O_4 - MnZnFe_2O_4/H_2O$ hybrid nanofluid, under various inputs of P_0, D_f, S_0, Φ_1 and Φ_2. From the computations, it is evident that the positive variation in P_0, D_f, S_0 and Φ_1 leads to higher absolute values of skin friction coefficients, showing a decrease in the velocity of fluid. Table 3.5 gives the details of Nusselt number as it relates to the porosity parameter P_0, Darcian parameter D_f, suction parameter S_0, volume fraction Φ_1 and Prandtl number Pr. The findings reveal that the Nusselt number $Re_x^{-\frac{1}{2}} Nu_x$ falls for the positive variation in porosity parameter P_0 and Darcian parameter D_f while inverse trend is observed for the increasing values of suction parameter S_0, volume concentration Φ_1 and Prandtl number for both nanofluid and hybrid nanofluid flow cases.

Table 3.6 illustrates the impacts of suction parameter S_0, chemical reaction rate constant σ and Schmidt number Sc on the concentration boundary layer. An opposite influence is shown by porosity parameter P_0 and Darcian parameter D_f. Moreover, Table 3.7 provides the results of the density of motile micro-organism $Re_x^{-\frac{1}{2}} Nn_x$. For the enhancing values of porosity parameter P_0, Darcian parameter D_f and chemical reaction rate σ density of motile micro-organism falls whereas a rise in the suction parameter S_0, Peclet number Pe, bioconvection parameter Ω and Schmidt number S_c cause an increase in density of motile micro-organisms.

TABLE 3.3: Missing conditions of $Re_x^{\frac{1}{2}} C_{f_x}$

P_0	D_f	S_0	Φ_1	Φ_2	T_{f_1}	T_{f_2}
0.1	25	0	0.03	0.05	[-1.1, -0.1]	[-1.1, -0.1]
0.3					[-1.1, -0.3]	[-1.2, -0.2]
0.5					[-1.3, -0.5]	[-1.2, -0.5]
0.8					[-1.3, -0.8]	[-1.3, -0.9]
	45				[-1.1, -0.2]	[-1.1, -0.2]
	65				[-1.1, -0.2]	[-1.1, -0.2]
	85				[-1.1, -0.3]	[-1.1, -0.3]
		0.6			[-1.5 , 0.0]	[-1.5 , 0.6]
		1.2			[-2.0 , 1.5]	[-2 .0, 1.5]
		1.8			[-2.7 , 2.8]	[-2.7 , 2.8]
			0.06		[-1.1, -0.1]	[-1.1, -0.1]
			0.09		[-1.1, -0.1]	[-1.1 , 0.0]
			0.12		[-1.1, -0.1]	[-1.1, -0.1]
				0.07	- - - -	[-1.1, -0.1]
				0.09	- - - -	[-1.1, -0.1]
				0.11	- - - -	[-1.1 , -0.1]

TABLE 3.4: Results of $Re_x^{\frac{1}{2}} C_{f_x}$

P_0	D_f	S_0	Φ_1	Φ_2	$Re_x^{\frac{1}{2}} C_{f_x}$ *(NF)*	$Re_x^{\frac{1}{2}} C_{f_x}$ *(HNF)*
0.1	25	0	0.03	0.05	-1.1545	-1.3269
0.3					-1.2514	-1.4358
0.5					-1.3412	-1.5371
0.8					-1.4657	-1.6776
	45				-1.1605	-1.3327
	65				-1.1664	-1.3386
	85				-1.1723	-1.3445
		0.6			-1.5345	-1.7711
		1.2			-1.9993	-2.3151
		1.8			-2.5269	-2.9329
			0.06		-1.2579	-1.4346
			0.09		-1.3672	-1.5493
			0.12		-1.4837	-1.6720
				0.07	- - - -	-1.4004
				0.09	- - - -	-1.4771
				0.11	- - - -	-1.5571

TABLE 3.5: Results of $Re_x^{-\frac{1}{2}} Nu_x$

P_0	D_f	S_0	Φ_1	Φ_2	Pr	$Re_x^{-\frac{1}{2}} Nu_x$ *(NF)*	$Re_x^{-\frac{1}{2}} Nu_x$ *(HNF)*
0.1	25	0	0.03	0.05	1	0.5783	0.5917
0.3						0.5599	0.5722
0.5						0.5434	0.5548
0.8						0.5216	0.5319
	45					0.5777	0.5911
	65					0.5770	0.5905
	85					0.5764	0.5899
		0.6				1.0081	1.0137
		1.2				1.5050	1.5028
		1.8				2.0410	2.0313
			0.06			0.5858	0.6007
			0.09			0.5944	0.6107
			0.12			0.6042	0.6218
				0.07		- - - -	0.5976
				0.09		- - - -	0.6040
				0.11		- - - -	0.6107
					5	1.5885	1.6514
					7	1.9253	2.0056
					10	2.3506	2.4527

TABLE 3.6: Results of $Re_x^{-\frac{1}{2}} Sh_x$

P_0	D_f	S_0	Φ_1	Φ_2	Pr	σ	E_0	Pe	Ω	Sc	$Re_x^{-\frac{1}{2}} Sh_x$ *(NF)*	$Re_x^{-\frac{1}{2}} Sh_x$ *(HNF)*
0.1	25	0	0.03	0.05	1	0	1	0.1	0	1	0.5692	0.5668
0.3											0.5514	0.5492
0.5											0.5354	0.5334
0.8											0.5141	0.5124
	45										0.5686	0.5663
	65										0.5680	0.5657
	85										0.5674	0.5652
		0.6									0.9975	0.9948
		1.2									1.4926	1.4901
		1.8									2.0264	2.0241
			0.06								0.5676	0.5669
			0.09								0.5671	0.5677
			0.12								0.5675	0.5693
				0.07							- - - -	0.5666
				0.09							- - - -	0.5668
				0.11							- - - -	0.5685
					5						0.5692	0.5668
					7						0.5692	0.5668
					10						0.5692	0.5668
						1					0.8490	0.8478
						3					1.2178	1.2172
						5					1.4944	1.4940
							2				0.5692	0.5668
							3				0.5692	0.5668
							4				0.5692	0.5668
								0.2			0.5692	0.5668
								0.3			0.5692	0.5668
								0.4			0.5692	0.5668
									0.4		0.5692	0.5668
									0.8		0.5692	0.5668
									1.2		0.5692	0.5668
										1.5	0.7470	0.7444
										2	0.8983	0.8957
										2.5	1.0319	1.0293

TABLE 3.7: Results of $Re_x^{-\frac{1}{2}}Nn_x$

P_0	D_f	S_0	Φ_1	Φ_2	Pr	σ	E_0	Pe	Ω	Sc	$Re_x^{-\frac{1}{2}}Nn_x$ *(NF)*	$Re_x^{-\frac{1}{2}}Nn_x$ *(HNF)*
0.1	25	0	0.03	0.05	1	0	1	0.1	0	1	0.634	0.6108
0.3											0.5946	0.5923
0.5											0.5778	0.5757
0.7											0.5625	0.5606
	45										0.6127	0.6103
	65										0.6121	0.6097
	85										0.6114	0.6091
		0.6									1.0866	1.0838
		1.2									1.6335	1.6308
		1.8									2.2223	2.2198
			0.06								0.6117	0.6109
			0.09								0.6111	0.6118
			0.12								0.6105	0.6135
				0.07							- - - -	0.6106
				0.09							- - - -	0.6108
				0.11							- - - -	0.6115
					5						0.6134	0.6108
					7						0.6134	0.6108
					10						0.6132	0.6108
						1					0.6377	0.6352
						2					0.6556	0.6532
						3					0.6706	0.6682
							2				0.6134	0.6108
							3				0.6134	0.6108
							4				0.6134	0.6108
								0.2			0.6580	0.6553
								0.3			0.7029	0.7001
								0.4			0.7483	0.7454
									0.4		0.6291	0.6266
									0.8		0.6449	0.6423
									1.2		0.6606	0.6580
										1.5	0.8035	0.8008
										2	0.9652	0.9625
										2.5	1.1082	1.1054

3.6.2 Velocity Profile

Figure 3.2 illustrates the influence of local porosity parameter P_0 on $f'(\xi)$. It is evident that both the nanofluids $NiZnFe_2O_4/H_2O$ and the hybrid nanofluid $MnZnFe_2O_4-NiZnFe_2O_4/H_2O$, experience a significant decrease in the velocity of flow as the values of P_0 increase. The porosity parameter P_0 is inversely proportional to the Darcian drag force. As the porosity increases and the Darcian drag force decreases, fluid flow becomes more permeable through the porous medium. However, this happens at the expense of a reduction in the fluid velocity.

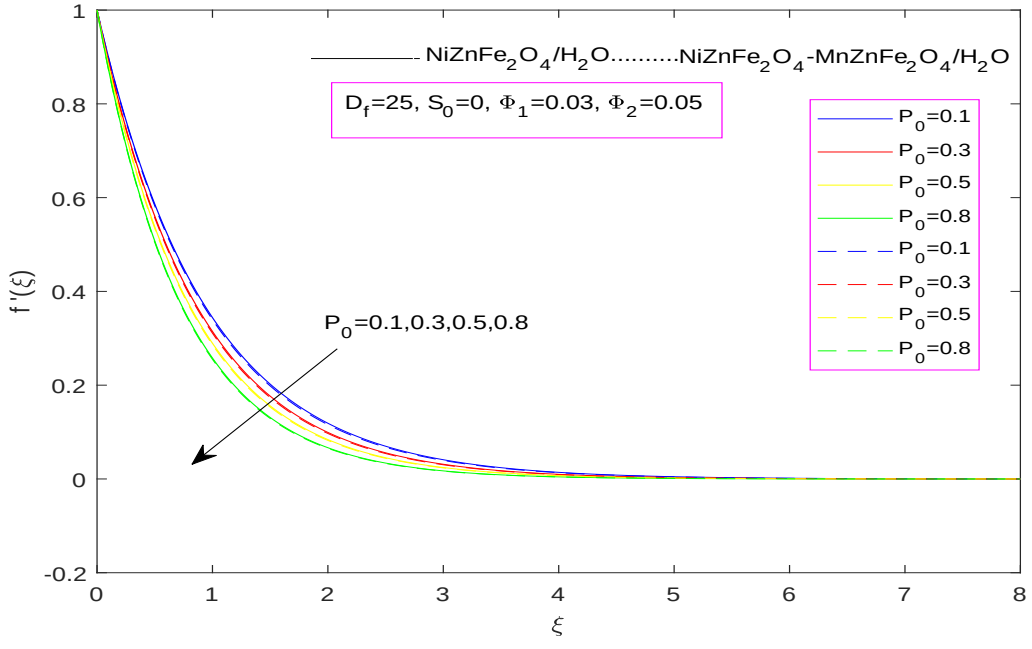

FIGURE 3.2: Impact of P_0 on $f'(\xi)$

Figure 3.3 discloses the result for the velocity profile against the Darcian parameter D_f. The observed decrease in the velocity profile $f'(\xi)$ with increasing D_f is explained by inertial effects. These effects introduce a force that drags the fluid backward, acting as a resistance and causing a reduction in the fluid's speed. Another important factor influencing the fluid flow characteristics is the suction parameter S_0. From Figure 3.4, it is evident that the velocity profile is enhanced for the rising values of suction parameter S_0. Mass transfer processes that take place at the wall's suction region are considered to be a cause of this impact. The

system's overall velocity decreases as a result of suction-generated flow motion that opposes the main flow.

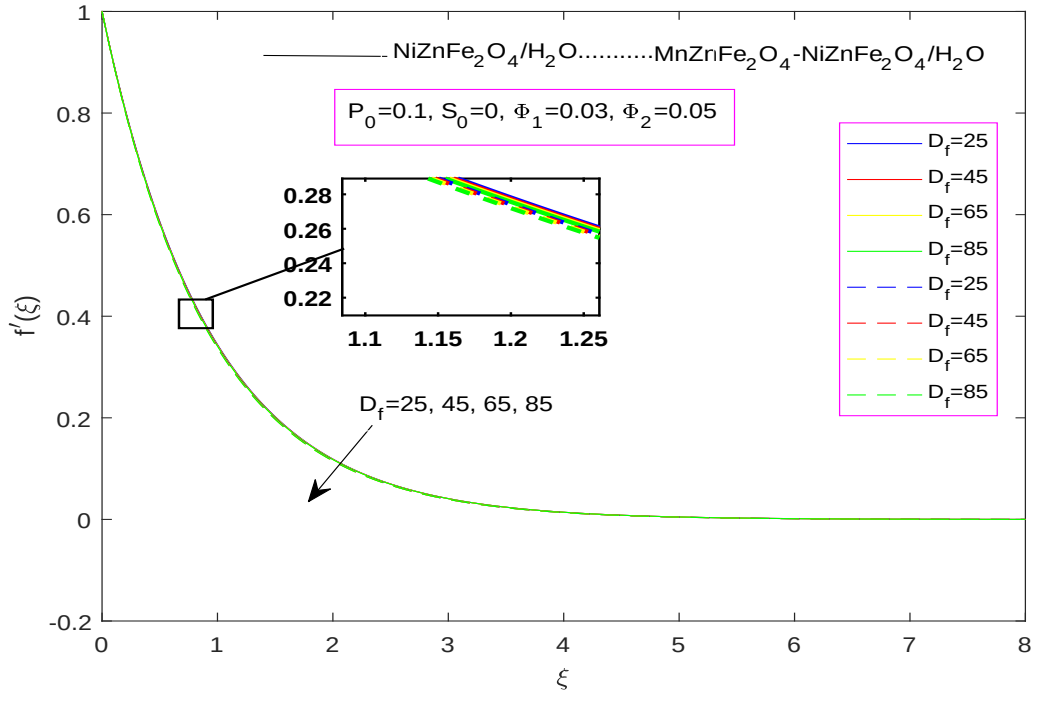

FIGURE 3.3: Impact of D_f on $f'(\xi)$

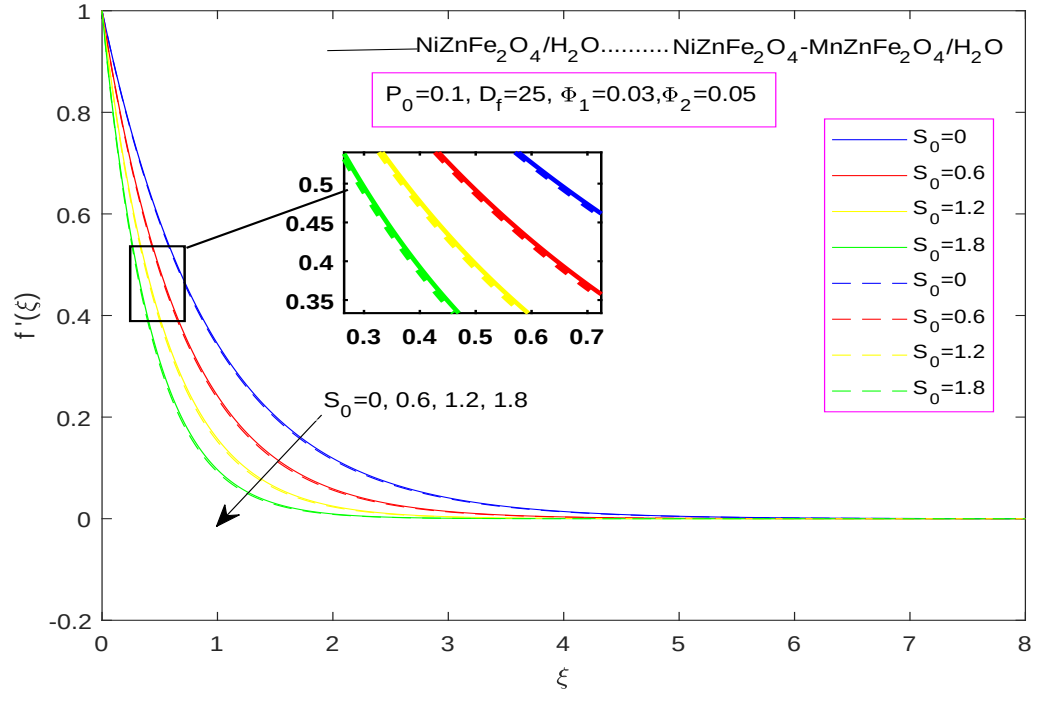

FIGURE 3.4: Impact of S_0 on $f'(\xi)$

3.6.3 Temperature Profile

Figures 3.5 to 3.9 present the characteristics of the temperature profile $\theta(\xi)$ with respect to various parameters, including the porosity parameter P_0, Darcian parameter D_f, suction parameter S_0, volume fraction Φ_1, and Prandtl number Pr. Figure 3.5 illustrates the influence of the porosity parameter P_0 on temperature profile $\theta(\xi)$. The rising values of P_0 enhance the temperature profile. From Figure 3.6, it is evident that the temperature profile $\theta(\xi)$ is enlarged for a positive variation in the Darcian parameter D_f.

From Figure 3.7, it is clear that the temperature profile $\theta(\xi)$ increases for the higher values of suction parameter S_0. The rising values of suction parameter $S_0 > 0$ lowers the temperature and decreases the thickness of the thermal boundary layer. Fluid temperature decreases when S_0 is increased because more nanofluid is drawn out.

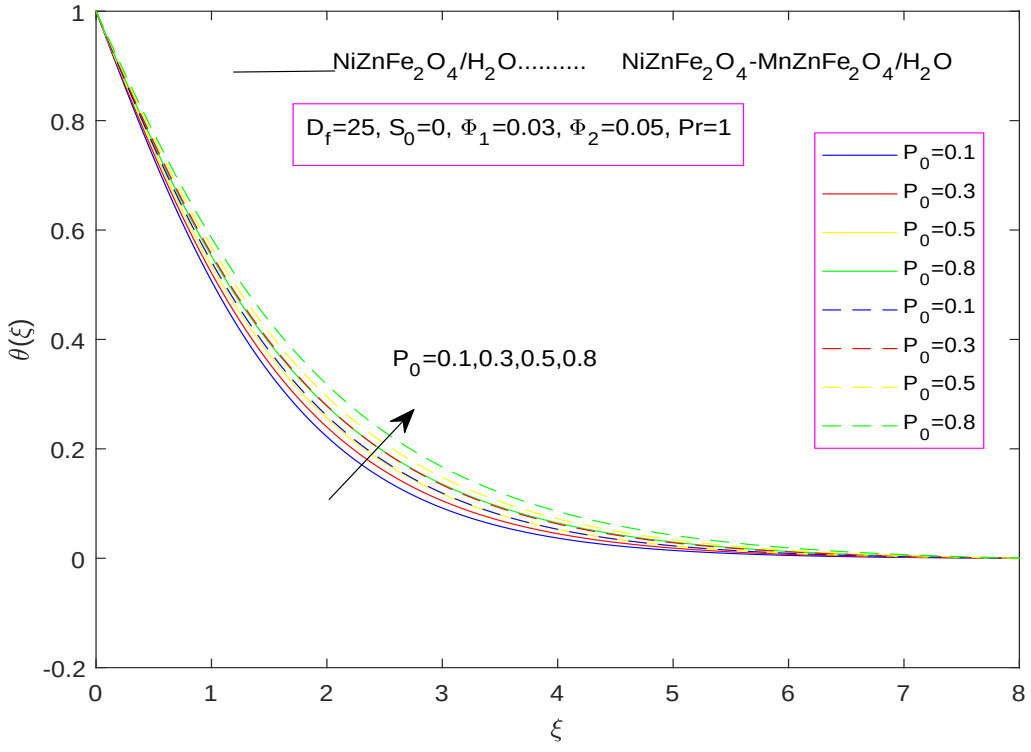

FIGURE 3.5: Impact of P_0 on $\theta(\xi)$

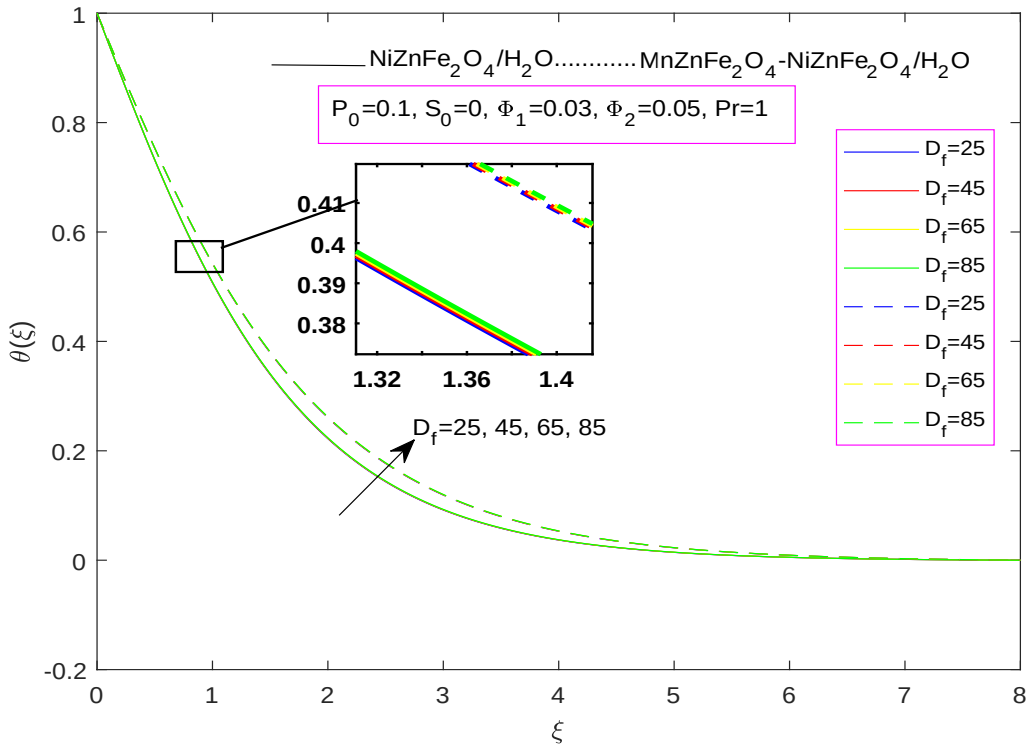

FIGURE 3.6: Impact of D_f on $\theta(\xi)$

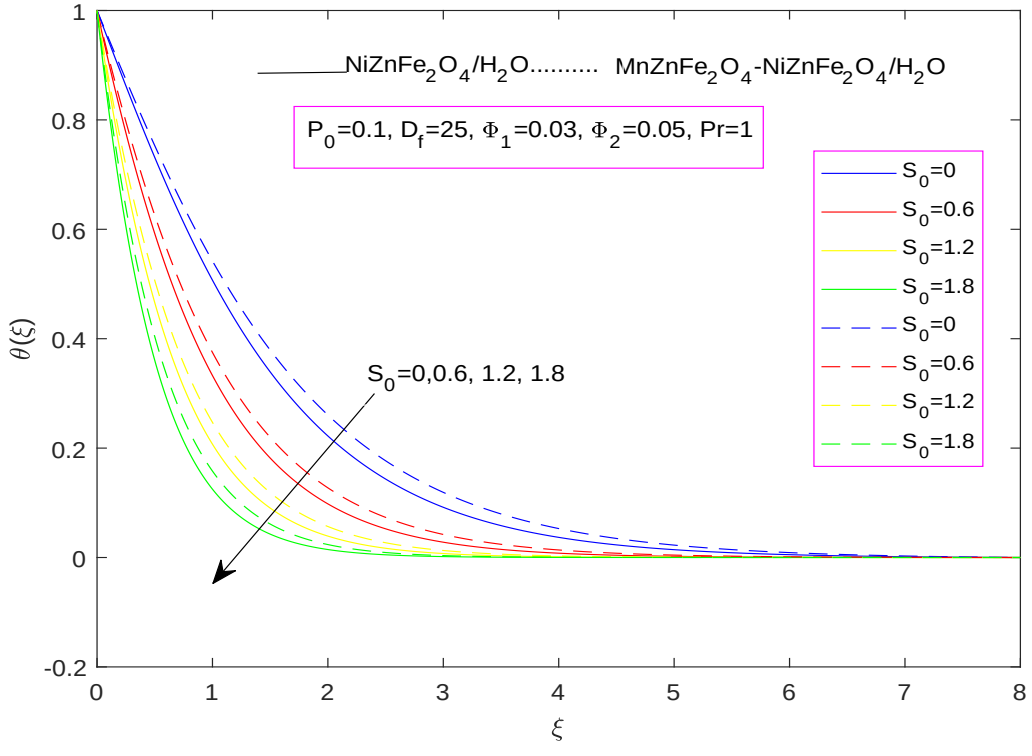

FIGURE 3.7: Impact of S_0 on $\theta(\xi)$

The outcomes in Figure 3.8 show that the volume fraction Φ_1 of $MnZnFe_2O_4$ in the hybrid nanofluid and temperature have a positive correlation. This means that the enhancing values of Φ_1 causes an increase in the temperature profile $\theta(\xi)$. This relationship can be explained by the higher volume fraction's elevated thermal conductivity.

Thus, the temperature within the nanofluid rises as a result of the enhanced thermal conductivity. The temperature variations of the fluid (for both nanofluid and hybrid nanofluids) with various values of Pr, are shown in Figure 3.9. The fluid temperature is observed to decline as Pr increases, which is consistent with a decrease in the thermal diffusivity as Pr grows.

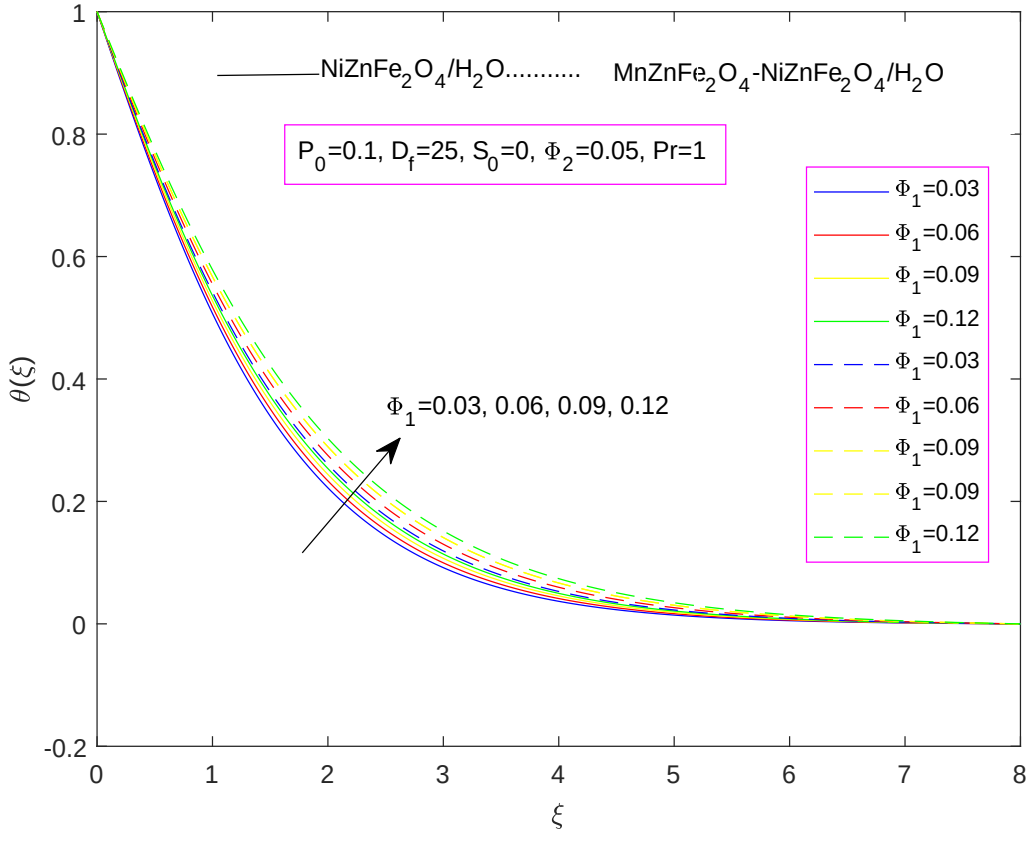

FIGURE 3.8: Impact of Φ_1 on $\theta(\xi)$

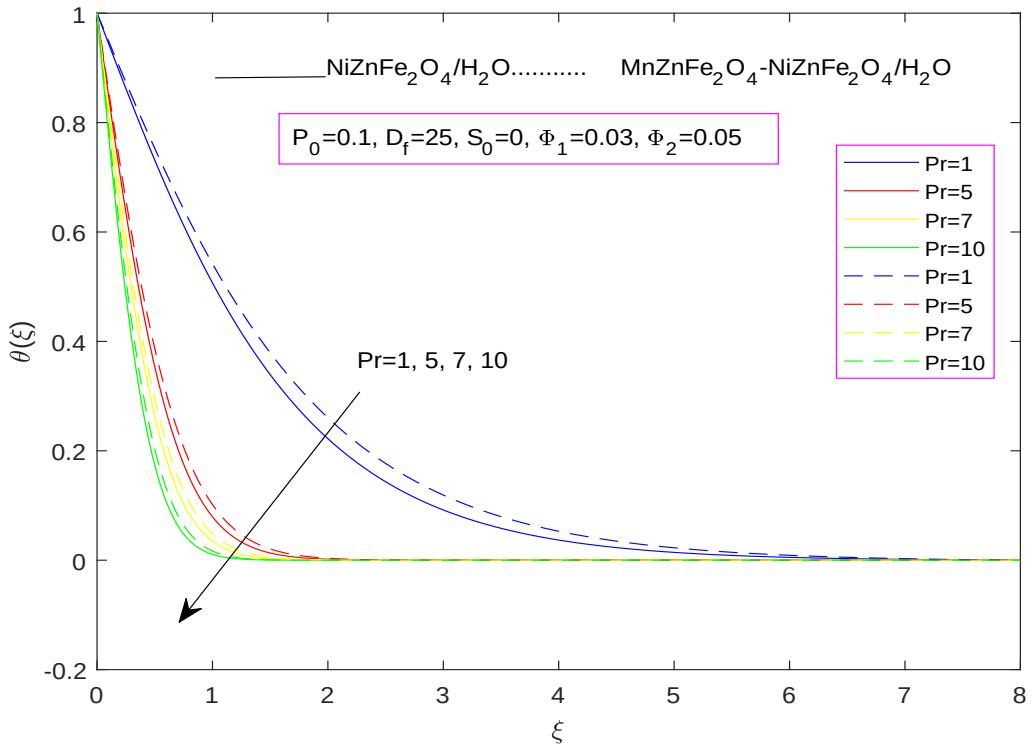

FIGURE 3.9: Impact of Pr on $\theta(\xi)$

3.6.4 Concentration Profile

The concentration of nanoparticles in a fluid significantly influences the fluid's properties and applications. Figure 3.10 discloses the effect of the local porosity parameter P_0 on $\phi(\xi)$. As the porosity parameter P_0 increases, the fluid's flow rate decreases, resulting in the accumulation of nanoparticles and, consequently, an elevated concentration of nanoparticles. An illustration of increase in the concentration profile $\phi(\xi)$ is depicted in Figure 3.11. By increasing the Darcian parameter D_f, the concentration profile $\phi(\xi)$ increases. From Figure 3.12, it is evident that $\phi(\xi)$ is dimmed as the suction parameter S_0 is enhanced. Figure 3.13 expose that $\phi(\xi)$ falls for a positive variation in Φ_1. Figure3.14 illustrates the physical impacts of σ. A decrease in the concentration is associated with a decline in the rate of a chemical reaction, indicating a diminishing level of reaction activity. So, as the chemical rate σ is increased, the concentration profile $\phi(\xi)$ is decreased. Figure

3.15 displays the effect of the Schmidt number S_c on $\phi(\xi)$ and the associated thinning of the concentration layer thickness is also observed. It is relevant to mention that S_c characterizes the ratio of momentum diffusivity (kinematic viscosity) to the mass diffusivity in a fluid. When S_c increases, it implies that the mass diffusivity is relatively lower as compared to the momentum diffusivity. As the mass diffusivity decreases with higher S_c values, the diffusion of the substance becomes less efficient. Consequently, the concentration profiles $\phi(\xi)$ exhibits a decrease.

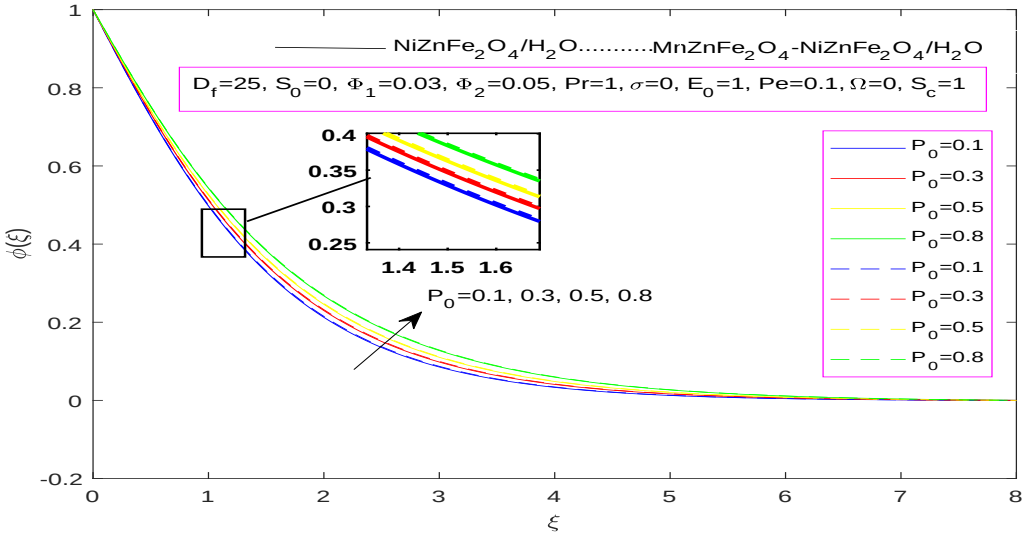

FIGURE 3.10: Impact of P_0 on $\phi(\xi)$

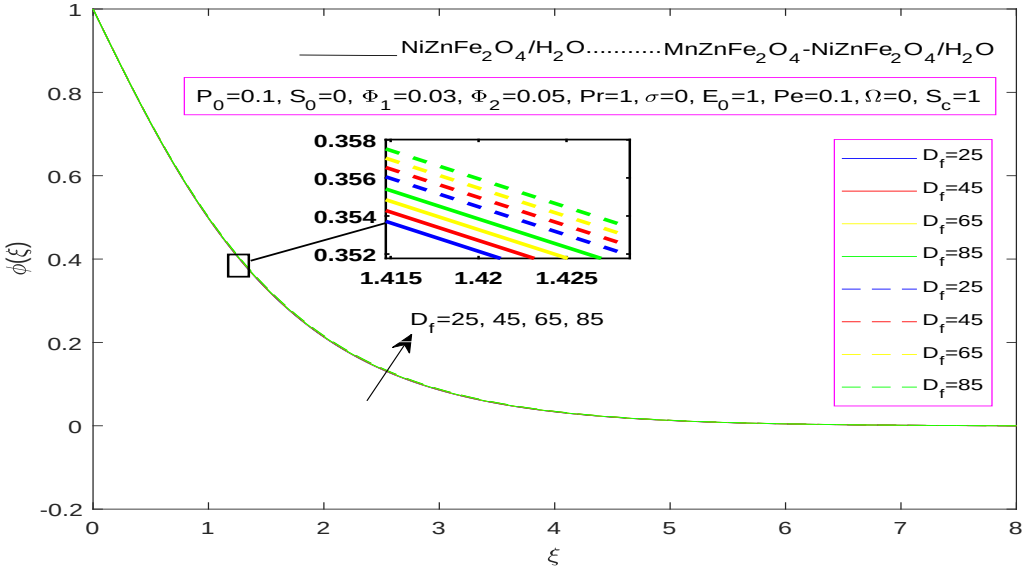

FIGURE 3.11: Impact of D_f on $\phi(\xi)$

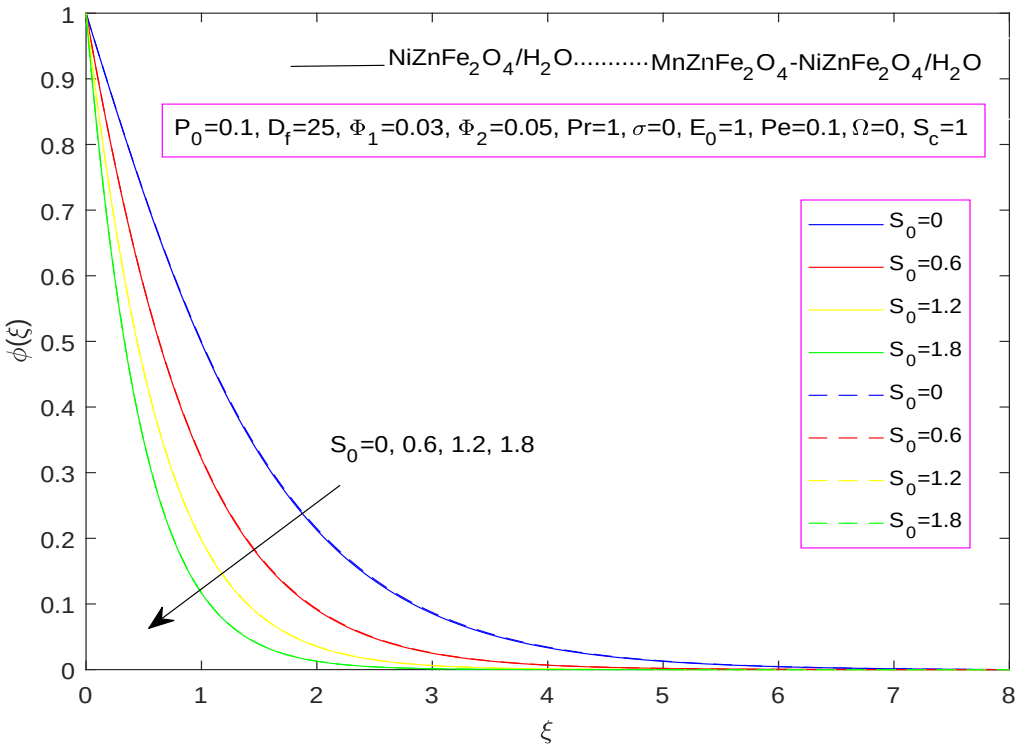

FIGURE 3.12: Impact of S_0 on $\phi(\xi)$

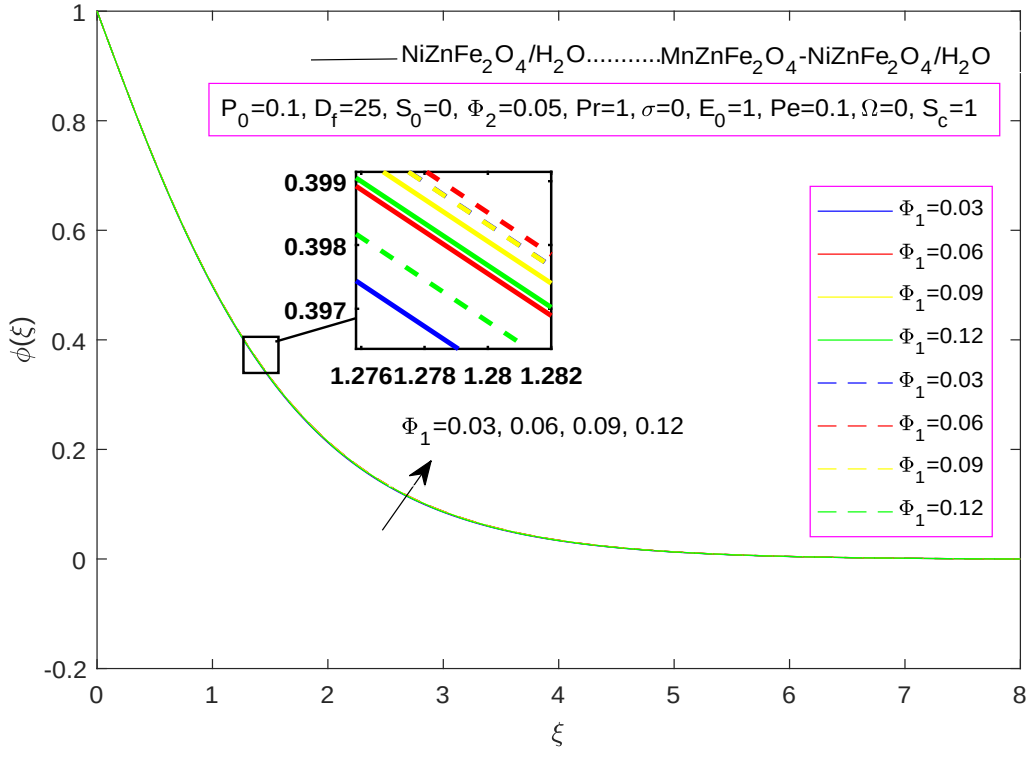

FIGURE 3.13: Impact of Φ_1 on $\phi(\xi)$

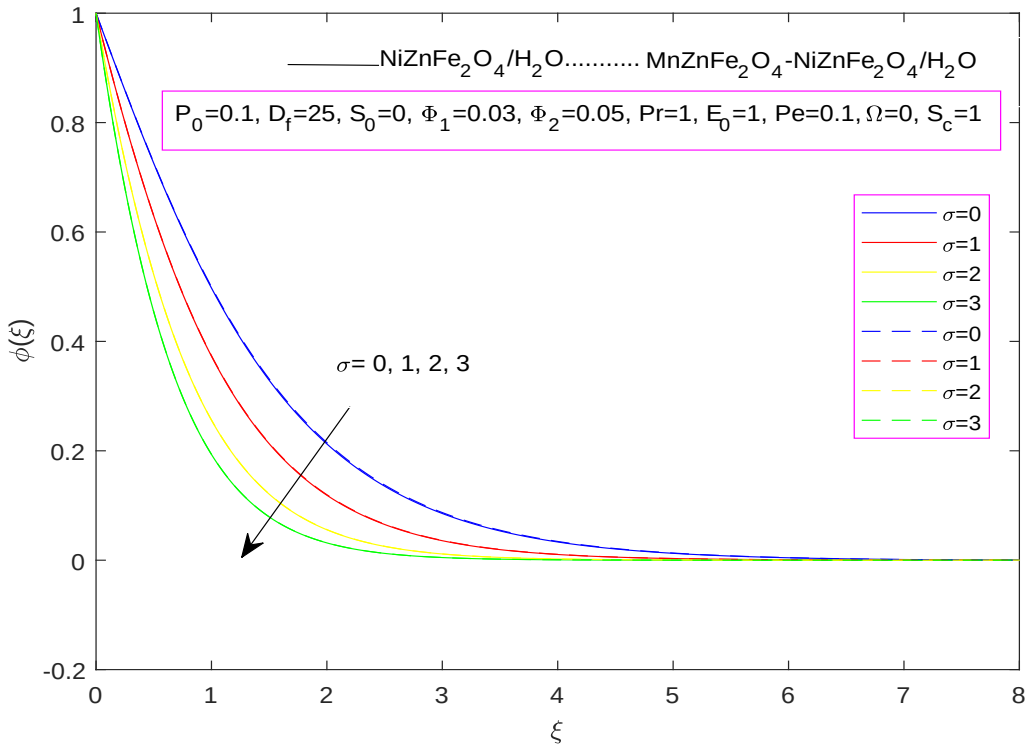

FIGURE 3.14: Impact of σ on $\phi(\xi)$

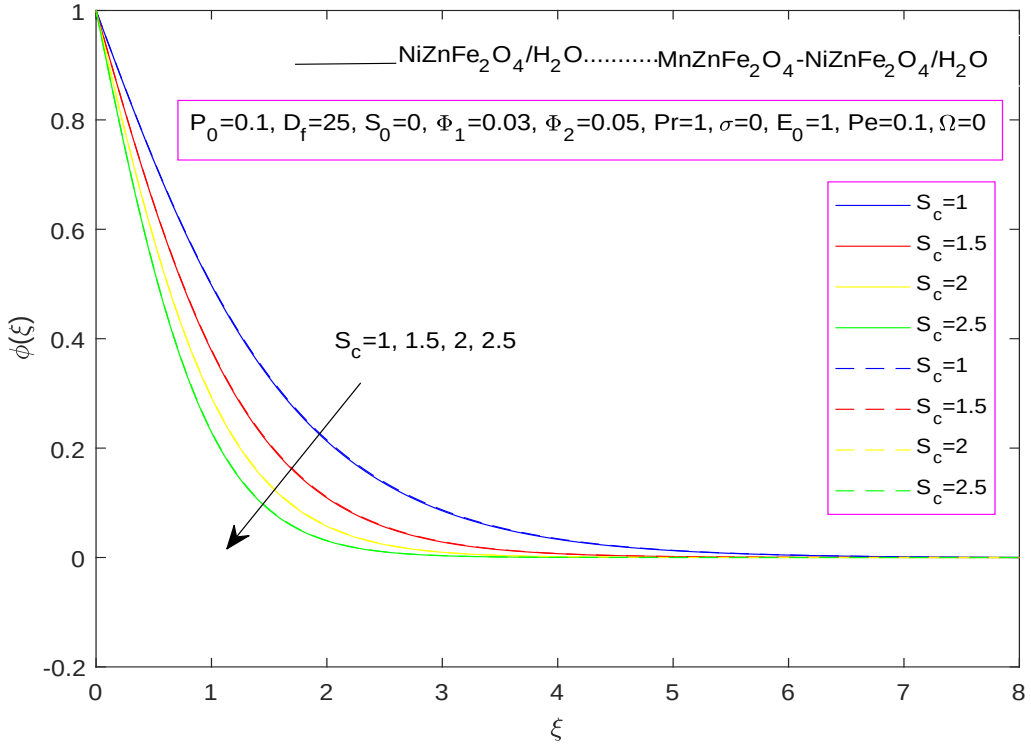

FIGURE 3.15: Impact of S_c on $\phi(\xi)$

3.6.5 Motile Profile

Figure 3.16 is sketched with the observation that the density of micro-organisms $G(\xi)$ is enhanced with a positive variation in P_0. Figure 3.17 makes it evident that the motile profile $G(\xi)$ increases significantly with a positive change in the Darcian parameter D_f. A decreasing trend of density of the motile micro-organism $G(\xi)$ with the larger values of the suction parameter S_0 is disclosed in Figure 3.18.

The relationship between σ and $G(\xi)$ is illustrated in Figure 3.19. Elevated values of σ trigger a detrimental chemical reaction that diminishes the concentration gradient, consequently reducing the density of motile $G(\xi)$. This occurs because liquid species are able to dissolve more effectively under these conditions. The impact of the Peclet number Pe on $G(\xi)$ is clearly illustrated in Figure 3.20.

The Peclet number Pe holds great significance in the study of microorganism swimming in a fluid. It elucidates the movement of substances within the fluid. An increase in Peclet Pe number enhances the speed of fluid particles, but concurrently, the diffusivity of microbes decreases with rising Peclet levels. Consequently, there is a reduction in the distribution of micro-rotations. Hence, the behavior of $G(\xi)$ exhibits a noticeable decline. From Figure 3.21, it is evident that higher values of Ω correspond to a decreasing trend in $G(\xi)$. The surface concentration diminishes with an increase in Ω. Consequently, particle strength weakens, leading to a reduction in mass and contributing to the degradation of motile profile $G(\xi)$.

Figure 3.22 illustrates the impact of the bioconvection Schmidt number S_c on the density of motile microorganisms. The figure distinctly shows that the density of motile microorganisms $G(\xi)$ follows a decreasing trend with the bioconvection Schmidt number S_c. Increasing values of S_c generally indicate a decrease in the microorganism diffusion, leading to a reduction in both the density of motile microorganisms and the thickness of the thermal boundary layer.

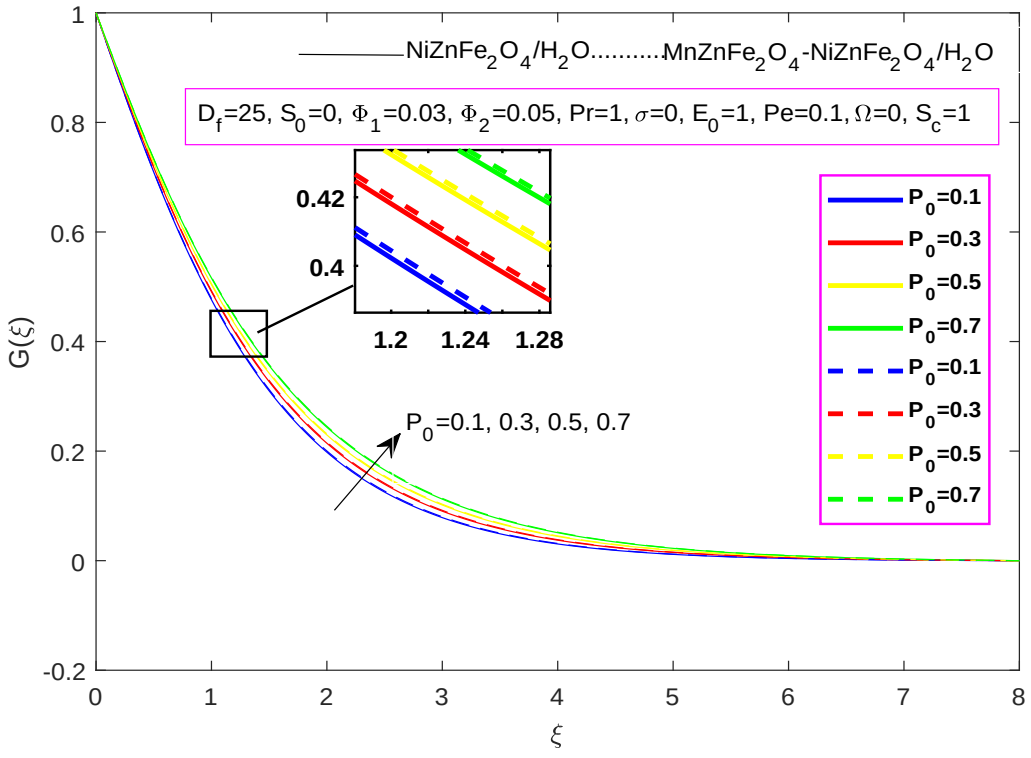

FIGURE 3.16: Impact of P_0 on $G(\xi)$

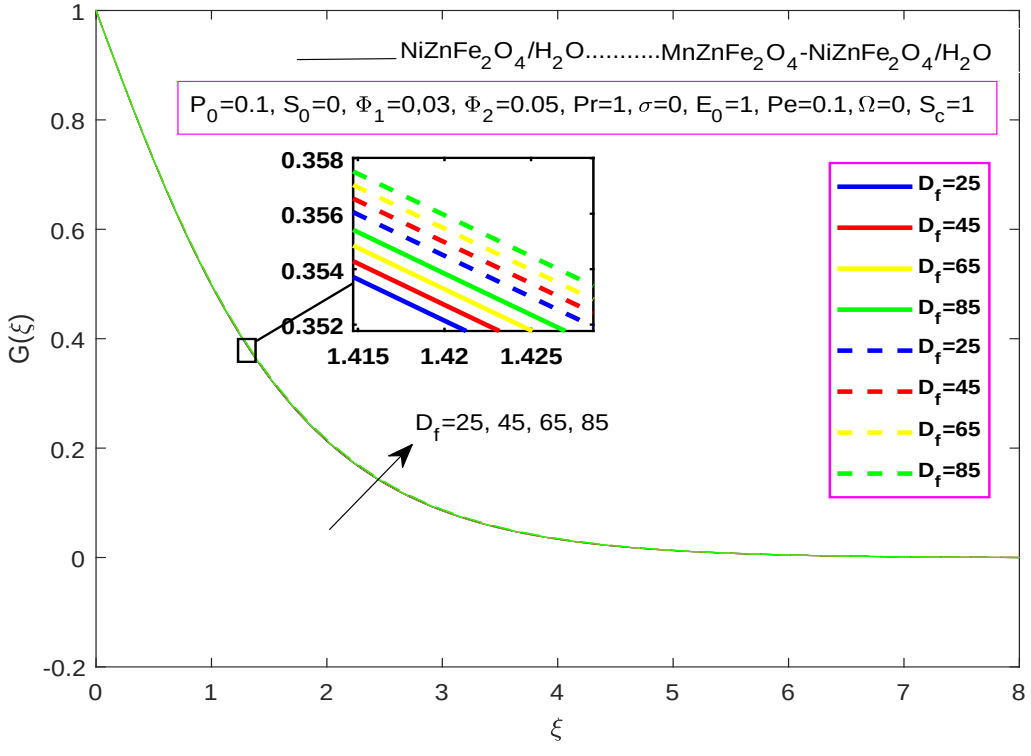

FIGURE 3.17: Impact of D_f on $G(\xi)$

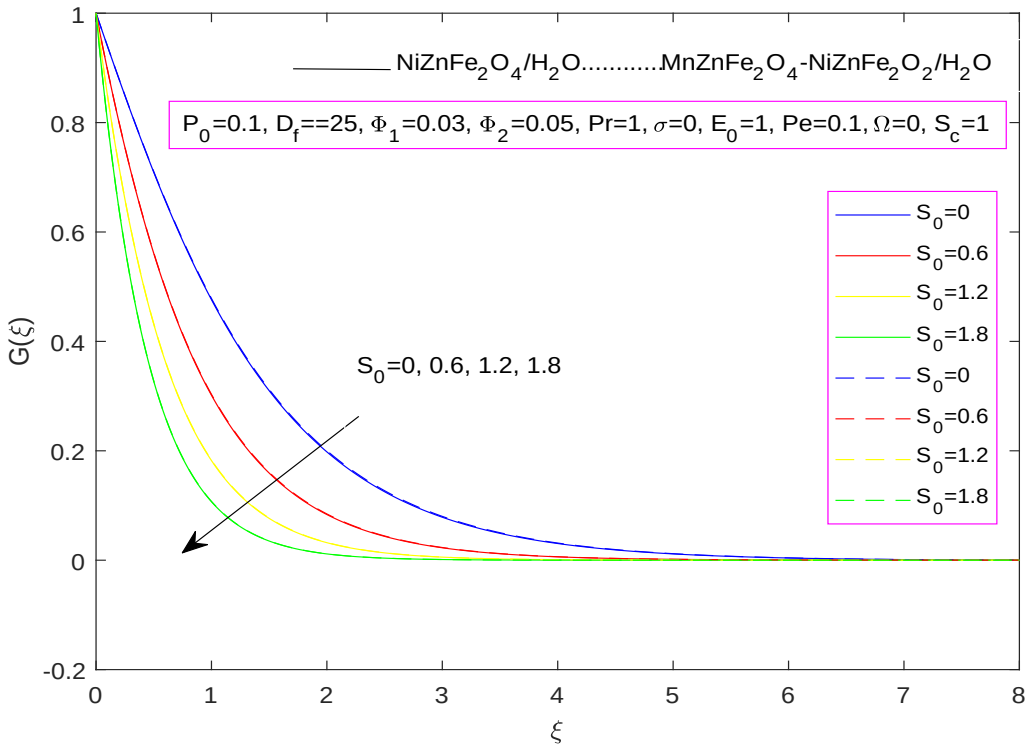

FIGURE 3.18: Impact of S_0 on $G(\xi)$

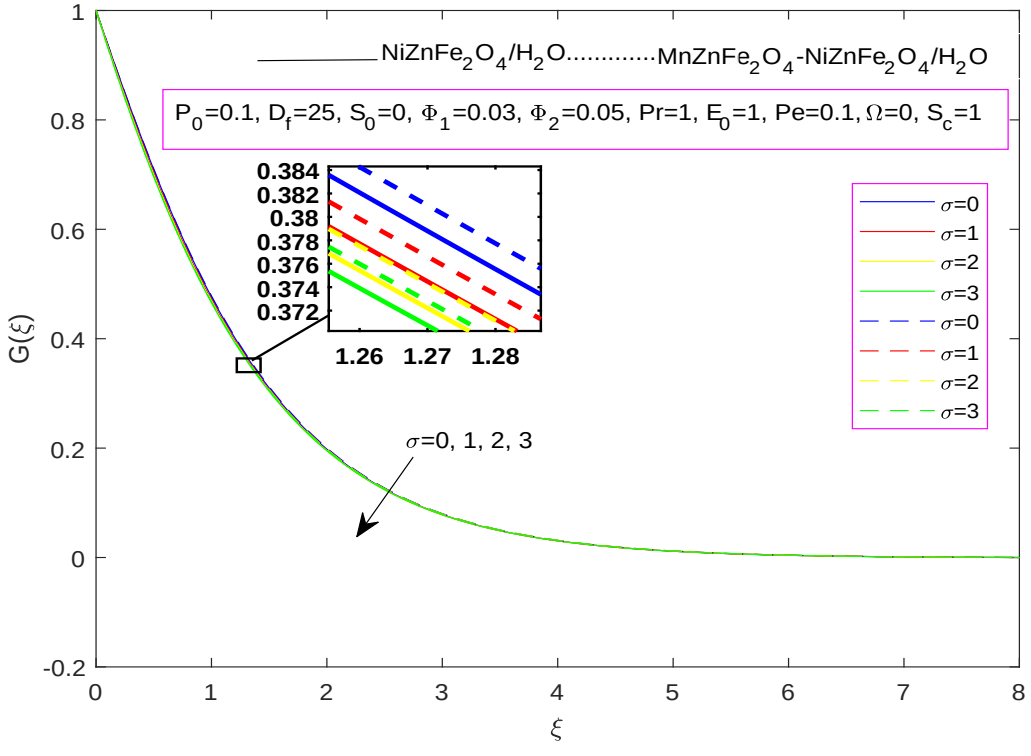

FIGURE 3.19: Impact of σ on $G(\xi)$

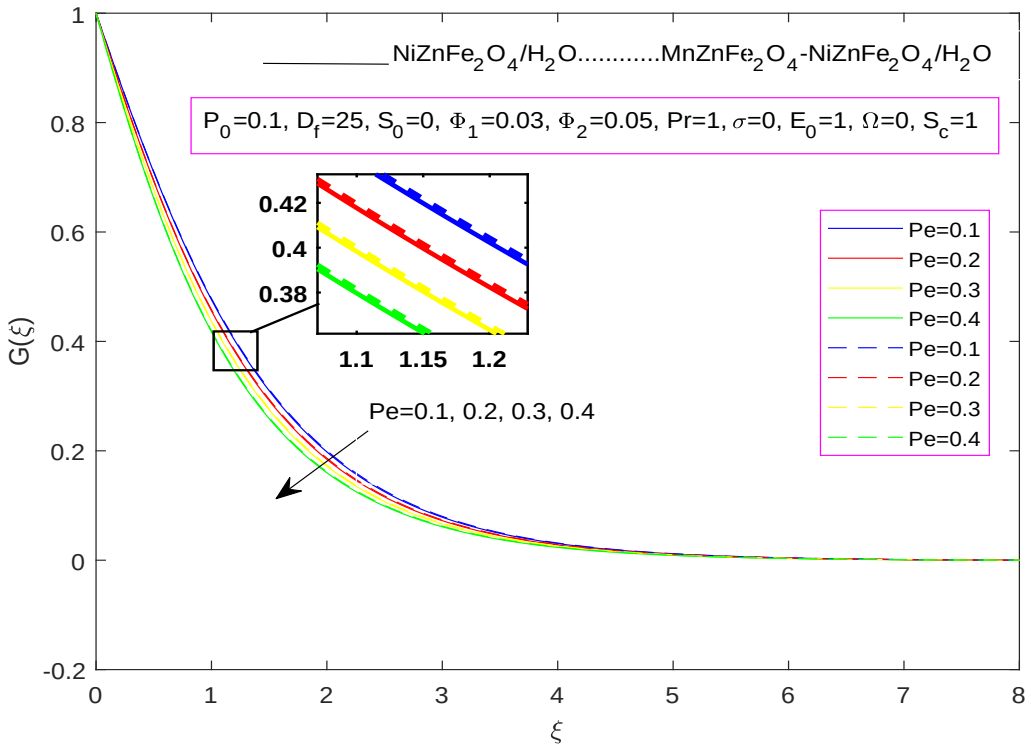

FIGURE 3.20: Impact of Pe on $G(\xi)$

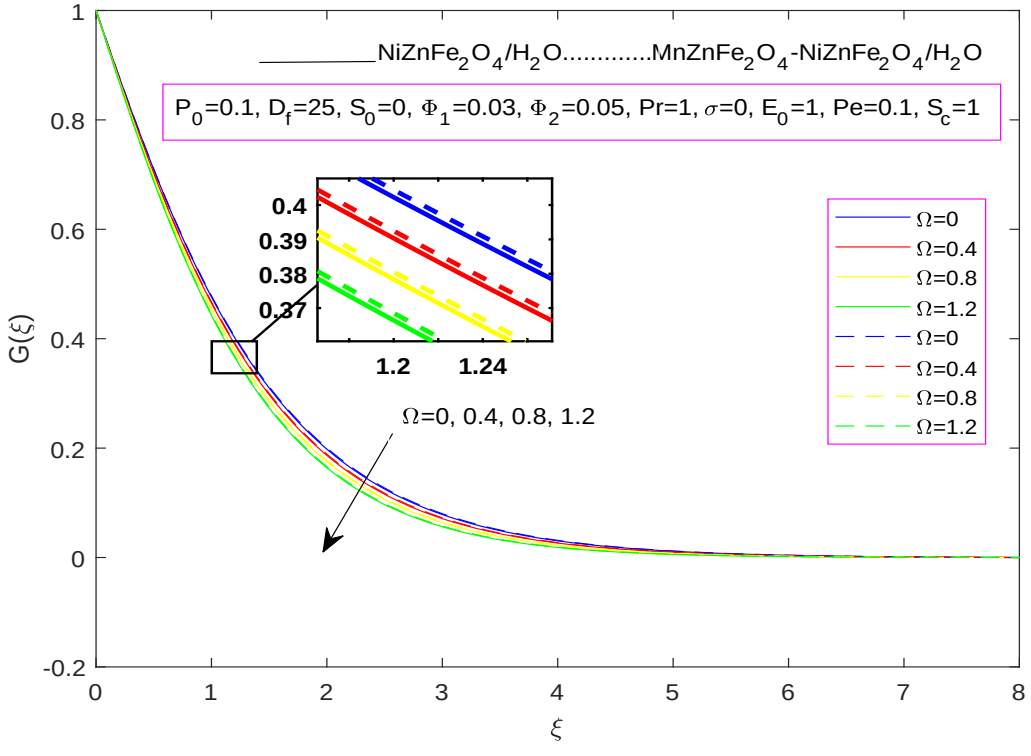

FIGURE 3.21: Impact of Ω on $G(\xi)$

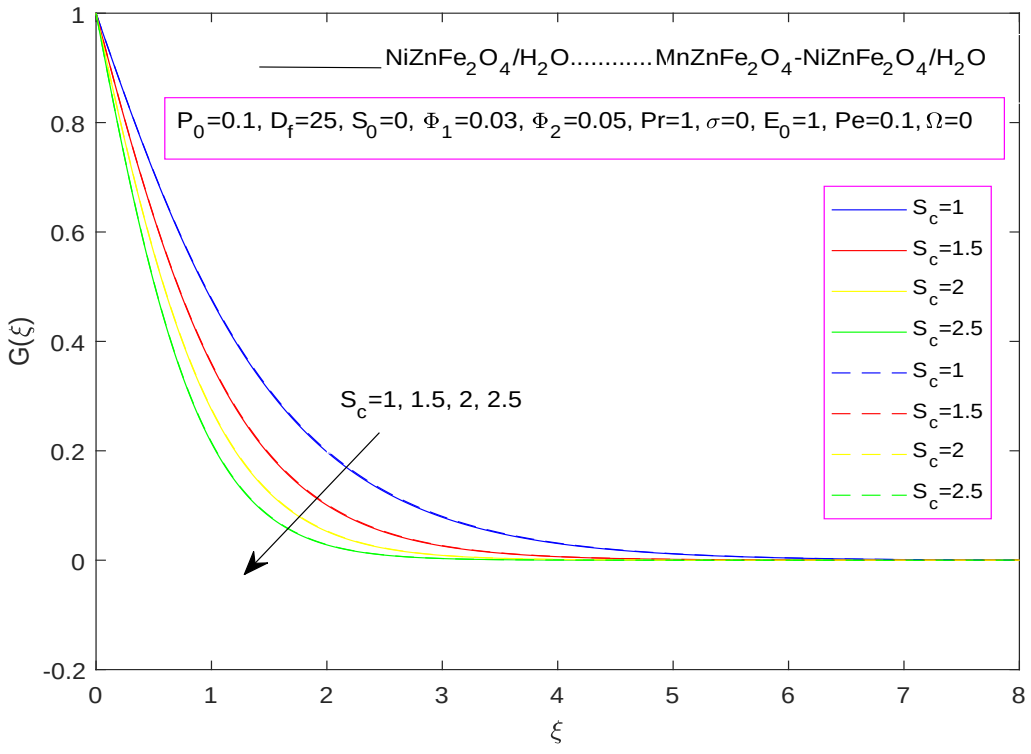

FIGURE 3.22: Impact of S_c on $G(\xi)$

Chapter 4

Flow Analysis of Hybrid Casson Nanofluid Containing Motile Micro-Organisms Subjected to Cattaneo-Christov Double Diffusion

4.1 Introduction

The model analyzed in Chapter 3, has been given a new direction by introducing the engine oil based hybrid nanofluid ($TiO_2 + Ag$) and by incorporating the impacts of Casson and magnetic field, in the momentum equation. In addition, magnetic field, thermal radiation and Cattaneo-Christov heat flux, in the energy equation has been incorporated. Furthermore, the Cattaneo-Christov mass flux, has been incorporated in the concentration equation. These various effects enables us to investigate how their combined influence affects the flow of fluid over a stretching sheet. By conducting numerical simulations and analysis, we delve into

the intricate interplay of these effects, scrutinizing their collective impact on the overall behavior of the flow.

4.2 Mathematical Modeling

A two dimensional $(2D)$ flow of a hybrid nanoliquid $(TiO_2 + Ag)/EO$ along a sheet with stretching velocity $U_w = cx$, $(c > 0)$ through a porous medium has been taken into account. Motile microbes are engaged in the flow, and their motion is caused by the bioconvection phenomenon. The fluid flow is subjected to a perpendicularly applied magnetic field of uniform strength. In addition, radiative flux, chemical processes and heat source/sink are considered.

The mathematical form of the flow model, based on the relevant conservation

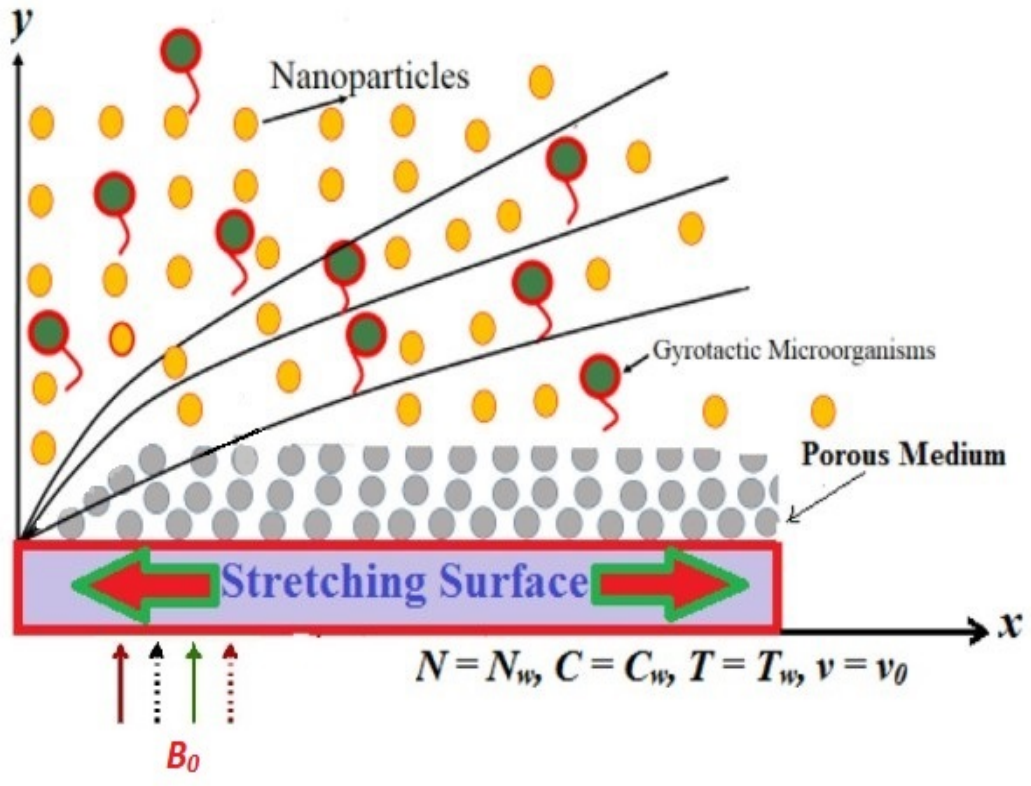

FIGURE 4.1: Geometry of the problem.

principles, has been presented in the form of the following partial differential equations [46, 47]:

Mass conservation equation:

$$\frac{\partial u}{\partial x}+\frac{\partial v}{\partial y}=0. \tag{4.1}$$

Momentum equation:

$$u\frac{\partial u}{\partial x}+v\frac{\partial u}{\partial y}=\frac{\mu_{hnf}}{\rho_{hnf}}\left(\frac{\beta+1}{\beta}\right)\frac{\partial^2 u}{\partial y^2}-\frac{\mu_{hnf}}{\rho_{hnf}k^*}u-\frac{C_b}{\rho_{hnf}\sqrt{(k^*)}}u^2\frac{\sigma_{hnf}}{\rho_{hnf}}B_0^2u. \tag{4.2}$$

Energy equation:

$$\begin{aligned}u\frac{\partial T}{\partial x}+v\frac{\partial T}{\partial y}=\frac{\kappa_{hnf}}{(\rho C_p)_{hnf}}\left(\frac{\partial^2 T}{\partial y^2}\right)-\lambda\Bigg(u\frac{\partial u}{\partial x}\frac{\partial T}{\partial x}+v\frac{\partial v}{\partial y}\frac{\partial T}{\partial y}+u\frac{\partial v}{\partial x}\frac{\partial T}{\partial y}+v\frac{\partial u}{\partial y}\frac{\partial T}{\partial x}\\+u^2\frac{\partial^2 T}{\partial x^2}+v^2\frac{\partial^2 T}{\partial y^2}+2uv\frac{\partial^2 T}{\partial x\partial y}\Bigg)+\frac{\sigma_{hnf}}{(C_p)_{hnf}\rho_{hnf}}B_0^2u^2-\frac{1}{(\rho C_p)_{hnf}}\left(\frac{\partial q_r}{\partial y}\right).\end{aligned} \tag{4.3}$$

Concentration equation:

$$\begin{aligned}u\frac{\partial C}{\partial x}+v\frac{\partial C}{\partial y}=D_B\frac{\partial^2 C}{\partial y^2}-K_r^2(C-C_\infty)\left(\frac{T}{T_\infty}\right)^{m_1}exp\left(\frac{-E^*}{k^*T}\right)-\alpha\Bigg(u\frac{\partial u}{\partial x}\frac{\partial C}{\partial x}\\+v\frac{\partial v}{\partial y}\frac{\partial C}{\partial y}+u\frac{\partial v}{\partial x}\frac{\partial C}{\partial y}+v\frac{\partial u}{\partial y}\frac{\partial C}{\partial x}+u^2\frac{\partial^2 C}{\partial x^2}+v^2\frac{\partial^2 C}{\partial y^2}+2uv\frac{\partial^2 C}{\partial x\partial y}\Bigg)\end{aligned} \tag{4.4}$$

Motile equation:

$$v\frac{\partial N}{\partial x}+u\frac{\partial N}{\partial y}+\frac{1}{(C_w-C_\infty)}\frac{\partial(N\frac{\partial C}{\partial y})}{\partial y}bW_c=D_n\frac{\partial^2 N}{\partial y^2}. \tag{4.5}$$

Boundary Conditions:

The following boundary conditions (BCs) have been assumed to physically analyze and numerically compute the solution of the above equations [46]:

$$\left.\begin{aligned}y=0:\ u(x,0)=U_w+\left(\frac{\beta+1}{\beta}\right)W_1\mu_{hnf}(B)\frac{\partial u}{\partial y},\ v(x,0)=-v_0,\\\frac{\partial T}{\partial y}=-\frac{h}{k_f}(T_w-T),\ C(x,0)=C_w,\ N(x,0)=N_w.\\y\to\infty:\ u\to 0,\ T\to T_\infty,\ C\to C_\infty,\ N\to N_\infty.\end{aligned}\right\} \tag{4.6}$$

Here u and v are horizontal and vertical velocities respectively. Also μ_{hnf} is viscosity.

4.2.1 Thermo-physical Properties

The valueable thermo-physical properties of NF and HNF are shown in Table 4.1

TABLE 4.1: Thermo-physical properties of nano-sized particles and base fluid.

Properties	TiO_2	Ag	Engine Oil
Density, $\rho(\frac{kg}{m^3})$	4250	10500	884
Specific heat, $C_p(\frac{J}{kgK})$	686.2	235	1910
Thermal conductivity, $k(\frac{W}{mK})$	8.9838	429	0.144
Electric conductivity, σ $(\frac{\Omega}{m})$	2.4×10^6	6.3×10^7	1×10^{-7}

The formulation of different thermo-physical properties for both nanofluid and hybrid nanofluid are tabulated in Table 3.1.

4.2.2 Similarity Transformations

Consider the following similarity transformation to reduce the governing system to ordinary differential equations (ODEs):

$$\left.\begin{aligned} &\xi(x,y) = \sqrt{\frac{c}{\nu_f}}y, \quad \psi(x,y) = \sqrt{\nu_f c}xf(\xi), \quad \theta(\xi) = \frac{T-T_\infty}{T_w-T_\infty}, \\ &G(\xi) = \frac{N-N_\infty}{N_w-N_\infty}, \quad \phi_(\xi) = \frac{C-C_\infty}{C_w-C_\infty}. \end{aligned}\right\} \tag{4.7}$$

The symbol ξ represents the similarity variable. The velocity components in the x and y directions are denoted by u and v, respectively, while $f'(\xi)$, $\theta(\xi)$, $\phi(\xi)$ and $G(\xi)$ stand for the dimensionless momentum,temperature, concentration and motile profiles. Different parameters used in the upcoming ODEs and their BCs, have been listed in Table 4.2.

TABLE 4.2: Different dimensionless parameters of the governing model.

Symbols	**Name**	**Appearance**
M	Magnetic parameter	$M = \frac{\sigma_f}{c\rho_f} B_0^2$
Nr	Radiation parameter	$Nr = \frac{16\sigma^* T_\infty^3}{3k^* \nu_f (\rho C_p)_f}$
E_c	Eckert number	$E_c = \frac{c^2 x^2}{(C_p)_f (T_w - T_\infty)}$
η	Time relaxation parameter	$\eta = \lambda_T c = \lambda_C c$
Λ	Velocity slip parameter	$\Lambda = W_0 \sqrt{\frac{c}{\nu_f}} \mu_f$
Bi	Biot number	$Bi = \frac{h_f}{K_f} \sqrt{\frac{\nu_f}{c}} (T_w - T_\infty)$

Continuity equation (4.1) is satisfied identically, whereas (4.2)-(4.6) are transformed into the dimensionless form presented below.

4.2.3 Dimensionless Form of Momentum Equation

In this section, the governing momentum equation (4.2) to get the non-dimensional form: For this, we use the equations (3.11)-(3.13), (3.15) and (3.16) into the equation (4.2), we get the following form:

$$\begin{aligned}
&\big(cxf'(\xi)\big)\big(cf'(\xi)\big) - \big(\sqrt{c\nu_f} f(\xi)\big)\left(\frac{c^{3/2}x}{\sqrt{\nu_f}} f''(\xi)\right) = \frac{\mu_{hnf}(B)}{\rho_{hnf}}\left(\frac{\beta+1}{\beta}\right)\frac{c^2 x}{\nu_f} f'''(\xi) \\
&\quad - \frac{\mu_{hnf}}{\rho_{hnf} k^*}\big(cxf'(\xi)\big) - \frac{C_b}{\rho_{hnf}\sqrt{k^*}}\big(c^2 x^2 f'^2(\xi)\big) - \frac{\sigma_{hnf}}{\rho_{hnf}} B_0^2 cxf'(\xi).
\end{aligned}$$

$$\begin{aligned}
\Rightarrow \quad & c^2 x f'^2(\xi) - c^2 x f(\xi) f''(\xi) = \frac{\mu_{hnf}(B)}{\rho_{hnf}}\left(\frac{\beta+1}{\beta}\right)\frac{c^2 x}{\nu_f} f'''(\xi) - \frac{\mu_{hnf}}{\rho_{hnf} k^*}\big(cxf'(\xi)\big) \\
& - \frac{C_b}{\rho_{hnf}\sqrt{k^*}}\big(c^2 x^2 f'^2(\xi)\big) - \frac{\sigma_{hnf}}{\rho_{hnf}} B_0^2 cxf'(\xi).
\end{aligned}$$

$$\Rightarrow \quad c^2 x\big(f'^2 - ff''\big) = c^2 x\left(\frac{\mu_{hnf}(B)}{\rho_{hnf}\nu_f}\frac{\beta+1}{\beta} f''' - \frac{\mu_{hnf}}{\rho_{hnf} k^* c} f' - \frac{1}{\rho_{hnf}} D_f f'^2 - \frac{\sigma_{hnf}}{\rho_{hnf}} B_0^2 \frac{f'}{c}\right).$$

$$\Rightarrow \quad f'^2 - ff'' = \frac{\mu_{hnf}(B)}{\rho_{hnf}\nu_f}\left(\frac{\beta+1}{\beta}\right) f''' - \frac{\mu_{hnf}}{\rho_{hnf} k^* c} f' - \frac{1}{\rho_{hnf}} D_f f'^2 - \frac{\sigma_{hnf}}{\rho_{hnf}} B_0^2 \frac{f'}{c}.$$

$$\Rightarrow \quad \frac{\mu_{hnf}(B)}{\rho_{hnf}\nu_f}\left(\frac{\beta+1}{\beta}\right)f''' = f'^2 - ff'' + \frac{\mu_{hnf}}{\rho_{hnf}k^*c}f' + \frac{1}{\rho_{hnf}}D_f f'^2 + \frac{\sigma_{hnf}}{\rho_{hnf}}B_0^2\frac{f'}{c}.$$

$$\Rightarrow \quad \left(\frac{\beta+1}{\beta}\right)f''' = \nu_f\frac{\rho_{hnf}}{\mu_{hnf}(B)}\left(f'^2 - ff''\right) + \frac{\nu_f}{k^*c}f' + \frac{\nu_f}{\mu_{hnf}(B)}D_f f'^2 + \nu_f\frac{\sigma_{hnf}}{\rho_{hnf}}B_0^2\frac{f'}{c}.$$

$$\Rightarrow \quad \left(\frac{\beta+1}{\beta}\right)f''' = \Delta_1(f'^2 - ff'') + P_0 f' + \Delta_4 D_f f'^2 + \frac{P_a}{\rho_f}\sigma_{hnf}B_0^2\frac{f'}{c}.$$

Finally, the dimensionless form of the momemtum equation gets the form:

$$\left(\frac{\beta+1}{\beta}\right)f''' = \Delta_1(f'^2 - ff'') + P_0 f' + \Delta_4 D_f f'^2 + \Delta_5 PaMf'.$$

$$\Rightarrow \quad f''' = \left(\frac{\beta}{\beta+1}\right)\left(\Delta_1(f'^2 - ff'') + P_0 f' + \Delta_4 D_f f'^2 + \Delta_5 P_a M f'\right).$$

$$\Rightarrow \quad f''' = \left(\frac{\beta}{\beta+1}\right)\left(\Delta_1(f'^2 - ff'') + \Delta_4 D_f f'^2 + \left(P_0 + \Delta_5 PaM\right)f'\right). \tag{4.8}$$

4.2.4 Dimensionless Form of Energy Equation

In this section, the non-dimensionalization process for the energy equation (4.3) has been discussed. For this, the following derivatives are also required:

$$\frac{\partial^2 T}{\partial x \partial y} = 0. \qquad \text{(using(3.18))} \tag{4.9}$$

The radiation heat flux q_r can be expressed as:

$$q_r = -\frac{4}{3}\frac{\sigma*}{k*}\frac{\partial T^4}{\partial y}. \tag{4.10}$$

The Stefan-Boltzman constant is denoted by σ^* , and the absorption coefficient is represented by k^*. The Taylor series expansion can be taken in account to express T^4 about T_∞ as follows:

$$T^4 = T_\infty^4 + 4T_\infty^3(T - T_\infty) + 6T_\infty^2(T - T_\infty)^2 + ...$$

By neglecting the higher terms, we get

$$\begin{aligned} & T^4 = T_\infty^4 + 4T_\infty^3(T - T_\infty). \\ \Rightarrow \quad & T^4 = 4T_\infty^3 T - 3T_\infty^4. \\ \Rightarrow \quad & \frac{\partial T^4}{\partial y} = 4T_\infty^3 \frac{\partial T}{\partial y}. \end{aligned}$$

So, equation (4.10) becomes:

$$\begin{aligned} & q_r = -\frac{4}{3}\frac{\sigma*}{k*}(4T_\infty^3)\frac{\partial T}{\partial y}. \\ \Rightarrow \quad & \frac{\partial q_r}{\partial y} = -\frac{16}{3}\frac{\sigma*}{k*}T_\infty^3\frac{\partial^2 T}{\partial y^2}. \\ \Rightarrow \quad & \frac{\partial q_r}{\partial y} = -\frac{16}{3}\frac{\sigma*}{k*}T_\infty^3(T_w - T_\infty)\left(\frac{c}{\nu_f}\right)\theta''. \end{aligned} \tag{4.11}$$

The dimensionless form of (4.3) can be obtained by using equations (3.11)- (3.19), (4.9) and (4.11) as follows:

$$\begin{aligned} & cxf'(0) - \sqrt{c\nu_f}f(T_w - T_\infty)\sqrt{\frac{c}{\nu_f}}\theta' = \frac{\kappa_{hnf}}{(\rho C_p)_{hnf}}(T_w - T_\infty)\left(\frac{c}{\nu_f}\right)\theta'' - \lambda\Big(c^2xf'^2(0) \\ & + c^{3/2}\sqrt{\nu}_f ff'(T_w - T_\infty)(\frac{c}{\nu_f})\theta''(T_w - T_\infty)\sqrt{\frac{c}{\nu_f}}\theta' + (0)(T_w - T_\infty)\sqrt{\frac{c}{\nu_f}}\theta' \\ & - c^2xff''(0) + c^2x^2f'^2(0) + c\nu_f f^2(T_w - T_\infty)(\frac{c}{\nu_f})\theta'' - 2c^{3/2}\sqrt{\nu}_f xff'\Big) \\ & + \frac{\sigma_{hnf}}{(C_p)_{hnf}\rho_{hnf}}B_0^2c^2x^2f'^2 - \frac{1}{(\rho C_p)_{hnf}}\left(\frac{\partial q_r}{\partial y}\right). \end{aligned}$$

$$\Rightarrow \quad -c(T_w - T_\infty)f\theta' = \frac{\kappa_{hnf}}{(\rho C_p)_{hnf}}(T_w - T_\infty)\left(\frac{c}{\nu_f}\right)\theta'' - \lambda\big(c^2ff'(T_w - T_\infty)\theta' + c^2f^2.$$

$$\begin{aligned} \Rightarrow \quad & (T_w - T_\infty)\theta''\big) + \frac{\sigma_{hnf}}{(C_p)_{hnf}\rho_{hnf}}B_0^2c^2x^2f'^2 - \frac{1}{(\rho C_p)_{hnf}}\left(\frac{\partial q_r}{\partial y}\right). \\ & -c(T_w - T_\infty)f\theta' = \frac{\kappa_{hnf}}{(\rho C_p)_{hnf}}(T_w - T_\infty)(\frac{c}{\nu_f})\theta'' - \lambda\big(c^2ff'(T_w - T_\infty)\theta' \\ & \qquad + c^2f^2(T_w - T_\infty)\theta''\big) \\ & \qquad + \frac{1}{(\rho C_p)_{hnf}}\left(\frac{16}{3}\frac{\sigma*}{k*}(T_\infty^3)(T_w - T_\infty)(\frac{c}{\nu_f})\theta''\right). \end{aligned}$$

$$-c(T_w-T_\infty)f\theta' = \frac{\Delta_2}{\Delta_3}\frac{1}{Pr}(T_w-T_\infty)\frac{c}{\nu_f}\theta'' - \lambda c^2(T_w-T_\infty)\big(ff'\theta' + f^2\theta''\big) + \frac{\sigma_{hnf}}{(C_p)_{hnf}\rho_{hnf}}B_0^2c^2x^2f'^2 + \frac{1}{(\rho C_p)_{hnf}}\left(\frac{16}{3}\frac{\sigma*}{k*}(T_\infty^3)(T_w-T_\infty)\frac{c}{\nu_f}\theta''\right).$$

$$\Rightarrow \quad -f\theta' = \frac{\Delta_2}{\Delta_3}\frac{1}{Pr}\theta'' - \lambda c\big(ff'\theta' + f^2\theta''\big) + \frac{\sigma_{hnf}}{(T_w-T_\infty)(C_p)_{hnf}\rho_{hnf}}B_0^2cx^2f'^2 + \frac{1}{(\rho C_p)_{hnf}}\left(\frac{16}{3}\frac{\sigma*}{k*}T_\infty^3\frac{1}{\nu_f}\theta''\right).$$

$$\Rightarrow \quad -f\theta' = \frac{\Delta_2}{\Delta_3}\frac{1}{Pr}\theta'' - \eta\big(ff'\theta' + f^2\theta''\big) + \frac{\sigma_{hnf}}{(T_w-T_\infty)(C_p)_{hnf}\rho_{hnf}}B_0^2cx^2f'^2 + \left(\frac{16}{3}\frac{\sigma*}{k*}T_\infty^3\left(\frac{1}{\nu_f(\rho C_p)_f\Delta_3}\right)\theta''\right).$$

$$\Rightarrow \quad -f\theta' = \frac{\Delta_2}{\Delta_3}\frac{1}{Pr}\theta'' - \eta\big(ff'\theta' + f^2\theta''\big) + \frac{\sigma_{hnf}}{(T_w-T_\infty)(C_p)_{hnf}\rho_{hnf}}B_0^2cx^2f'^2 + \frac{Nr}{\Delta_3}\theta''.$$

$$\Rightarrow \quad -f\theta' = \frac{\Delta_2}{\Delta_3}\frac{1}{Pr}\theta'' - \eta\big(ff'\theta' + f^2\theta''\big) + \frac{\sigma_{hnf}}{(T_w-T_\infty)(C_p)_f\Delta_3 c}B_0^2c^2x^2f'^2\frac{\sigma_f}{\sigma_f} + \frac{Nr}{\Delta_3}\theta''.$$

$$\Rightarrow \quad -f\theta' = \frac{\Delta_2}{\Delta_3}\frac{1}{Pr}\theta'' - \eta\big(ff'\theta' + f^2\theta''\big) + \frac{\sigma_{hnf}}{\sigma_f}\frac{c^2x^2}{(T_w-T_\infty)(C_p)_f}\frac{B_0^2\sigma_f}{\rho_f c}\frac{1}{\Delta_3}f'^2 + \frac{Nr}{\Delta_3}\theta''.$$

$$\Rightarrow \quad -f\theta' = \frac{\Delta_2}{\Delta_3}\frac{1}{Pr}\theta'' - \eta\big(ff'\theta' + f^2\theta''\big) + \frac{ME_c}{\Delta_3}\Delta_5f'^2 + \frac{Nr}{\Delta_3}\theta''.$$

$$\Rightarrow \quad -f\theta' = \frac{\Delta_2}{\Delta_3}\frac{1}{Pr}\theta'' - \eta ff'\theta' - \eta f^2\theta'' + \frac{Nr}{\Delta_3}\theta'' + \frac{ME_c}{\Delta_3}\Delta_5f'^2.$$

$$\Rightarrow \quad -f\theta' = \left(\frac{\Delta_2}{\Delta_3}\frac{1}{Pr} - \eta f^2 + \frac{Nr}{\Delta_3}\right)\theta'' - \eta ff'\theta' + \frac{ME_c}{\Delta_3}\Delta_5f'^2.$$

$$\Rightarrow \quad \left(\frac{\Delta_2}{\Delta_3}\frac{1}{Pr} - \eta f^2 + \frac{Nr}{\Delta_3}\right)\theta'' = \eta ff'\theta' - f\theta' - \frac{ME_c}{\Delta_3}\Delta_5f'^2.$$

$$\Rightarrow \quad \theta'' = \frac{1}{\left(\frac{\Delta_2}{\Delta_3}\frac{1}{Pr} - \eta f^2 + \frac{Nr}{\Delta_3}\right)}\left((\eta ff' - f)\theta' - \frac{ME_c}{\Delta_3}\Delta_5f'^2\right).$$

Therefore, the dimensionless form of the equation (4.3) gets the form:

$$\theta'' = \frac{1}{\left(\frac{\Delta_2}{\Delta_3}\frac{1}{Pr} - \eta f^2 + \frac{Nr}{\Delta_3}\right)}\left((\eta ff' - f)\theta' - \frac{ME_c}{\Delta_3}\Delta_5f'^2\right). \tag{4.12}$$

4.2.5 Dimensionless Form of Concentration Equation

Now, for the conversion of equation (4.4) the following derivatives are required:

$$2uv\frac{\partial^2 C}{\partial x \partial y} = 0. \qquad \text{(using (3.21))} \tag{4.13}$$

Now, the dimensionless form of the concentration equation (4.4) can be obtained by using equations (3.11)-(3.15), (3.20)-(3.22) and (4.13) as shown below:

$$\begin{aligned} -c(C_w - C_\infty)f\phi' = \frac{c}{S_c}(C_w - C_\infty)\phi'' - \sigma c(C_w - C_\infty)(1+\delta\theta)^{m_1} exp\left(\frac{-E_0}{1+\delta\theta}\right)\phi \\ - \alpha\big(c^2(C_w - C_\infty)ff'\phi' + c^2(C_w - C_\infty)f^2\phi''\big). \end{aligned}$$

$$\begin{aligned} \Rightarrow -c(C_w - C_\infty)f\phi' = \frac{c}{S_c}(C_w - C_\infty)\phi'' - \sigma c(C_w - C_\infty)(1+\delta\theta)^{m_1} exp\left(\frac{-E_0}{1+\delta\theta}\right)\phi \\ - \alpha\big(+ c^2(C_w - C_\infty)ff'\phi' + c^2(C_w - C_\infty)f^2\phi''\big). \end{aligned}$$

$$\begin{aligned} \Rightarrow -c(C_w - C_\infty)f\phi' = \frac{c}{S_c}(C_w - C_\infty)\phi'' - \sigma c(C_w - C_\infty)(1+\delta\theta)^{m_1} exp\left(\frac{-E_0}{1+\delta\theta}\right)\phi \\ - \alpha c^2(C_w - C_\infty)\big(ff'\phi' + f^2\phi''\big). \end{aligned}$$

$$\Rightarrow \quad -f\phi' = \frac{1}{S_c}\phi'' - \sigma(1+\delta\theta)^{m_1} exp\left(\frac{-E_0}{1+\delta\theta}\right)\phi - \eta\big(ff'\phi' + f^2\phi''\big).$$

$$\Rightarrow \quad \frac{1}{S_c}\phi'' - \sigma(1+\delta\theta)^{m_1} exp\left(\frac{-E_0}{1+\delta\theta}\right)\phi - \eta\big(ff'\phi' + f^2\phi''\big).$$

$$\Rightarrow \quad \frac{1}{S_c}\phi'' - \eta f^2\phi'' + \big(f - \eta ff'\big)\phi' - \sigma(1+\delta\theta)^{m_1} exp\left(\frac{-E_0}{1+\delta\theta}\right)\phi = 0.$$

$$\Rightarrow \quad \left(\frac{1 - S_c\eta f^2}{S_c}\right)\phi'' + \big(f - \eta ff'\big)\phi' - \sigma(1+\delta\theta)^{m_1} exp\left(\frac{-E_0}{1+\delta\theta}\right)\phi = 0.$$

$$\Rightarrow \quad \phi'' = \left(\frac{S_c}{1 - S_c\eta f^2}\right)\left(\sigma(1+\delta\theta)^{m_1} exp\left(\frac{-E_0}{1+\delta\theta}\right)\phi - \big(f - \eta ff'\big)\phi'\right).$$

Therefore, the dimensionless form of the concentration equation (4.5) as follows:

$$\phi'' = \left(\frac{S_c}{1 - S_c\eta f^2}\right)\left(\sigma(1+\delta\theta)^{m_1} exp\left(\frac{-E_0}{1+\delta\theta}\right)\phi - \big(f - \eta ff'\big)\phi'\right). \tag{4.14}$$

4.2.6 Dimensionless Form of Motile Equation

The identical satisfaction of equation (4.5) is already discussed in Chapter 3.

$$G'' + S_c f G' = Pe\big(\phi''(\Omega + G) + \phi' G'\big). \tag{4.15}$$

The final dimensionless form of the governing equations is

$$f''' = \left(\frac{\beta}{1+\beta}\right)\big(\Delta_1(f'^2 - ff'') + \Delta_4 D_f f'^2 + \big(P_0 + \Delta_5 PaM\big)f'\big). \tag{4.16}$$

$$\theta'' = \frac{1}{\left(\frac{\Delta_2}{\Delta_3}\frac{1}{Pr} - \eta f^2 + \frac{Nr}{\Delta_3}\right)}\left((\eta f f' - f)\theta' - \frac{ME_c}{\Delta_3}\Delta_5 f'^2\right). \tag{4.17}$$

$$\phi'' = \left(\frac{S_c}{1 - S_c\eta f^2}\right)\left(\sigma(1+\delta\theta)^{m_1} exp\left(\frac{-E_0}{1+\delta\theta}\right)\phi - \big(f - \eta f f'\big)\phi'\right). \tag{4.18}$$

$$G'' = Pe\big(\phi''(\Omega + G) + \phi' G'\big) - S_c f G'. \tag{4.19}$$

4.2.7 Dimensionless Form of Boundary Conditions

The related BCs are converted into the dimensionless form by the following calculation.

- $v(x,0) = -v_0, \qquad at \quad y = 0.$

  $\Rightarrow \quad v_0 = -\sqrt{c\nu_f} f(\xi), \qquad at \quad y = 0.$

  $\Rightarrow \quad f(\xi) = \dfrac{v_0}{\sqrt{c\nu_f}}, \qquad at \quad \xi = 0.$

  $\Rightarrow \quad f(0) = \dfrac{v_0}{\sqrt{c\nu_f}},$

  $\Rightarrow \quad f(0) = S_0.$

- $u(x,0) = U_w + \left(\dfrac{\beta+1}{\beta}\right) W_1 \mu_{hnf}(B)\left(\dfrac{\partial u}{\partial y}\right), \qquad at \quad y = 0.$

  $\Rightarrow \quad cxf'(\xi) = cx + \left(\dfrac{\beta+1}{\beta}\right) W_0\big(\mu_f(1-\phi_1)^{-2.5}(1-\phi_2)^{-2.5}\big)\left(\dfrac{c^3/2f''(\xi)}{\sqrt{\nu_f}}\right),$

$$\Rightarrow \quad , cxf'(\xi) = cx + \left(\frac{\beta+1}{\beta}\right)\left(\sqrt{\frac{c}{\nu_f}}\mu_f W_0\right)\left((1-\phi_1)^{-2.5}(1-\phi_2)^{-2.5}\right)cxf''(\xi),$$

$$\Rightarrow \quad cxf'(\xi) = cx + \left(\frac{\beta+1}{\beta}\right)\frac{\Lambda}{\left((1-\phi_1)^{2.5}(1-\phi_2)^{2.5}\right)}cxf''(\xi),$$

$$\Rightarrow \quad f'(0) = 1 + \left(\frac{\beta+1}{\beta}\right)\frac{\Lambda}{\left((1-\phi_1)^{2.5}(1-\phi_2)^{2.5}\right)}f''(0),$$

$$\Rightarrow \quad f'(0) = 1 + \left(\frac{\beta+1}{\beta}\right)\frac{\Lambda}{\left((1-\phi_1)^{2.5}(1-\phi_2)^{2.5}\right)}f''(0).$$

- $\dfrac{\partial T}{\partial y} = -\dfrac{h}{k_f}(T_w - T),$ $at \quad y = 0.$

$$\Rightarrow \quad \sqrt{\frac{c}{\nu_f}}(T_w - T_\infty)\theta' = -\frac{h}{k_f}\big(T_w - T_\infty - (T_w - T_\infty)\theta(\xi)\big), \qquad at \quad \xi = 0.$$

$$\Rightarrow \quad \theta'(\xi)(T_w - T_\infty) = -\frac{h}{k_f}\sqrt{\frac{\nu_f}{c}}(T_w - T_\infty)(1-\theta(\xi)),$$

$$\Rightarrow \quad \theta'(\xi) = -Bi(1-\theta(\xi)),$$

$$\Rightarrow \quad \theta'(0) = -Bi(1-\theta(0)).$$

- $C(x,0) = C_w,$ $at \quad y = 0.$

$$\Rightarrow \quad C(x,0) = C_\infty + (C_w - C_\infty)\phi(\xi), \qquad at \quad \xi = 0.$$

$$\Rightarrow \quad \phi(\xi) = \frac{C_w - C_\infty}{C_w - C_\infty}, \qquad at \quad \xi = 0.$$

$$\Rightarrow \quad \phi(\xi) = 1, \qquad at \quad \xi = 0.$$

$$\Rightarrow \quad \phi(0) = 1.$$

- $N(x,0) = N_w,$ $at \quad y = 0.$

$$\Rightarrow \quad N(x,0) = N_\infty + (N_w - N_\infty)G(\xi), \qquad at \quad \xi = 0.$$

$$\Rightarrow \quad G(\xi) = \frac{N_w - N_\infty}{N_w - N_\infty}, \qquad at \quad \xi = 0.$$

$$\Rightarrow \quad G(\xi) = 1, \qquad at \quad \xi = 0.$$

$$\Rightarrow \quad G(0) = 1.$$

- $u \longrightarrow 0,$ $as \quad y \longrightarrow \infty.$

$$\Rightarrow \quad f'(\xi) \longrightarrow 0, \qquad as \quad \xi \longrightarrow \infty.$$

- $T \to T_\infty, \qquad as \quad y \longrightarrow \infty.$

$$\Rightarrow \quad \theta(\xi) \to 0, \qquad as \quad \xi \longrightarrow \infty.$$

- $C \to C_\infty, \qquad as \quad y \longrightarrow \infty.$

$$\Rightarrow \quad \phi(\xi) \to 0, \qquad as \quad \xi \longrightarrow \infty.$$

- $N \to N_\infty, \qquad as \quad y \longrightarrow \infty.$

$$\Rightarrow \quad G(\xi) \to 0, \qquad as \quad \xi \longrightarrow \infty.$$

Finally,

$$\left.\begin{aligned} &f = S_0, \quad f' = 1 + \left(\frac{\beta+1}{\beta}\right)\frac{\Lambda}{\left((1-\Phi_1)^{2.5}(1-\Phi_2)^{2.5}\right)}f''(0), \\ &\theta' = -Bi(1-\theta(0)), \quad G = 1, \quad \phi = 1 \quad as \quad \xi \to 0, \\ &f' \to 0, \quad \theta \to 0, \quad G \to 0, \quad \phi \to 0, \quad as \quad \xi \to \infty. \end{aligned}\right\} \tag{4.20}$$

The skin friction $Re_x^{\frac{1}{2}} C_{f_x}$, Nusselt number $Re_x^{-\frac{1}{2}} Nu_x$, Sherwood number $Re_x^{-\frac{1}{2}} Sh_x$ and density of motile micro-organism $Re_x^{-\frac{1}{2}} Nn_x$ in dimensionless form are similar as discussed in Chapter 3.

4.3 Solution Methodology

The numerical solutions are determined through the application of the shooting method, employing the fourth-order Runge-Kutta technique for computation. To tackle the solution of the ODE (4.16), the following notations have been adopted as an initial step:

$$f = G_1, \qquad f' = G_1' = G_2, \qquad f'' = G_1'' = G_2' = G_3.$$

The momentum equation is then transformed into the system of first-order ODEs shown below:

$$\left.\begin{aligned} G_1' &= G_2, & G_1(0) &= S_0, \\ G_2' &= G_3, & G_2(0) &= 1 + \left(\frac{\beta+1}{\beta}\right) \\ & & & \frac{\Lambda}{\big((1-\Phi_1)^{2.5}(1-\Phi_2)^{2.5}\big)} G_3(0), \\ G_3' &= \frac{\beta+1}{\beta}\big(\Delta_1(G_2^2 - G_1G_3)\big) + \Delta_4 D_f G_2^2 & & \\ &\quad + \big(P_0 + P_a\Delta_5 M\big)G_2, & G_3(0) &= p. \end{aligned}\right\} \quad (4.21)$$

The above IVP will be numerically solved by the Runge-Kutta method of order 4.

The domain of the problem is considered to be bounded i.e. $[0,\ \xi_\infty]$, where ξ_∞ is a positive real number, for which the variation in the solution is ignorable after $\xi = \xi_\infty$. The missing condition p is to be chosen such that:

$$G_2(\xi_\infty, p) = 0.$$

Newton's method will be used to find p. This method has the following iterative scheme.

$$p_{n+1} = p_n - \frac{G_2(\xi_\infty, p_n)}{(\frac{\partial}{\partial p} G_2(\xi_\infty, p))_{p=p_n}}.$$

We, further introduce the following notations:

$$\frac{\partial G_1}{\partial p} = G_4, \quad \frac{\partial G_2}{\partial p} = G_5, \quad \frac{\partial G_3}{\partial p} = G_6.$$

As a result of these new notations, the Newton's iterative scheme gets the form:

$$p_{n+1} = p_n - \frac{G_2(\xi_\infty, p_n)}{G_5(\xi_\infty, p_n)}.$$

Now, differentiating the system of three first order ODEs (4.21) with respect to p, we get another system of ODEs, as follows:

$$\left.\begin{aligned}
&G_4' = G_5, && G_4(0) = 0,\\
&G_5' = G_6, && G_5(0) = \left(\frac{\beta+1}{\beta}\right)\\
& && \frac{\Lambda}{\left((1-\Phi_1)^{2.5}(1-\Phi_2)^{2.5}\right)},\\
&G_6' = \left(\frac{\beta+1}{\beta}\right)\left(\Delta_1(2G_2G_5 - G_1G_6 - G_4G_3)\right)\\
&\quad + 2\Delta_4 D_f G_2 G_5 + \left(P_0 + P_a\Delta_5 M\right)G_5, && G_6(0) = 1.
\end{aligned}\right\} \tag{4.22}$$

The stopping criteria for the Newton's technique is set as:

$$| G_2(\xi_\infty, p) | < \epsilon.$$

where $\epsilon > 0$ is a sufficiently small number, which from now onward has been taken has been considered as 10^{-10}.

The ordinary differential equation (4.17) will be approximated by using the shooting technique and assuming f as a known function. The notations below have been used for the implementation of the shooting method:

$$\theta = H_1, \qquad \theta' = H_1' = H_2.$$

The energy equation (4.17) can be represented in the form of the following first-order ODEs:

$$\left.\begin{aligned}
&H_1' = H_2, && H_1(0) = 1,\\
&H_2' = \frac{1}{\left(\frac{\Delta_2}{\Delta_3}\frac{1}{Pr} - \eta G_1^2 + \frac{Nr}{\Delta_3}\right)}\Bigg((\eta G_1 G_2 - G_1)H_2 && \\
&\quad - \frac{ME_c}{\Delta_3}\Delta_5 G_2^2\Bigg), && H_2(0) = -Bi(1-\theta(0)).
\end{aligned}\right\} \tag{4.23}$$

The above IVP will be numerically solved by Runge-Kutta method of oder 4. The missing condition q is to be chosen such that,

$$H_1(\xi_\infty, q) = 0.$$

The above equation can be solved by using Newton's method with the following iterative formula.

$$q_{n+1} = q_n - \frac{H_1(\xi_\infty, q_n)}{(\frac{\partial}{\partial q} H_1(\xi_\infty, q))_{q=q_n}}.$$

To proceed further the following new notations, have been introduced:

$$\frac{\partial H_1}{\partial q} = H_3, \qquad \frac{\partial H_2}{\partial q} = H_4.$$

As a result of these new notations, the Newton's iterative scheme gets the form:

$$q_{n+1} = q_n - \frac{H_1(\xi_\infty, q_n)}{H_3(\xi_\infty, q_n)}.$$

Now, differentiating the above system of two first order ODEs with respect to q, we get another system of ODEs, as follows:

$$\left.\begin{aligned} H_3' &= H_4, & H_3(0) &= 0, \\ H_4' &= \frac{1}{\left(\frac{\Delta_2}{\Delta_3}\frac{1}{Pr} - \eta G_1^2 + \frac{Nr}{\Delta_3}\right)}\left((\eta G_1 G_2 - G_1) H_4\right), & H_4(0) &= -Bi. \end{aligned}\right\} \quad (4.24)$$

The stopping criteria for the Newton's method is set as:

$$\mid H_1(\xi_\infty, q) \mid < \epsilon.$$

Now, to solve equations (4.18) and (4.19) numerically by using the shooting technique, assume f, f', f'' and θ as known functions. The following notation have been taken:

$$\phi = T_1, \qquad \phi' = T_1' = T_2, \qquad G = T_3, \qquad G' = T_3' = T_4$$

The equations (4.18) and (4.19) are then transformed into the system of first-order coupled ODEs:

$$\left.\begin{aligned}
&T_1' = T_2, && T_1(0) = 1\\
&T_2' = \frac{S_c}{1 - S_c\eta G_1^2}\Bigg(\sigma(1+\delta\theta)^{m_1} exp\Bigg(\frac{-E_0}{1+\delta\theta}\Bigg)T_1\\
&- \big(G_1 - \eta G_1 G_2\big)T_2\Bigg), && T_2(0) = d\\
&T_3' = T_4, && T_3(0) = 1\\
&T_4' = Pe\Bigg(\frac{S_c}{1 - S_c\eta G_1^2}\Bigg(\sigma(1+\delta\theta)^{m_1} exp\Bigg(\frac{-E_0}{1+\delta\theta}\Bigg)T_1\\
&\quad - \big(G_1 - \eta G_1 G_2\big)T_2\Bigg)(\Omega + T_3) + T_2 T_4\Bigg) - ScfT_4, && T_4(0) = s.
\end{aligned}\right\} \tag{4.25}$$

To apply the fourth-order Runge-Kutta method for the numerical solution of the mentioned initial value problem, it is crucial to judiciously select the conditions d and s within the system of equations. The absent conditions d and s in the given system of equations must be chosen in a manner that ensures:

$$T_1(\xi_\infty, d) = 0, \qquad T_3(\xi_\infty, s) = 0.$$

Newton's method will be used to find d and s. This method has the following iterative scheme.

$$\begin{bmatrix} d \\ s \end{bmatrix}_{(n+1)} = \begin{bmatrix} d \\ s \end{bmatrix}_{(n)} - \begin{bmatrix} \frac{\partial T_1}{\partial d} & \frac{\partial T_1}{\partial s} \\ \frac{\partial T_3}{\partial d} & \frac{\partial T_3}{\partial s} \end{bmatrix}^{-1}_{(n)} \begin{bmatrix} T_1 \\ T_3 \end{bmatrix}_{(n)}.$$

Furthermore, the following notations will be useful for computing the entries of the Jacobian matrix.

$$\begin{aligned}
&\frac{\partial T_1}{\partial d} = T_5, && \frac{\partial T_2}{\partial d} = T_6, && \frac{\partial T_3}{\partial d} = T_7, && \frac{\partial T_4}{\partial d} = T_8,\\
&\frac{\partial T_1}{\partial s} = T_9, && \frac{\partial T_2}{\partial s} = T_{10}, && \frac{\partial T_3}{\partial s} = T_{11}, && \frac{\partial T_4}{\partial s} = T_{12}.
\end{aligned}$$

Newton's iterative scheme will change the form after utilizing the above mentioned notations as follows:

$$\begin{bmatrix} d \\ s \end{bmatrix}_{(n+1)} = \begin{bmatrix} d \\ s \end{bmatrix}_{(n)} - \begin{bmatrix} T_5 & T_9 \\ T_7 & T_{11} \end{bmatrix}^{-1}_{(n)} \begin{bmatrix} T_1 \\ T_3 \end{bmatrix}_{(n)}.$$

Now, differentiating (4.25) the system of four first order ODEs with respect to d and s, we get another system of ODEs as follows:

$$\left.\begin{aligned}
&T_5' = T_6, && T_5(0) = 0,\\
&T_6' = \frac{S_c}{1 - S_c\eta G_1^2}\left(\sigma(1+\delta\theta)^{m_1} exp\left(\frac{-E_0}{1+\delta\theta}\right)T_5\right.\\
&\quad \left. - \big(G_1 - \eta G_1 G_2\big)T_6\right), && T_6(0) = 1,\\
&T_7' = T_8, && T_7(0) = 0,\\
&T_8' = Pe\left(\frac{S_c}{1 - S_c\eta G_1^2}\left(\sigma(1+\delta\theta)^{m_1} exp\left(\frac{-E_0}{1+\delta\theta}\right)T_1 - \big(G_1 - \eta G_1 G_2\big)T_2\right)T_7\right.\\
&\quad + (\Omega + T_3)\left(\frac{S_c}{1 - S_c\eta G_1^2}\left(\sigma(1+\delta\theta)^{m_1} exp\left(\frac{-E_0}{1+\delta\theta}\right)T_5\right.\right.\\
&\quad \left.\left. - \big(G_1 - \eta G_1 G_2\big)T_6 + T_6T_4 + T_2T_8\right) - ScfT_7 && T_8(0) = 0,\\
&T_9' = T_{10}, && T_9(0) = 0,\\
&T_{10}' = \frac{S_c}{1 - S_c\eta G_1^2}\left(\sigma(1+\delta\theta)^{m_1} exp\left(\frac{-E_0}{1+\delta\theta}\right)T_9\right.\\
&\left. - \big(G_1 - \eta G_1 G_2\big)T_{10}\right), && T_{10}(0) = 0,\\
&T_{11}' = T_{12}, && T_{11}(0) = 0,\\
&T_{12}' = Pe\left(\frac{S_c}{1 - S_c\eta G_1^2}\left(\sigma(1+\delta\theta)^{m_1} exp\left(\frac{-E_0}{1+\delta\theta}\right)T_1 - \big(G_1 - \eta G_1 G_2\big)T_2\right)T_{11}\right.\\
&\quad + (\Omega + T_3)\left(\frac{S_c}{1 - S_c\eta G_1^2}\left(\sigma(1+\delta\theta)^{m_1} exp\left(\frac{-E_0}{1+\delta\theta}\right)T_9\right.\right.\\
&\quad \left.\left. - \big(G_1 - \eta G_1 G_2\big)T_{10} + T_{10}T_4 + T_2T_{12}\right) - ScfT_{12}, && T_{12}(0) = 1.
\end{aligned}\right\} \tag{4.26}$$

The stopping criteria for the Newton's method is set as:

$$max\left\{\mid T_1(\xi_\infty, d)\mid, \mid T_3(\xi_\infty, s)\mid\right\} < \epsilon.$$

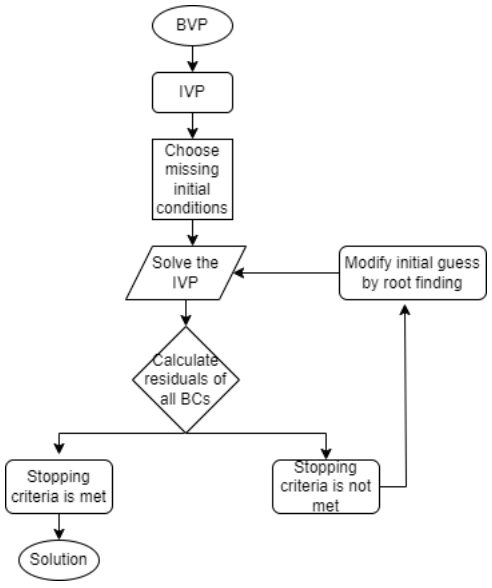

FIGURE 4.2: **Flow diagram of the shooting technique.**

4.4 Results Interpretation

After transforming the governing PDEs describing the fluid flow into a system of ODEs, several crucial parameters emerge. The influence of these dimensionless parameters on dimensionless velocity, temperature, concentration and motile microorganism profiles is thoroughly investigated through the graphical representation. Moreover, the dynamic behaviour of the computed skin friction, Sherwood and Nusselt number will also be assessed.

4.4.1 Skin Friction (C_f), Nusselt (Nu) and Sherwood Numbers (Sh) and Density of Motile Micro-organisms (Nn)

Here, different physical quantities of interest will be analyzed through their computed values. Table 3 displays how $Re_x^{\frac{1}{2}} C_{f_x}$ behaves when subjected to various physical quantities. The skin friction is shown to decrease as the values of β, D_f, P_0, M, S_0, Φ_1, and Φ_2 are enhanced.

In Table 4.3, T_{f_1} and T_{f_2} are the intervals for the choice of missing condition p while computing the skin friction coefficient for nanofluid and hybrid nanofluid respectively. It is observed that for the computation of Nusselt number and Sherwood number, there is a great flexibility in the choice of the missing initial condition. The Nusselt number $Re_x^{-\frac{1}{2}} Nu_x$ falls for the rising values of β, P_0, and M but an augmentation for the rising values of S_0, Φ_1, and Pr is noticed, as shown in Table 4.4. Additionally, the Nusselt number exhibits a tendency of dimming for positive variations in η, Nr, and E_c.

The trend of the Sherwood number $Re_x^{-\frac{1}{2}} Sh_x$ and density distribution of motile micro-organisms $Re_x^{-\frac{1}{2}} Nn_x$ are revealed in Tables 4.6, 4.7, 4.8. The tables clearly shows that the Sherwood number is increased for rising values of D_f, S_0, Φ_1, S_c, and σ whereas the an opposite behavior is shown for increasing values of β, P_0, M, Φ_1, Pr, E_0 and η. The value of density distribution of motile micro-organism $Re_x^{-1/2} Nn_x$ falls for the rising values of β, P_0, M and Φ_2 but an enhancement for the rising values of D_f, S_0, Φ_1, η, S_c, Pe, σ and Ω is noticed.

TABLE 4.3: Missing conditions of $Re_x^{\frac{1}{2}} C_{f_x}$

β	D_f	P_0	M	S_0	Φ_1	Φ_2	T_{f_1}	T_{f_2}
1	25	0.1	0.6	0	0.09	0.09	[-0.6 , 0.5]	[-0.7 , 0.3]
5							[-0.9, -0.3]	[-0.9, -0.4]
7							[-1.0, -0.4]	[-0.9, -0.4]
9							[-1.0, -0.4]	[-1.0, -0.5]
	45						[-0.7 , 0.4]	[-0.7 , 0.2]
	65						[-0.7 , 0.3]	[-0.7 , 0.2]
	85						[-0.7 , 0.2]	[-0.7 , 0.1]
		0.3					[-0.7 , 0.3]	[-0.7 , 0.1]
		0.5					[-0.8 , 0.2]	[-0.7 , 0.0]
		0.8					[-0.8 , 0.0]	[-0.8, -0.1]
			1.2				[-0.8, -0.1]	[-0.7, -0.1]
			1.6				[-0.8, -0.3]	[-0.8, -0.2]
			2				[-0.9, -0.5]	[-0.8, -0.3]
				0.6			[-0.8 , 1.0]	[-0.8 , 0.7]
				1.2			[-1.0 , 1.6]	[-1.0 , 1.2]
				1.8			[-1.2 , 2.2]	[-1.2 , 1.8]
					0.12		[-0.7 , 0.7]	[-0.6 , 0.3]
					0.15		[-0.7 , 0.5]	[-0.6 , 0.4]
					0.18		[-0.6 , 0.6]	[-0.6 , 0.5]
						0.12	- - - -	[-0.7 , 0.2]
						0.15	- - - -	[-0.6 , 0.2]
						0.18	- - - -	[-0.6 , 0.2]

TABLE 4.4: Results of $Re_x^{\frac{1}{2}} C_{f_x}$ for nanofluid TiO_2/EO and hybrid nanofluid $(TiO_2 + Ag)/EO$ for $\Lambda = 1$.

β	D_f	P_0	M	S_0	Φ_1	Φ_2	$Re_x^{\frac{1}{2}} C_{f_x}$ *(NF)*	$Re_x^{\frac{1}{2}} C_{f_x}$ *(HNF)*
1	25	0.1	0.6	0	0.09	0.09	-0.8887	-1.1010
5							-1.2075	-1.5171
7							-1.2427	-1.5633
9							-1.2635	-1.5906
	45						-0.8910	-1.1028
	65						-0.8932	-1.1046
	85						-0.8954	-1.1064
		0.3					-0.9344	-1.1503
		0.5					-0.9767	-1.1961
		0.8					-1.0351	-1.2593
			1.2				-0.9917	-1.1802
			1.6				-1.0515	-1.2281
			2				-1.1060	-1.2728
				0.6			-1.0253	-1.3072
				1.2			-1.1740	-1.5305
				1.8			-1.3294	-1.7565
					0.12		-0.9378	-1.1500
					0.15		-0.9890	-1.2011
					0.18		-1.0425	-1.2548
						0.12	- - - -	-1.1718
						0.15	- - - -	-1.2433
						0.18	- - - -	-1.3159

TABLE 4.5: $Re_x^{-\frac{1}{2}} Nu_x$ for nanofluid TiO_2/EO and hybrid nanofluid $(TiO_2 + Ag)/EO$ for $\Lambda = 1$.

β	P_0	M	S_0	Φ_1	Φ_2	Pr	η	Nr	E_c	$Re_x^{-\frac{1}{2}} Nu_x$ *(NF)*	$Re_x^{-\frac{1}{2}} Nu_x$ *(HNF)*
1	0.1	0.6	0	0.09	0.09	6.2	0.1	0.3	0.1	0.1863	0.2398
5										0.1854	0.2382
7										0.1853	0.2379
9										0.1852	0.2378
	0.3									0.1859	0.2391
	0.5									0.1855	0.2383
	0.8									0.1849	0.2372
		1.6								0.1736	0.2264
		2								0.1693	0.2217
		2.6								0.1632	0.2150
			0.6							0.2127	0.2748
			1.2							0.2252	0.2913
			1.5							0.3563	0.3016
				0.12						0.1974	0.2539
				0.15						0.2092	0.2689
				0.18						0.2218	0.2848
					0.12					- - - -	0.2598
					0.15					- - - -	0.2810
					0.18					- - - -	0.3036
						7.2				0.1873	0.2416
						8.2				0.1881	0.2429
						9.2				0.1888	0.2440
							0.2			0.1869	0.2406
							0.3			0.1876	0.2414
							0.4			0.1882	0.2421
								0.5		0.1792	0.2305
								0.7		0.1729	0.2223
								0.9		0.1673	0.2150
									0.2	0.1785	0.2322
									0.3	0.1707	0.2245
									0.4	0.1629	0.2168

TABLE 4.6: $Re_x^{-\frac{1}{2}} Sh_x$ and $Re_x^{-\frac{1}{2}} Nn_x$ for nanofluid TiO_2/EO and hybrid nanofluid $(TiO_2 + Ag)/EO$ for $\Phi_2 = 0.09$, $Pr = 6.2$, $\eta = 0.1$, $Nr = 0.3$, $E_c = 0.1$, $S_c = 1$, $\sigma = 0$, $E_0 = 4$, $Pe = 0.1$, $\Omega = 0$, $Bi = 0.2$ and for $\Lambda = 1$.

β	D_f	P_0	M	S_0	Φ_1	$Re_x^{-\frac{1}{2}} Sh_x$ *(NF)*	$Re_x^{-\frac{1}{2}} Sh_x$ *(HNF)*	$Re_x^{-\frac{1}{2}} Nn_x$ *(NF)*	$Re_x^{-\frac{1}{2}} Nn_x$ *(HNF)*
1	25	0.1	0.6	0	0.09	0.5468	0.5216	0.5817	0.5557
3						0.5164	0.4921	0.5511	0.5260
5						0.5073	0.4832	0.5418	0.5170
7						0.5029	0.4790	0.5374	0.5127
	45					0.5463	0.5212	0.5811	0.5553
	65					0.5457	0.5208	0.5805	0.5549
	85					0.5452	0.5204	0.5800	0.5545
		0.3				0.5312	0.5063	0.5657	0.5401
		0.5				0.5167	0.4922	0.5509	0.5257
		0.8				0.4968	0.4728	0.5306	0.5058
			0.8			0.5344	0.5131	0.5690	0.5470
			1			0.5226	0.5049	0.5570	0.5387
			1.2			0.5116	0.4971	0.5457	0.5307
				0.4		0.8514	0.8185	0.8952	0.8626
				0.8		1.2408	1.2016	1.2504	1.2142
				1.2		1.7609	1.7154	1.6410	1.6031
					0.12	0.5456	0.5221	0.5804	0.5562
					0.15	0.5447	0.5227	0.5793	0.5567
					0.18	0.5439	0.5232	0.5784	0.5571

TABLE 4.7: $Re_x^{-\frac{1}{2}} Sh_x$ and $Re_x^{-\frac{1}{2}} Nn_x$ for nanofluid TiO_2/EO and hybrid nanofluid $(TiO_2 + Ag)/EO$ for $\beta = 1$, $D_f = 25$, $P_0 = 0.1$, $M = 0.6$, $S_0 = 0$, $\Phi_1 = 0.09$, $\sigma = 0$, $E_0 = 4$, $Pe = 0.1$, $\Omega = 0$, $Bi = 0.2$ and for $\Lambda = 1$.

Φ_2	Pr	η	Nr	E_c	S_c	$Re_x^{-\frac{1}{2}} Sh_x$ *(NF)*	$Re_x^{-\frac{1}{2}} Sh_x$ *(HNF)*	$Re_x^{-\frac{1}{2}} Nn_x$ *(NF)*	$Re_x^{-\frac{1}{2}} Nn_x$ *(HNF)*
0.09	6.2	0.1	0.3	0.1	1	0.5468	0.5261	0.5817	0.5557
0.12						- - - -	0.5156	- - - -	0.5495
0.15						- - - -	0.5105	- - - -	0.5442
0.18						- - - -	0.5062	- - - -	0.5396
	7.2					0.5468	0.5216	0.5817	0.5557
	8.2					0.5468	0.5216	0.5817	0.5557
	9.2					0.5468	0.5216	0.5817	0.5557
		0.2				0.5540	0.5277	0.5822	0.5561
		0.3				0.5614	0.5342	0.5827	0.5566
		0.4				0.5691	0.5408	0.5832	0.5571
			0.5			0.5468	0.5216	0.5817	0.5557
			0.7			0.5468	0.5216	0.5817	0.5557
			0.9			0.5468	0.5216	0.5817	0.5557
				0.2		0.5468	0.5216	0.5817	0.5557
				0.3		0.5468	0.5216	0.5817	0.5557
				0.4		0.5468	0.5216	0.5817	0.5557
					3	1.0879	1.0473	1.1496	1.1079
					5	1.4623	1.4113	1.5424	1.4904
					7	1.7670	1.7077	1.8621	1.8016

TABLE 4.8: $Re_x^{-\frac{1}{2}} Sh_x$ and $Re_x^{-\frac{1}{2}} Nn_x$ for nanofluid TiO_2/EO and hybrid nanofluid $(TiO_2 + Ag)/EO$ for $\beta = 1$, $D_f = 25$, $P_0 = 0.1$, $M = 0.6$, $S_0 = 0$, $\Phi_1 = 0.09$, $\Phi_2 = 0.09$, $Pr = 6.2$, $\eta = 0.1$, $Nr = 0.3$, $E_c = 0.1$, $S_c = 1$ and for $\Lambda = 1$.

σ	E_0	Pe	Ω	Bi	$Re_x^{-\frac{1}{2}} Sh_x$ *(NF)*	$Re_x^{-\frac{1}{2}} Sh_x$ *(HNF)*	$Re_x^{-\frac{1}{2}} Nn_x$ *(NF)*	$Re_x^{-\frac{1}{2}} Nn_x$ *(HNF)*
0	4	0.1	0	0.2	0.5468	0.5216	0.5817	0.55557
1					0.5644	0.5402	0.5831	0.5573
3					0.5978	0.5755	0.5860	0.5603
5					0.6293	0.6085	0.5887	0.5631
	8				0.5468	0.5216	0.5817	0.5557
	12				0.5468	0.5216	0.5817	0.5557
	16				-.5468	0.5216	0.5817	0.5557
		0.2			0.5468	0.5216	0.6238	0.5961
		0.3			0.5468	0.5216	0.6663	0.6370
		0.4			0.5468	0.5216	0.7093	0.6782
			0.4		0.5468	0.5216	0.5962	0.5698
			0.8		0.5468	0.5216	0.6108	0.5838
			1.2		0.5468	0.5216	0.6254	0.5979
				0.4	0.5468	0.5216	0.5817	0.5557
				0.6	0.5468	0.5216	0.5817	0.5557
				0.8	0.5468	0.5216	0.5817	0.5557

4.4.2 Velocity Field

In Figure 4.3, we observe the effect of β on $f'(\eta)$. As β escalates, the velocity profile, represented by $f'(\xi)$, decreases. Essentially, for the higher values of Casson parameter β, the yield stress of the fluid decreases. Consequently, the fluid behaves more like a Newtonian fluid, characterized by a constant viscosity, and the velocity profile becomes flatter. This behavior is a result of the rheological properties associated with Casson fluid models. In Figure 4.4, the velocity profile behavior is depicted, illustrating a notable trend. As the Darcian drag force parameter D_f tends to larger values, the velocity experiences a decreasing impact. This signifies that higher values of D_f lead to a more pronounced damping effect on the velocity

profile within the system. The Darcian drag force parameter has a significant influence on fluid flow through porous media, and its increase tends to impede the flow, resulting in a diminishing velocity profile. From Figure 4.5, it is evident that $f'(\xi)$ decreases as P_0 increases. This phenomenon can be attributed to the physical relationship between the local porosity parameter P_0 and the Darcian drag force. Physically, the local porosity parameter P_0 is inversely proportional to the Darcian drag force D_f. In other words, as P_0 increases, the Darcian drag force tends to decrease. When the Darcian drag force is reduced due to a higher P_0, the Darcy number is affected. The dimensionless Darcy parameter signifies the ratio of viscous forces to inertial forces, and it plays a role in determining the impact of the Darcian drag force on the fluid flow. An increase in the Darcy number implies a slower growth of the Darcian drag force, which in turn, enhances the fluid flow flexibility within the porous medium. Consequently, this increased flexibility and reduced resistance result in a decline in the fluid velocity, as shown in Figure 4.5. In Figure 4.6, the impact of the magnetic parameter M on the velocity profile is illustrated. As the applied transverse magnetic field increases, the fluid velocity decreases. This behavior is attributed to the presence of the Lorentz force, which acts as a resistive force within electrically conducting nanofluids interacting with the applied magnetic field. The Lorentz force is a crucial factor that influences the fluid dynamics in this scenario. As the magnetic field intensity, represented by M increases, the Lorentz force also intensifies. This heightened Lorentz force acts against the fluid flow, resulting in a decline in the fluid velocity. This decreasing trend in the fluid velocity due to the Lorentz force is evident for both conventional and hybrid nanofluids. Regardless of the type of nanofluid, the Lorentz force's influence increases with higher magnetic field, leading to a notable reduction in the fluid velocity. In Figure 4.7, it is apparent that an increase in the suction parameter S_0 leads to a decrease in the fluid velocity. When suction is applied, it creates a negative pressure gradient, effectively drawing fluid into the boundary or reducing the pressure within the system. This negative pressure gradient can hinder the movement and flow of the fluid, resulting in a decrease in fluid velocity. From Figure 4.8, it is clear that as Φ_1 rises, there is an observed elevation in

the velocity profile. This phenomenon could be attributed to the introduction of nanoparticles, which contribute to the increased energy and acceleration of fluid flow.

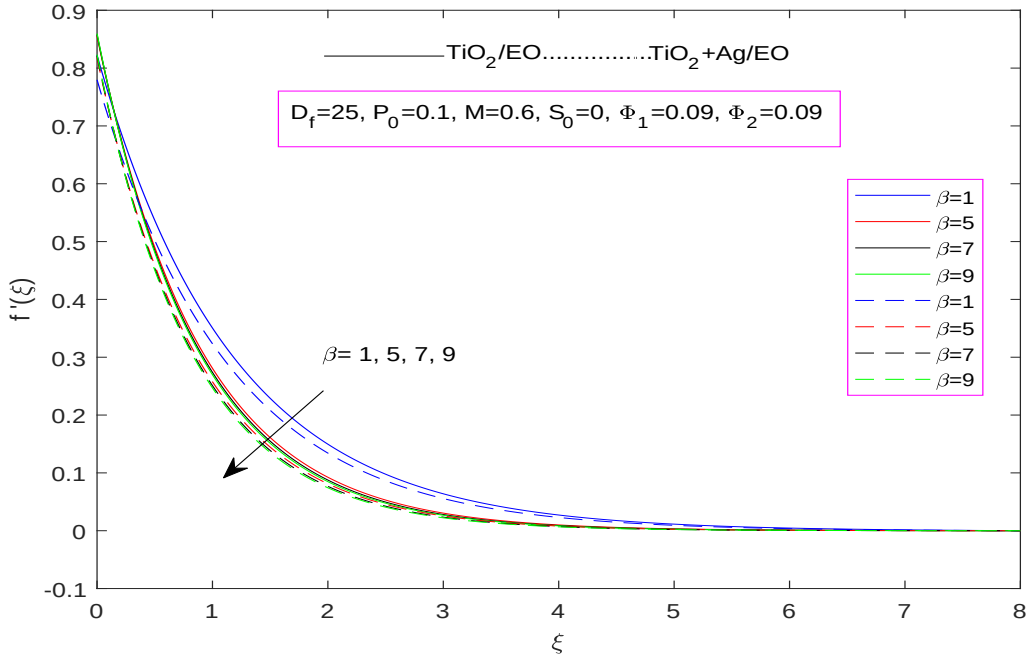

FIGURE 4.3: Impact of β on $f'(\xi)$

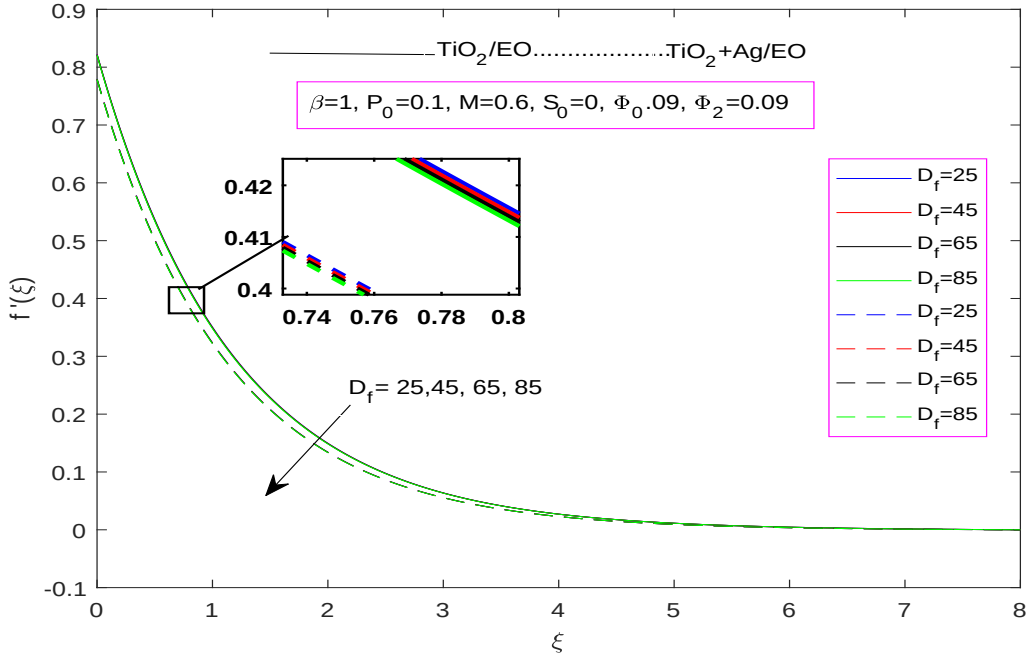

FIGURE 4.4: Impact of D_f on $f'(\xi)$

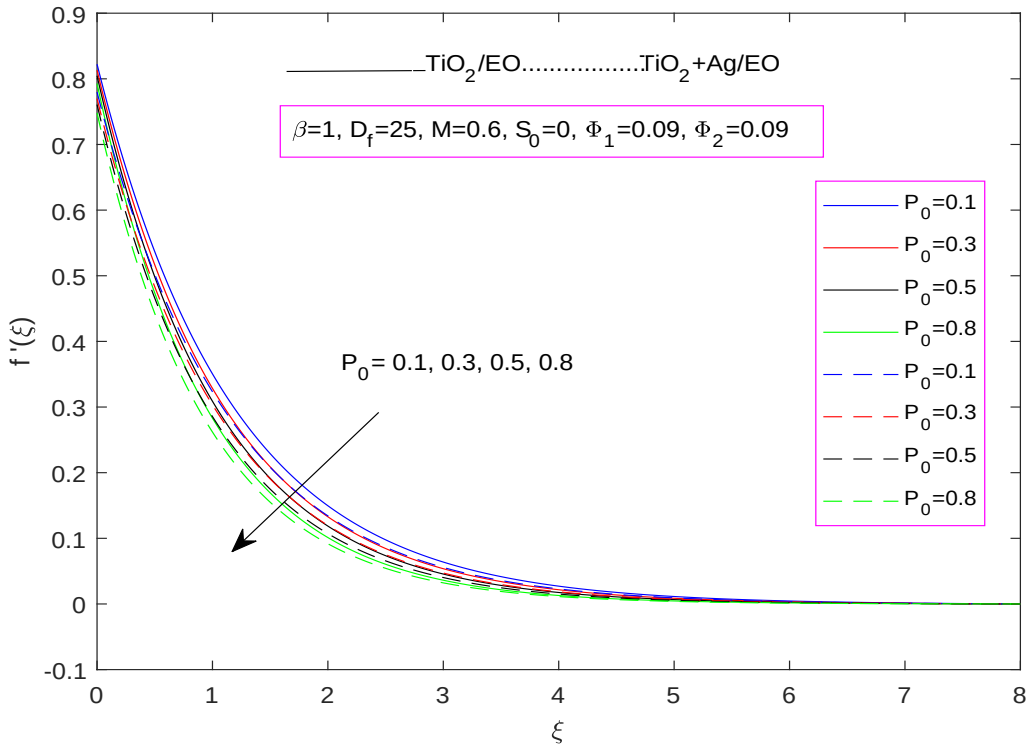

FIGURE 4.5: Impact of P_0 on $f'(\xi)$

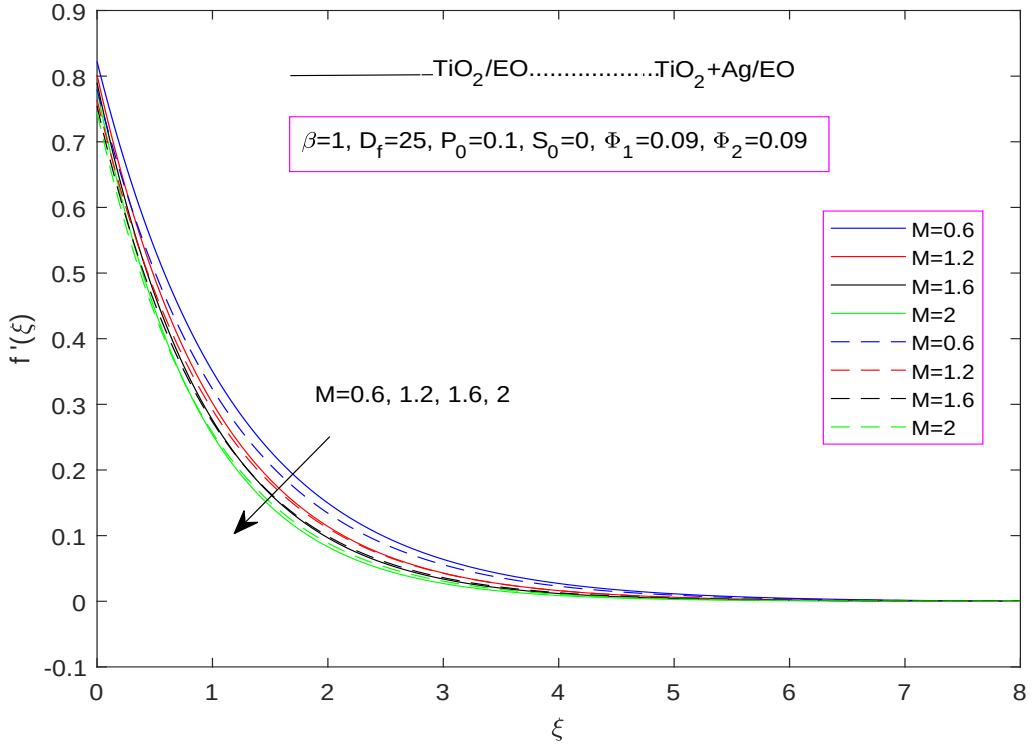

FIGURE 4.6: Impact of M on $f'(\xi)$

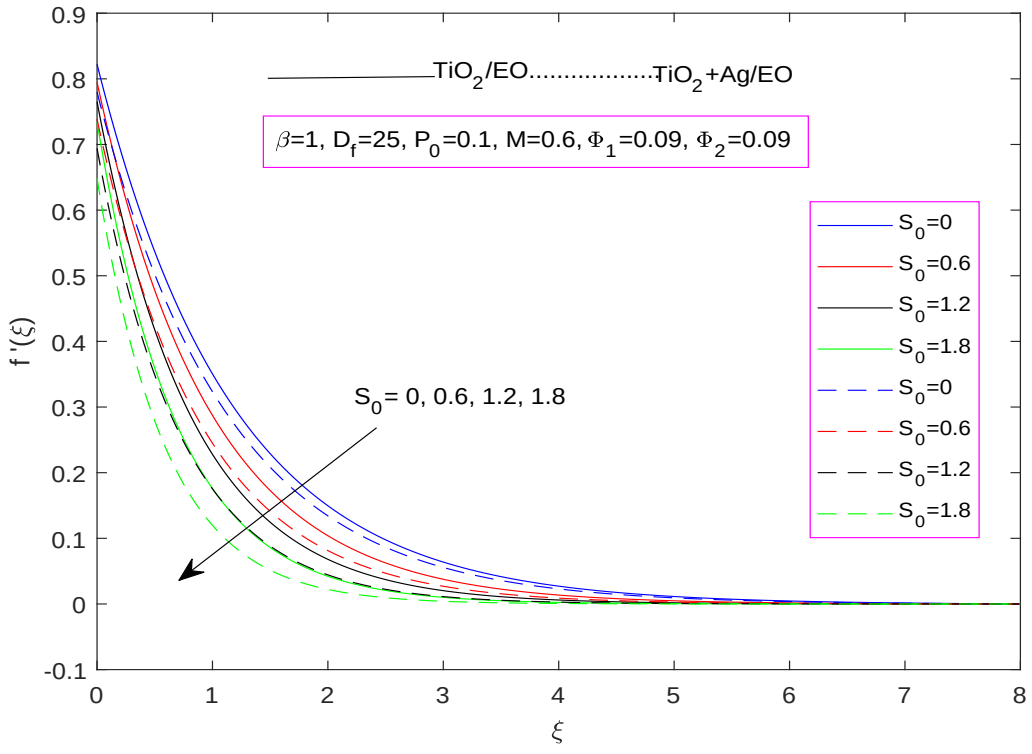

FIGURE 4.7: Impact of S_0 on $f'(\xi)$

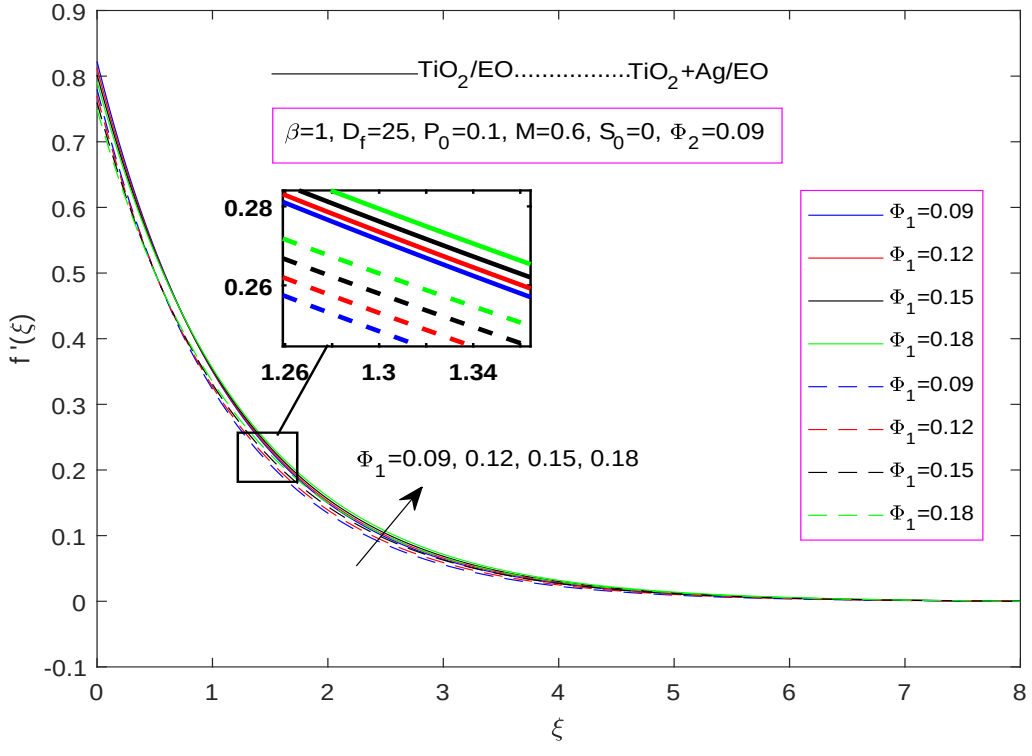

FIGURE 4.8: Impact of Φ_1 on $f'(\xi)$

4.4.3 Temperature Field

In Figure 4.9, the temperature profile behavior is depicted as a function of the Casson parameter β. The observed increasing pattern in the temperature profile indicates a decrease in the heat transfer rate and an increase in the thickness of thermal boundary layer as β increases. The Casson parameter β plays a significant role in determining the rheological behavior of non-Newtonian fluids. As β increases, the flow becomes more shear-thinning, meaning the fluid's viscosity decreases with increasing shear rate. This change in the rheological behavior impacts the velocity and temperature profiles within the fluid. As mentioned, a growth in the temperature profile and an increase in the thermal boundary layer thickness occur because the increase in β leads to a reduction in the velocity boundary layer. This is due to a reduced convective heat transfer, causing a decrease in the heat transfer rate through the fluid.

In Figure 4.10, the depicted trend illustrates that increasing the value of the local porosity parameter P_0 leads to a subsequent increase in temperature within the system. The local porosity parameter P_0 is a measure of the porous nature of the medium through which the fluid is flowing. An increase in P_0 suggests a higher degree of porous structure or permeability within the medium. This increase in porosity allows for better fluid flow and enhances heat exchange between the fluid and the surrounding medium. As P_0 increases, the porous medium offers less resistance to the flow of the fluid, enabling more efficient convective heat transfer. Consequently, the temperature within the system rises because the fluid can more effectively absorb or dissipate heat, depending on the specific context and conditions of the system.

From Figure 4.11, it is evident that the temperature of the nanofluid rises as the magnetic parameter M increases. Additionally, thickness of thermal boundary layer rises for the enhancing values of M. As M has an inverse relationship with the density of the nanofluid. When M increases, the density of the nanofluid decreases. A decrease in density due to an increase in M implies a reduced mass

of fluid per unit volume. In turn, this decrease in density allows the nanofluid to absorb more heat, causing a temperature increase. The findings from Figure 4.12, indicate a decrease in $\theta(\xi)$ within the flow regime, primarily influenced by the dominant effect of suction parameter S_0. The suction parameter S_0 represents the suction effect at the boundary of the system.

Figure 4.13, illustrates that $\theta(\xi)$ is enhanced with increasing values of Φ_1. When nanoparticles are added to a fluid, they can enhance heat transfer due to their increased surface area and thermal conductivity compared to the base fluid. This enhanced heat transfer is a result of various mechanisms, including improved thermal conduction and convection. As Φ_1 increases, there are more nanoparticles available to participate in heat transfer processes, leading to higher temperatures within the fluid. The graph in Figure 4.14, illustrates how the temperature field changes with variations in Pr. The Prandtl number is defined as the ratio of momentum diffusivity to thermal diffusivity $Pr = \frac{\nu}{\alpha}$, where ν and α are kinematic viscosity and thermal diffusivity respectively. In physical terms, an increase in Pr signifies a reduction in thermal diffusivity, subsequently resulting in a decrease in thermal boundary layer thickness. This reduction in the boundary layer thickness leads to the lower temperature within the boundary layer and consequently a decline in $\theta(\xi)$. As Pr increases, the heat transfer rate within the system enhanced, leading to a reduction in $\theta(\xi)$. The higher Pr signifies that the fluid can more effectively conduct heat.

In Figure 4.15, highlights that $\theta(\xi)$ diminishes as the relaxation time parameter η increases, a relationship commonly observed in viscoelastic fluids. In Figure 4.16, it is illustrated that the temperature within the boundary layer, as represented by $\theta(\xi)$, increases in correlation with the fluctuation in Nr. The dimensionless parameter Nr represents the effect of thermal radiation on heat transfer. When Nr values increase, it signifies a higher intensity. Thermal radiation is a process by which heat is transferred in the form of electromagnetic waves, and higher Nr values indicate more effective radiation-induced heat transfer. Consequently, $\theta(\xi)$

exhibits an increase, showcasing the impact of thermal radiation on temperature distribution.

In Figure 4.17, it is demonstrated that the Eckert number E_c governs the effect of heat dissipation on temperature, and this effect intensifies as E_c is increased. The Eckert number E_c characterizes the ratio of kinetic energy to enthalpy. It quantifies the influence of kinetic energy changes on the thermal behavior of a fluid during a process. In fluid dynamics, it is often associated with heat dissipation effects. As E_c increases, it signifies that the kinetic energy variations have a more substantial influence on the thermal behavior of the fluid. In the context of heat dissipation, a higher E_c implies that more kinetic energy of the fluid is converted into thermal energy. This effect results in a rise in temperature.

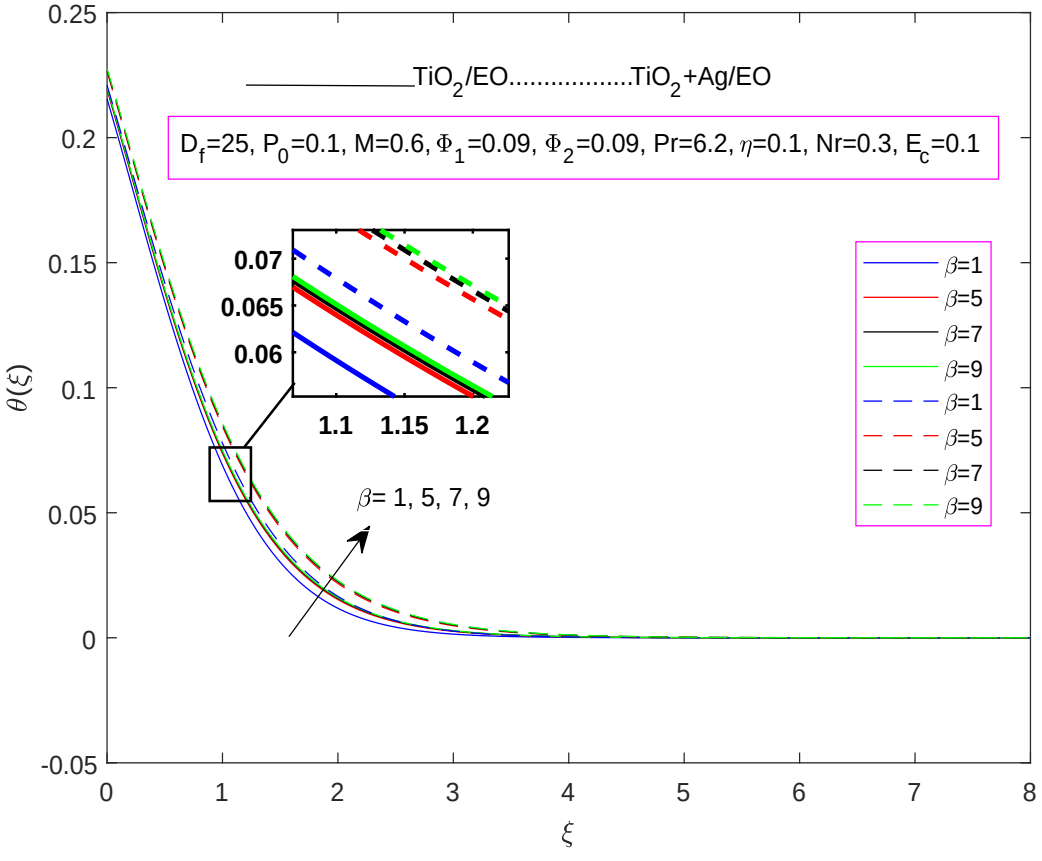

FIGURE 4.9: Impact of β on $\theta(\xi)$

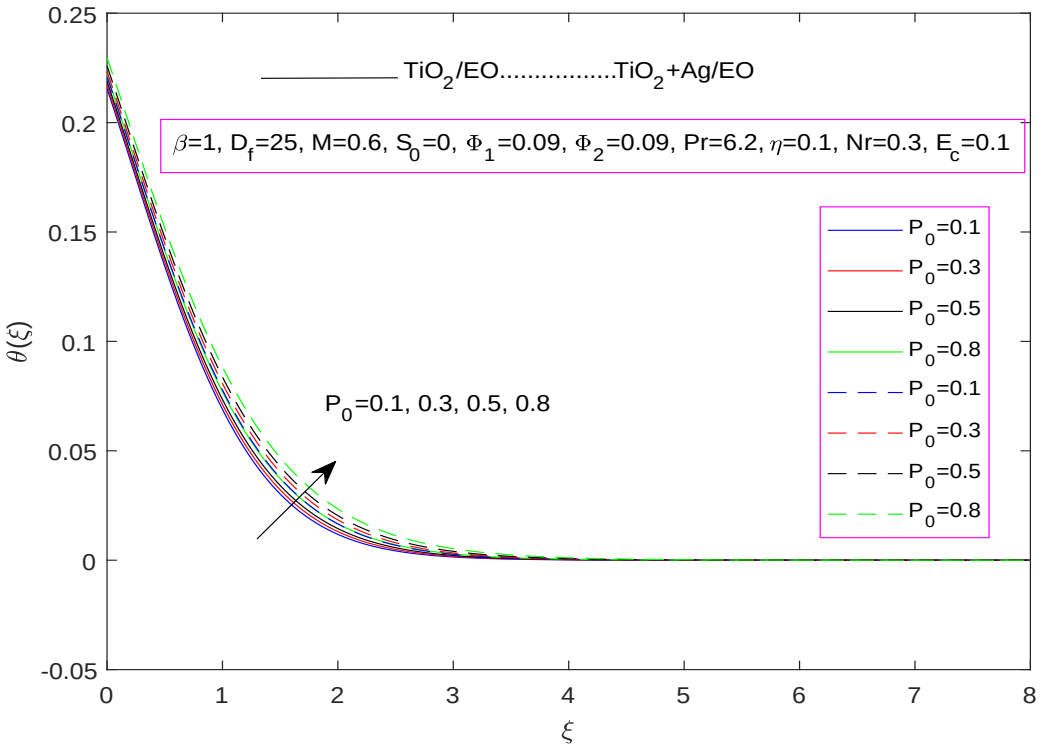

FIGURE 4.10: Impact of P_0 on $\theta(\xi)$

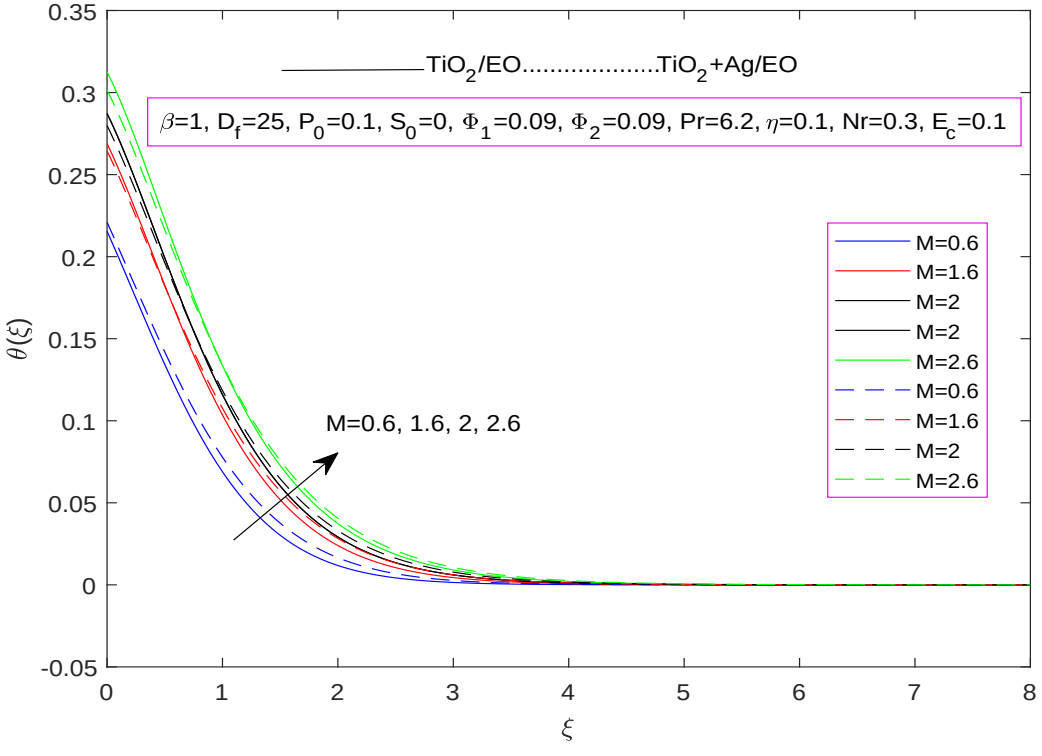

FIGURE 4.11: Impact of M on $\theta(\xi)$

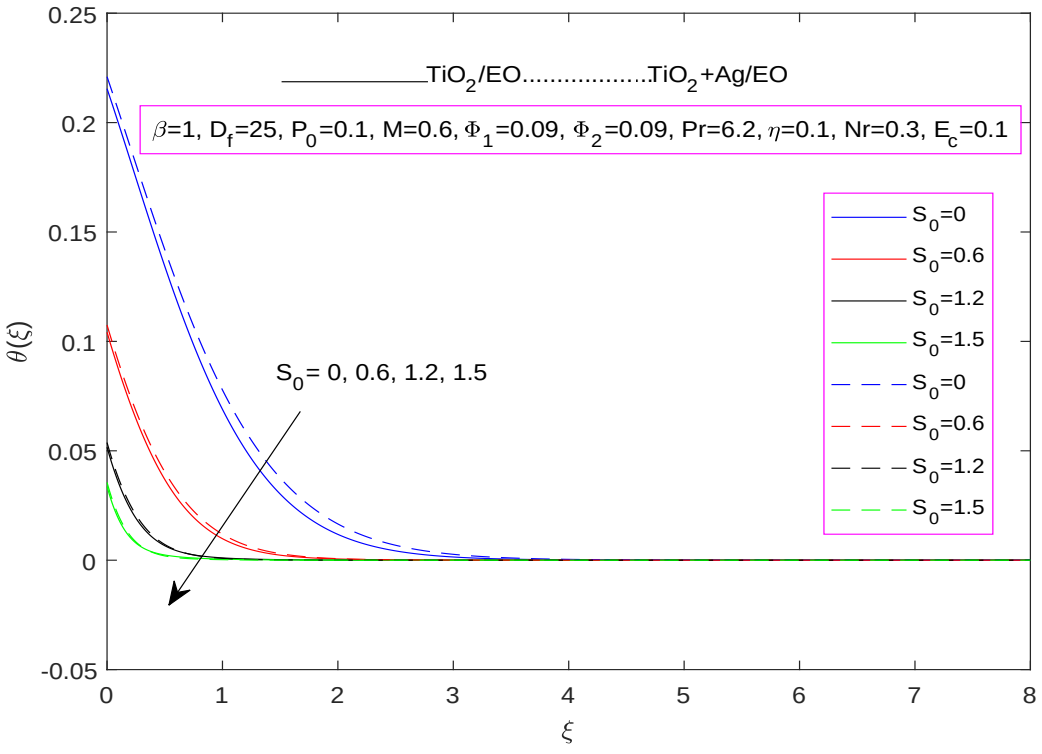

FIGURE 4.12: Impact of S_0 on $\theta(\xi)$

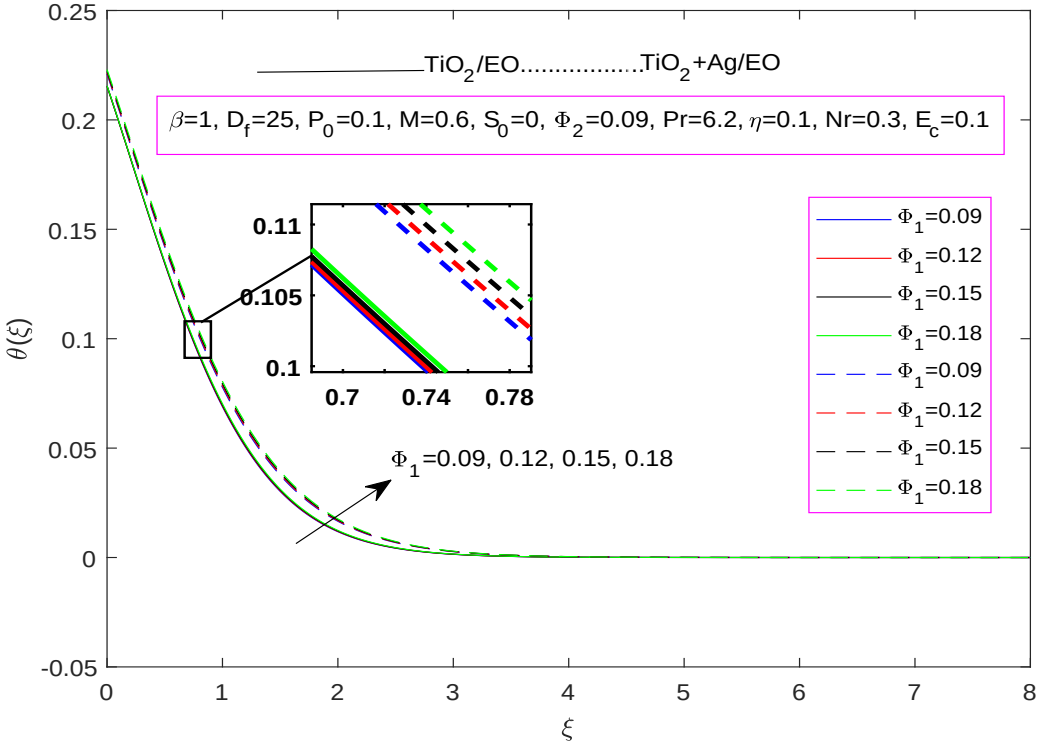

FIGURE 4.13: Impact of Φ_1 on $\theta(\xi)$

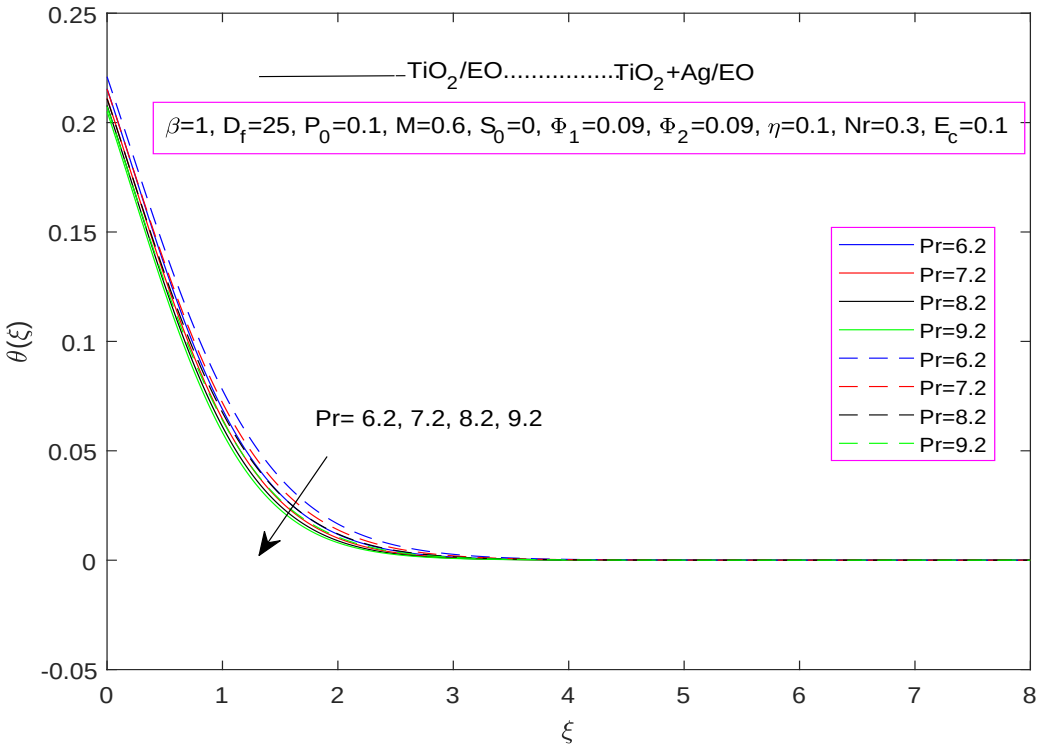

FIGURE 4.14: Impact of Pr on $\theta(\xi)$

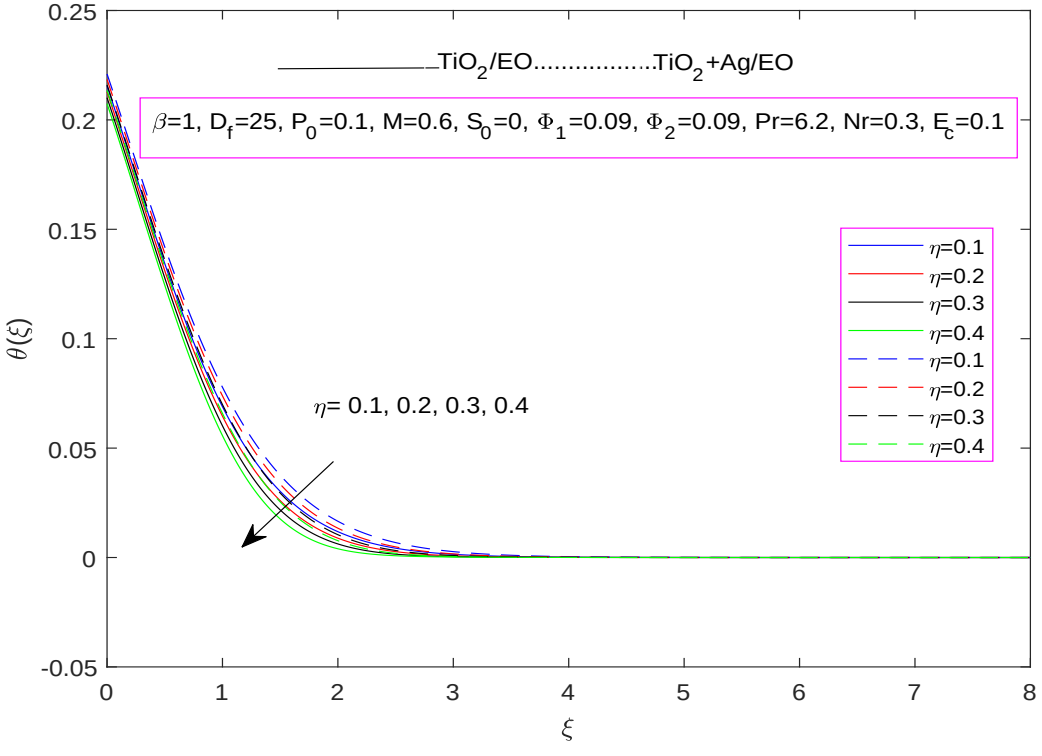

FIGURE 4.15: Impact of η on $\theta(\xi)$

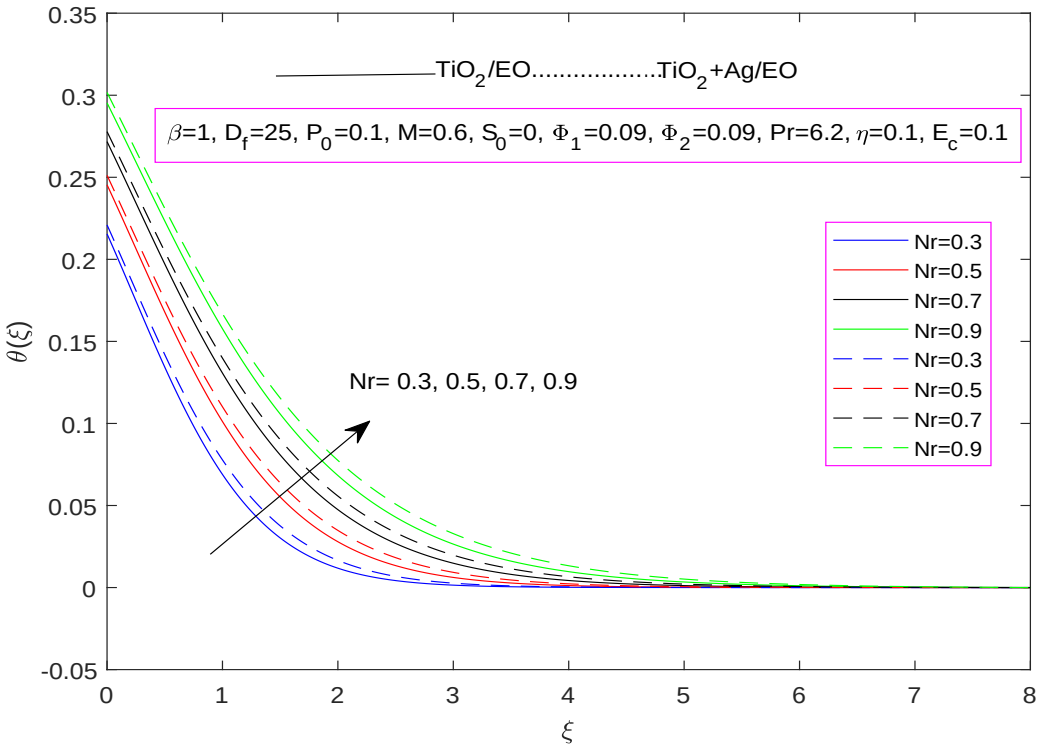

FIGURE 4.16: Impact of Nr on $\theta(\xi)$

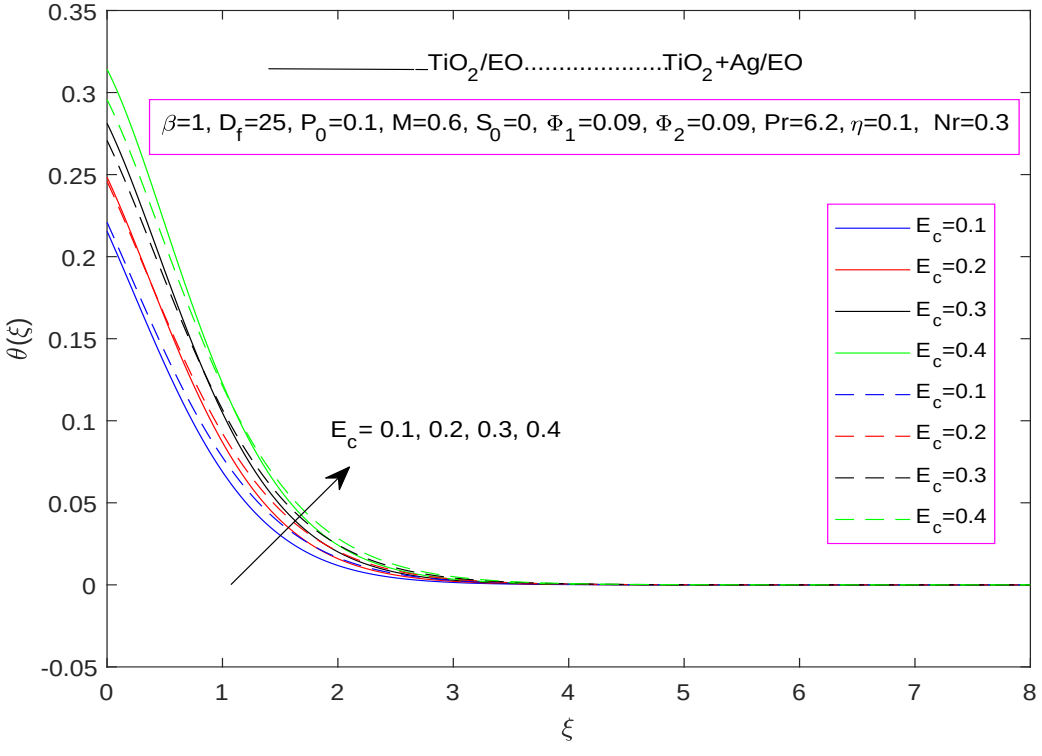

FIGURE 4.17: Impact of E_c on $\theta(\xi)$

4.4.4 Concentration Field

Figure 4.18 shows the concentration profile's reduction as the Casson parameter increases. A higher Casson parameter may lead to the increased yield stress or more significant shear-thinning behavior, making it more difficult for the fluid to disperse and mix, resulting in the reduced concentration profiles. An illustration of increase in the concentration profile $\phi(\xi)$ is depicted in Figure 4.19 for the positive variation in Darcian parameter D_f.

Figure 4.20 discloses the effect of the local porosity parameter P_0 on $\phi(\xi)$. It appears that increasing P_0 results in a less intense concentration profile. A higher P_0 can lead to a reduction in $\phi(\xi)$. This could be due to increased dispersion and mixing of the concentration within the system as the void spaces allow for greater fluid movement and distribution, resulting in a more spread out and less intense concentration profile. The impact of the magnetic parameter M on the concentration profile is disclosed in Figure 4.21 which reflect that as M rises, $\phi(\xi)$ enhanced. From Figure 4.22, it is evident that $\phi(\xi)$ is dimmed as the suction parameter S_0 enhanced. Figure 4.23 exposed that $\phi(\xi)$ falls for positive variation in Φ_1. From Figure 4.24, it is clear that $\phi(\xi)$ declines for the rising values of relaxation parameter η.

Figure 4.25 displays the effect of the Schmidt number S_c on $\phi(\xi)$ and the associated thinning of the concentration layer thickness is also observed. It is relevant to mention that S_c characterizes the ratio of momentum diffusivity (kinematic viscosity) to mass diffusivity in a fluid. A rise in S_c suggests that the mass diffusivity is comparatively smaller than the momentum diffusivity. As mass diffusivity decreases with higher S_c values, the diffusion of the substance becomes less efficient. Consequently, the concentration profiles $\phi(\xi)$ exhibits a decrease.

Figure 4.26 illustrates the physical impacts of σ. By facilitating more efficient liquid species dissolution, positive variation of σ results in a detrimental chemical reaction that reduces the concentration gradient. So, as the chemical rate constant σ is increased, the concentration profile $\phi(\xi)$ is decreased.

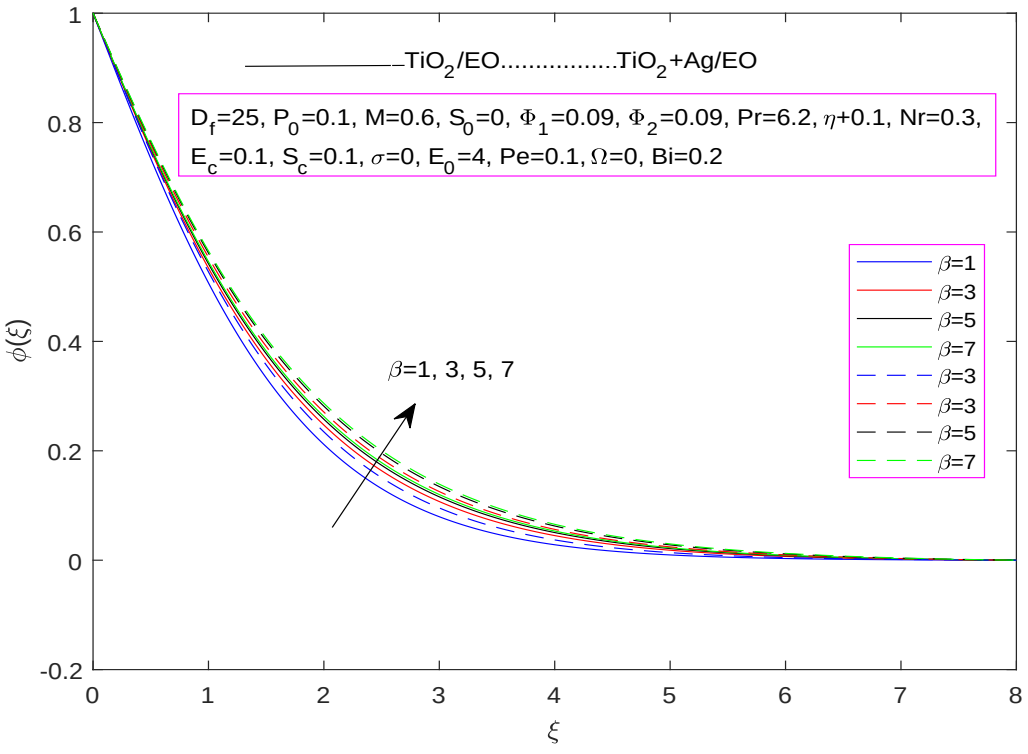

FIGURE 4.18: Impact of β on $\phi(\xi)$

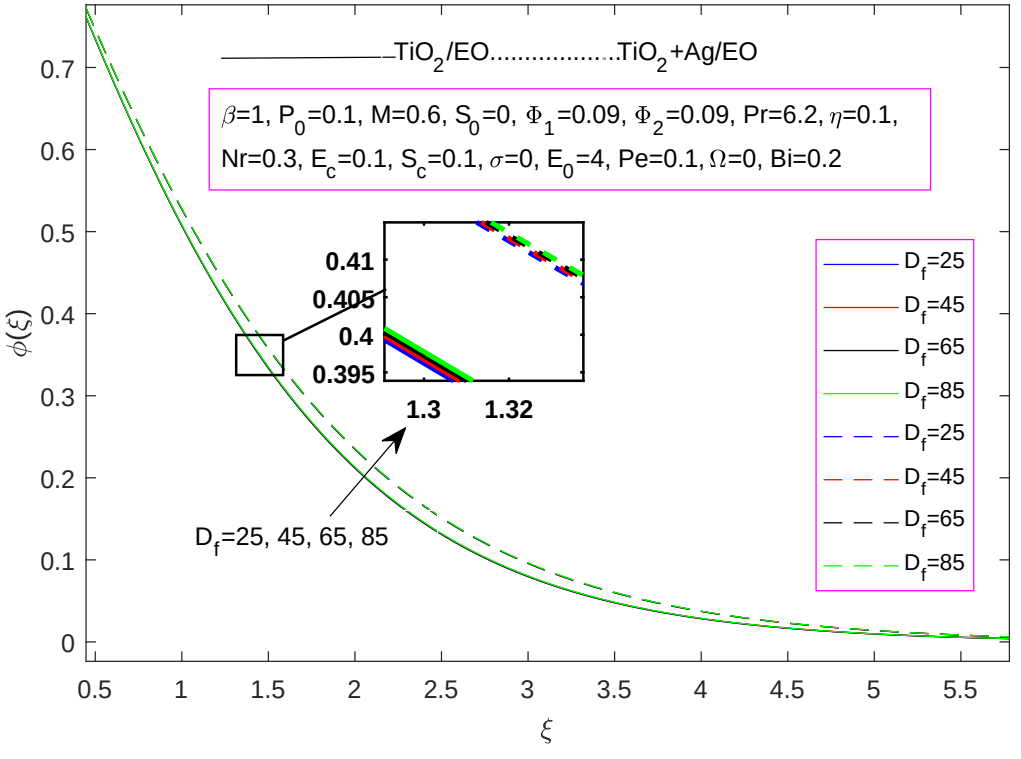

FIGURE 4.19: Impact of D_f on $\phi(\xi)$

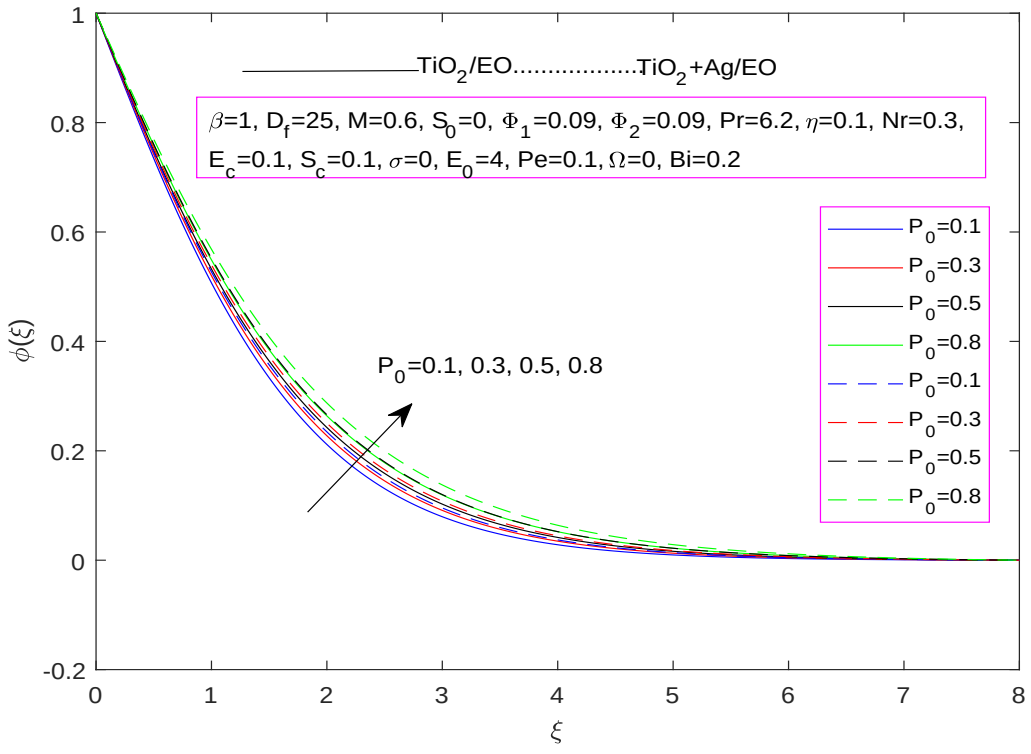

FIGURE 4.20: Impact of P_0 on $\phi(\xi)$

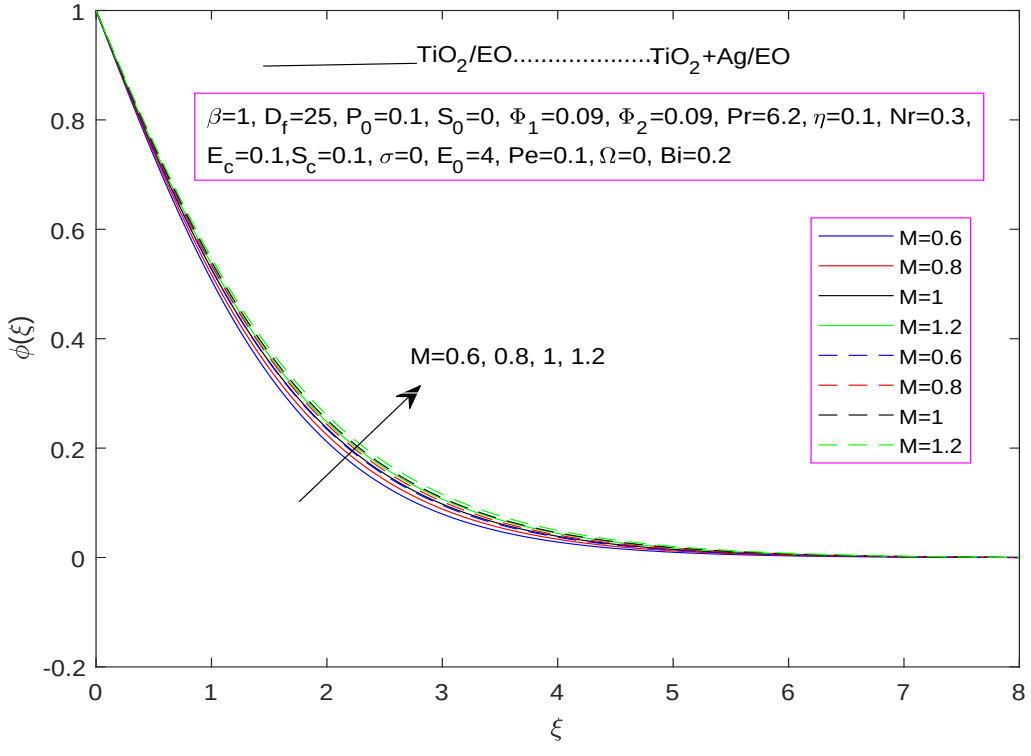

FIGURE 4.21: Impact of M on $\phi(\xi)$

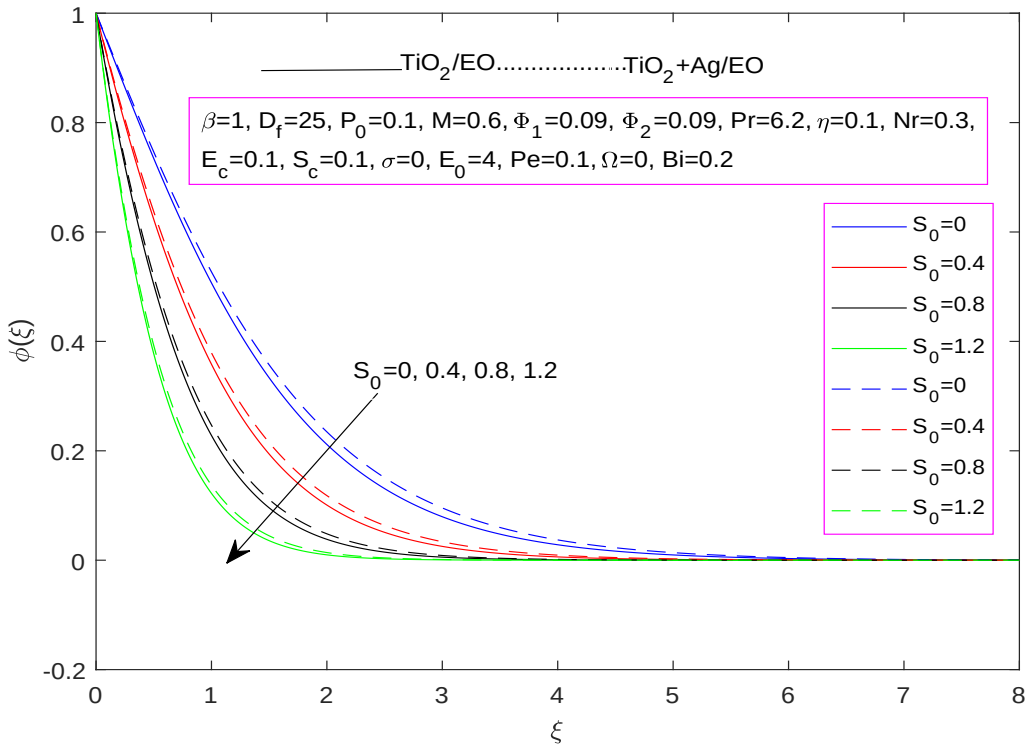

FIGURE 4.22: Impact of S_0 on $\phi(\xi)$

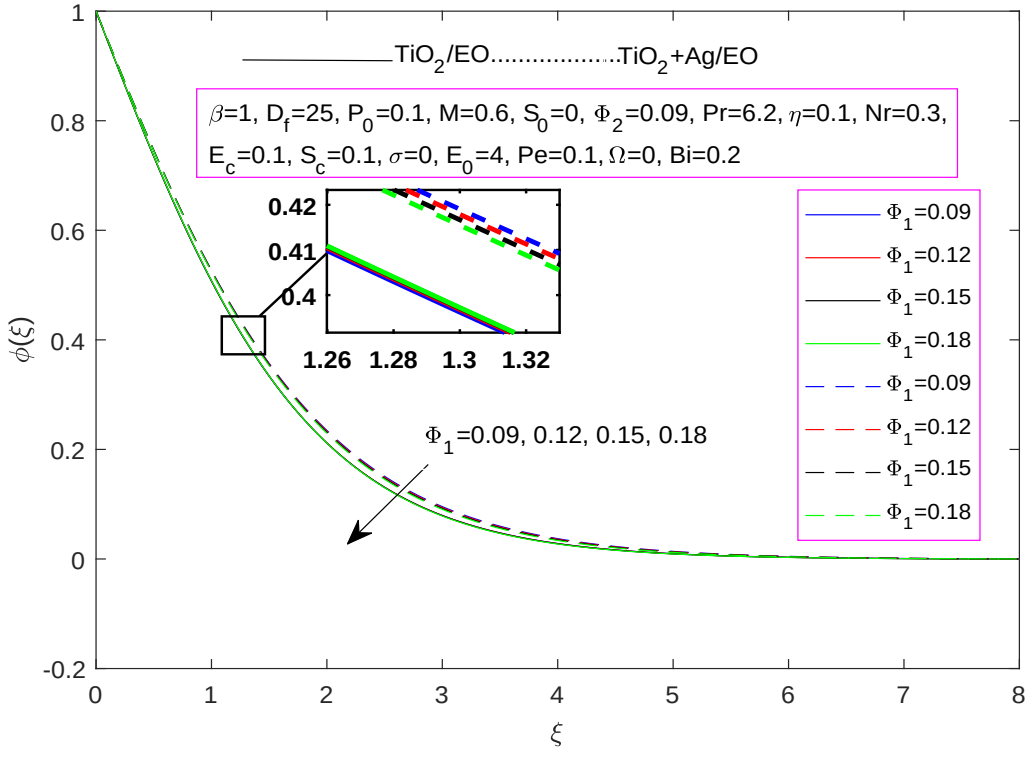

FIGURE 4.23: Impact of Φ_1 on $\phi(\xi)$

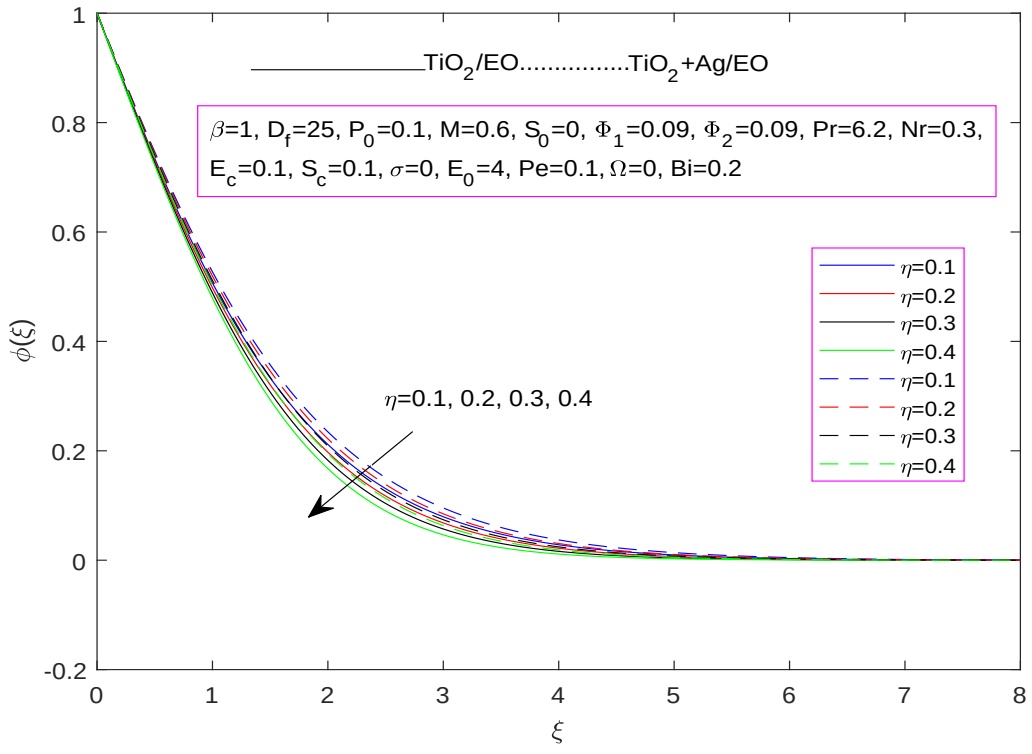

FIGURE 4.24: Impact of η on $\phi(\xi)$

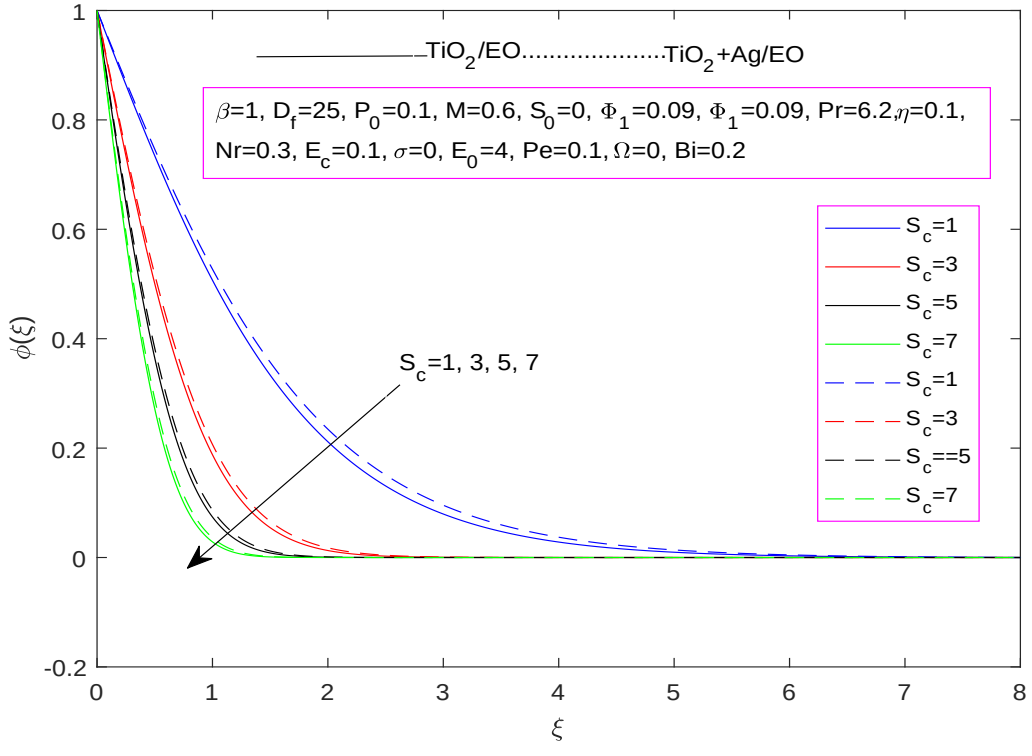

FIGURE 4.25: Impact of S_c on $\phi(\xi)$

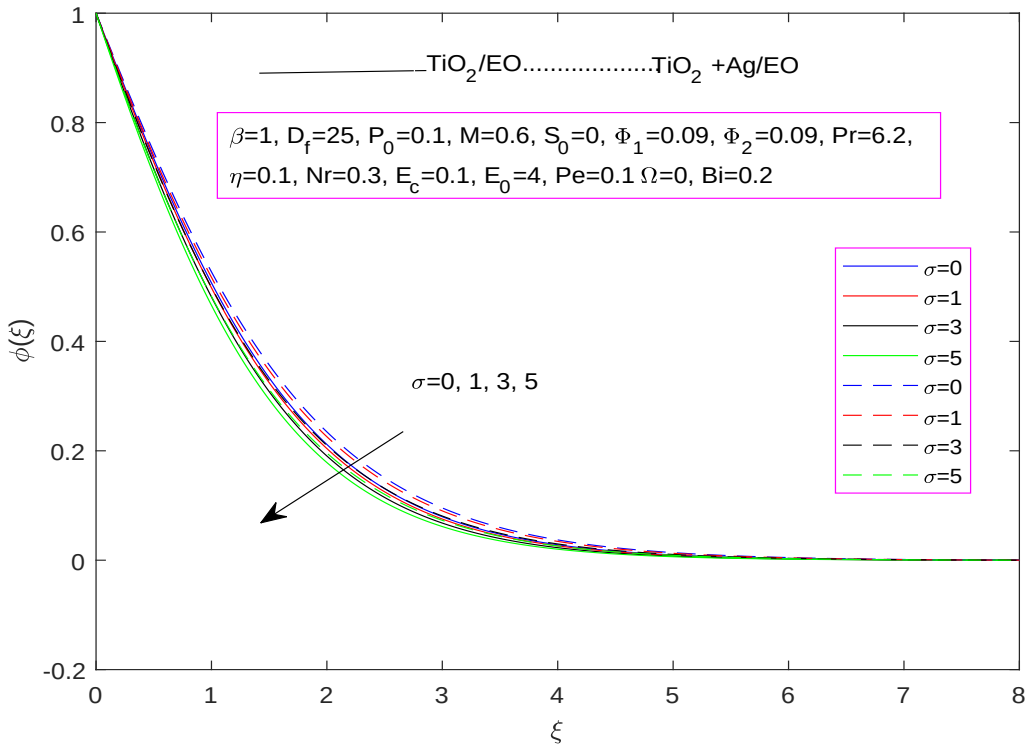

FIGURE 4.26: Impact of σ on $\phi(\xi)$

4.4.5 Motile Field

Figure 4.27 portrays the behavior of the motile profile concerning the Casson parameter β. As β rises, the flow tends to exhibit more shear-thinning behavior i.e increasing shear rate cause decrease in viscosity of fluid. As mentioned earlier, the growth in the motile profile and expansion of the thermal boundary layer occur because higher values of β results in a reduction of the velocity boundary layer. Figure 4.28 makes it evident that the motile profile $G(\xi)$ increases significantly with a positive change in the Darcian parameter D_f. Figures (4.29, 4.30) are sketched with the observation that the density of micro-organisms $G(\xi)$ is enhanced with the positive variation in M and P_0. The decreasing trend of density of motile micro-organism $G(\xi)$ with the larger values of suction parameter S_0 is disclosed in Figure 4.31. From Figure 4.32, it is evident that with the enhancing values of Φ_1, density distribution of motile micro-organisms shows a dimming behavior. Figure 4.33 discloses the relation between relaxation parameter η and $G(\xi)$.

Figure 4.34 illustrates the impact of the bioconvection Schmidt number S_c on the density of motile microorganisms $G(\xi)$. The figure distinctly shows that $G(\xi)$ decreases as S_c increases. Elevated S_c values typically indicate a reduced microorganism diffusion, leading to a decrease in $G(\xi)$ and the thermal boundary layer thickness. The relationship between σ and $G(\xi)$ is illustrated in Figure 4.35. Elevated values of σ trigger a detrimental chemical reaction that diminishes the concentration gradient, consequently reducing the density of motile microorganisms $G(\xi)$. This occurs as liquid species are able to dissolve more effectively under these conditions. The impact of the Peclet number Pe on $G(\xi)$ is clearly illustrated in Figure 4.36. The Peclet number Pe holds great significance in the study of microorganism swimming in a fluid. It can be defined as the ratio of microbe diffusion to the product of the chemotaxis constant and the maximum cell swimming speed. An increase in Pe enhances the speed of fluid particles, simultaneously leading to a reduction in the diffusivity of microbes. Consequently, higher Peclet levels result in a decreased distribution of micro-rotations. Thus density of motile microorganisms $G(\xi)$ is reduced. The data presented in Figure 4.37 clearly shows that as the values of Ω increase, the behavior of $G(\xi)$ exhibits a noticeable decline. The surface concentration diminishes with the increasing value of $G(\xi)$. Consequently, both particle strength and mass decrease, leading to a degradation in the density profiles.

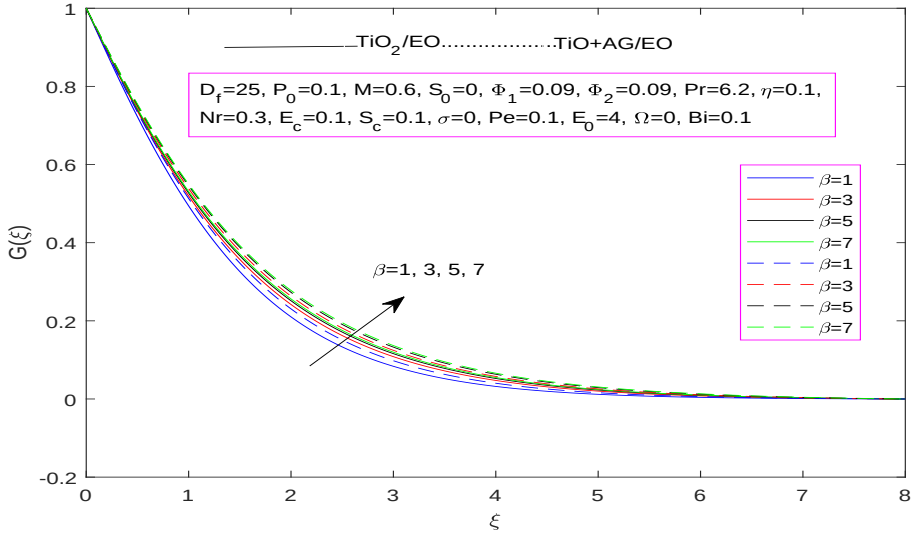

FIGURE 4.27: Impact of β on $G(\xi)$

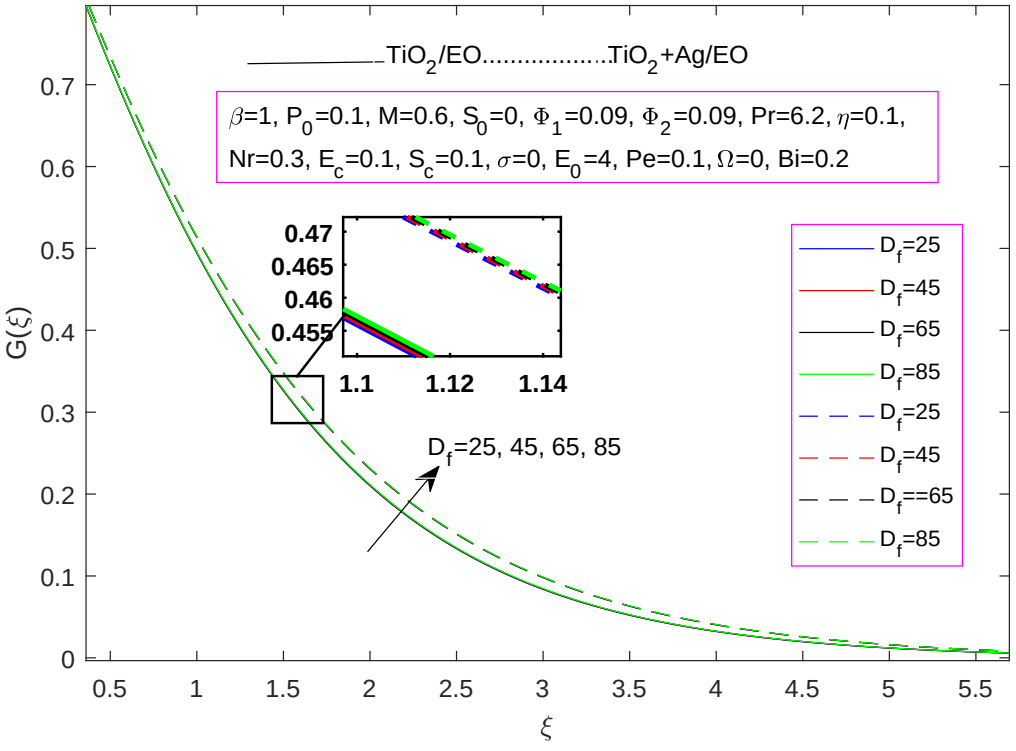

FIGURE 4.28: Impact of D_f on $G(\xi)$

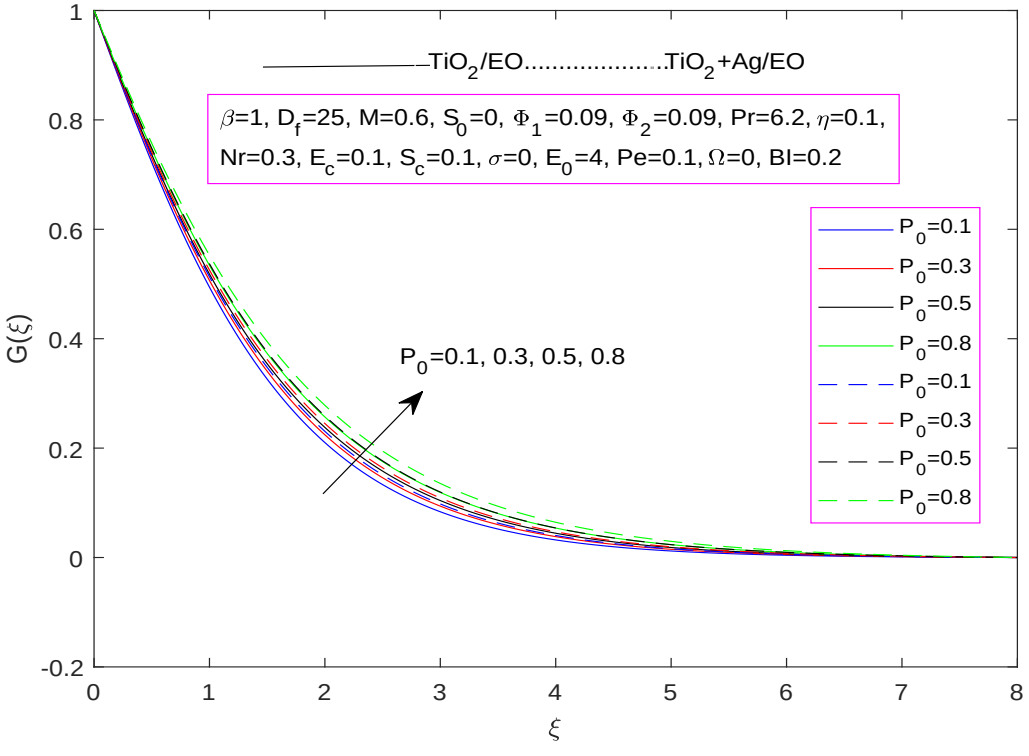

FIGURE 4.29: Impact of P_0 on $G(\xi)$

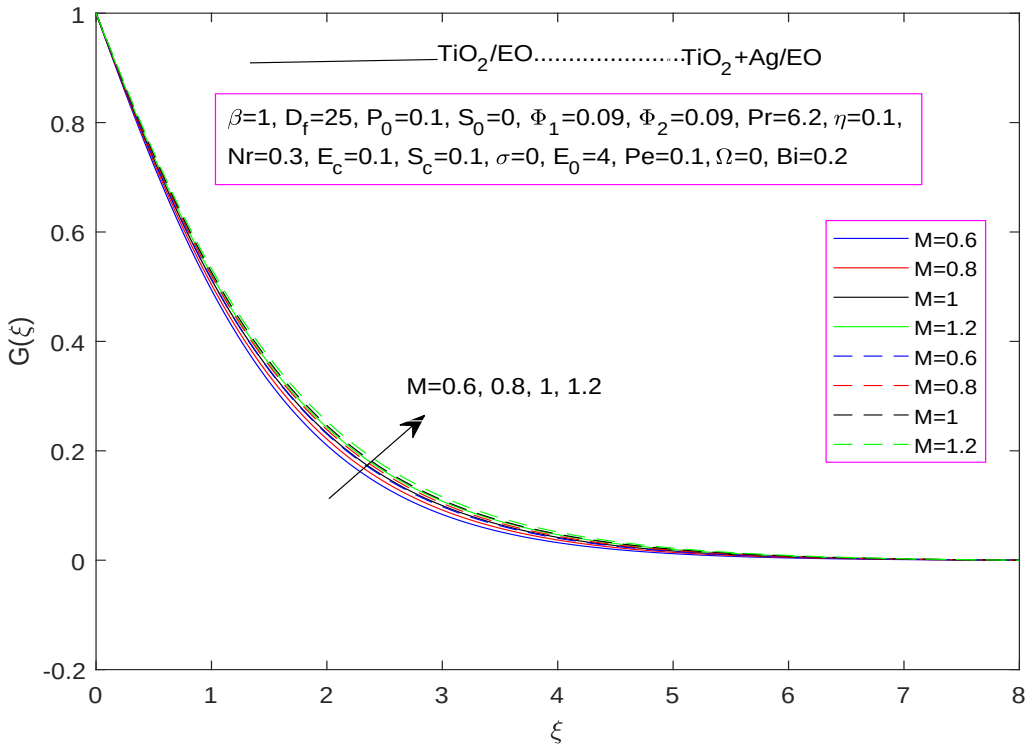

FIGURE 4.30: Impact of M on $G(\xi)$

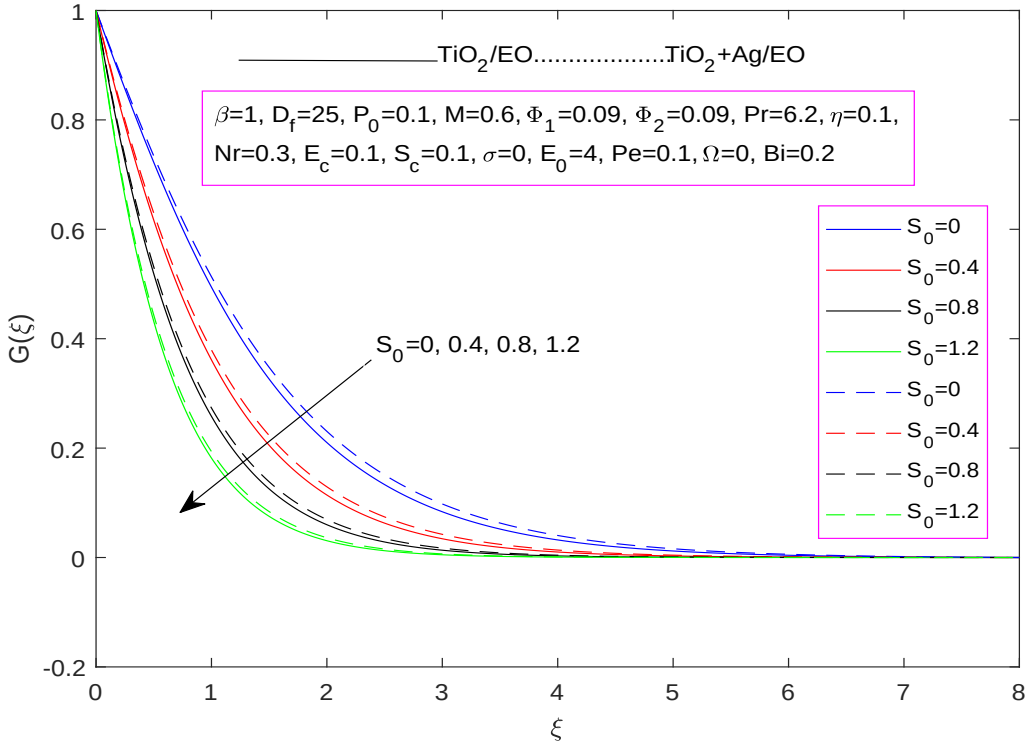

FIGURE 4.31: Impact of S_0 on $G(\xi)$

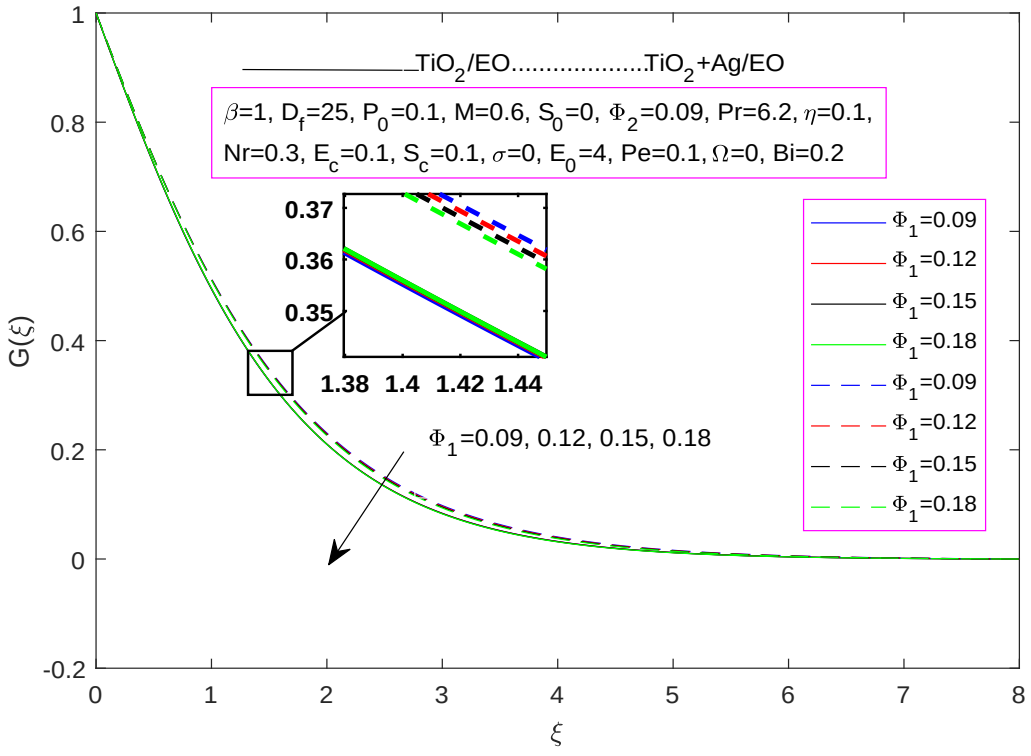

FIGURE 4.32: Impact of Φ_1 on $G(\xi)$

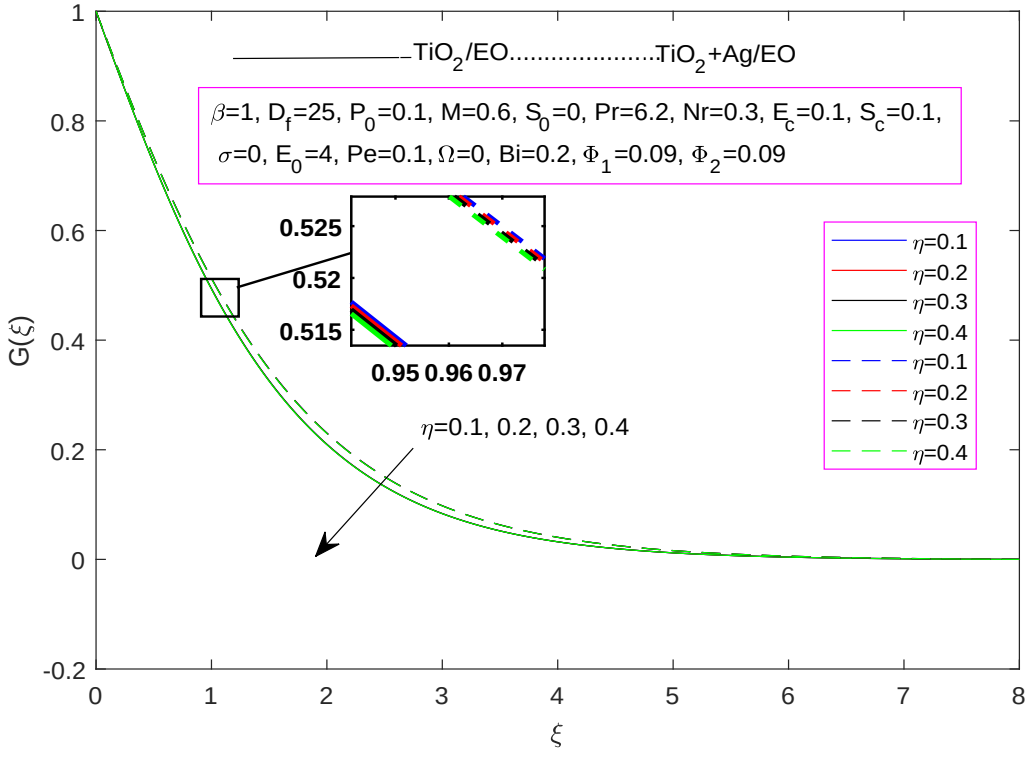

FIGURE 4.33: Impact of η on $G(\xi)$

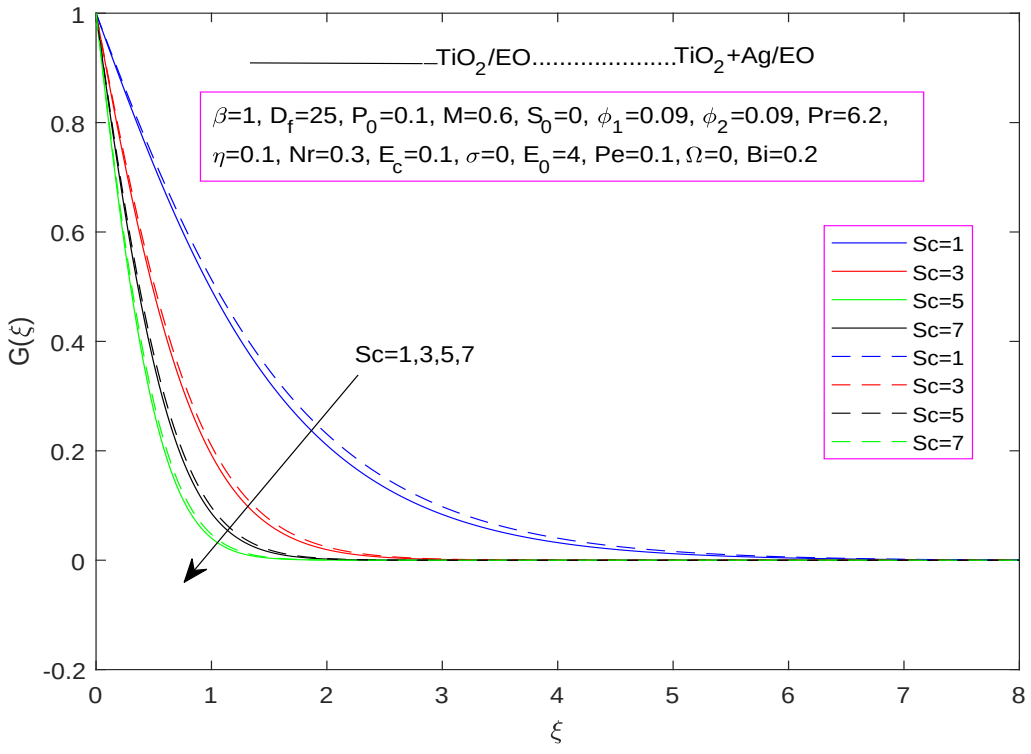

FIGURE 4.34: Impact of S_c on $G(\xi)$

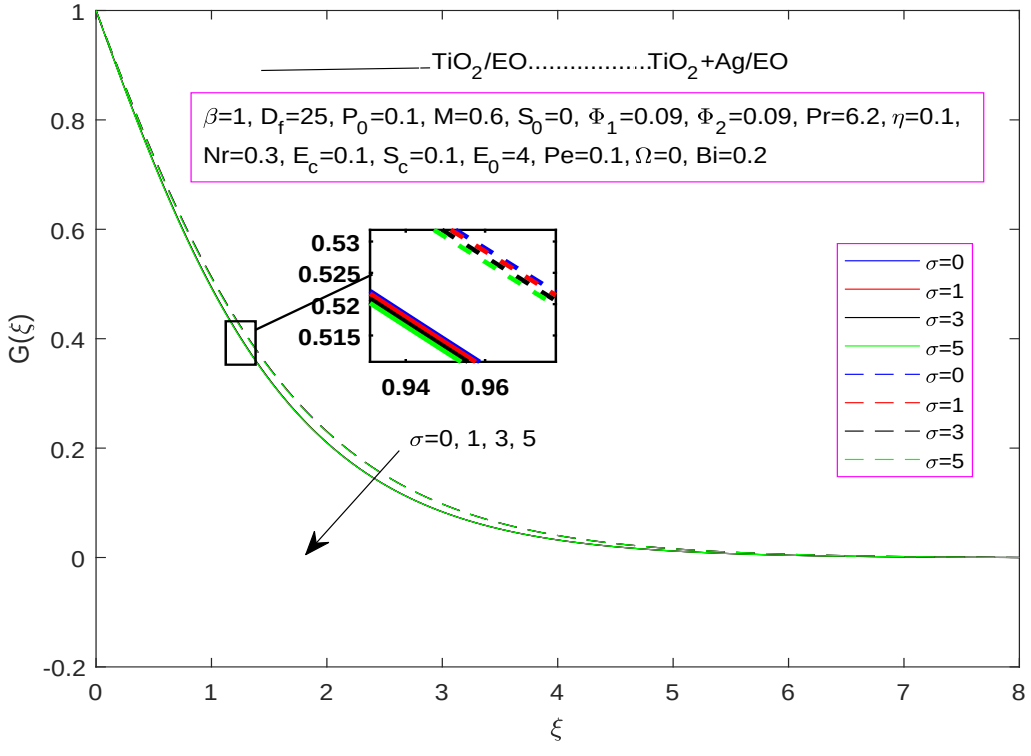

FIGURE 4.35: Impact of σ on $G(\xi)$

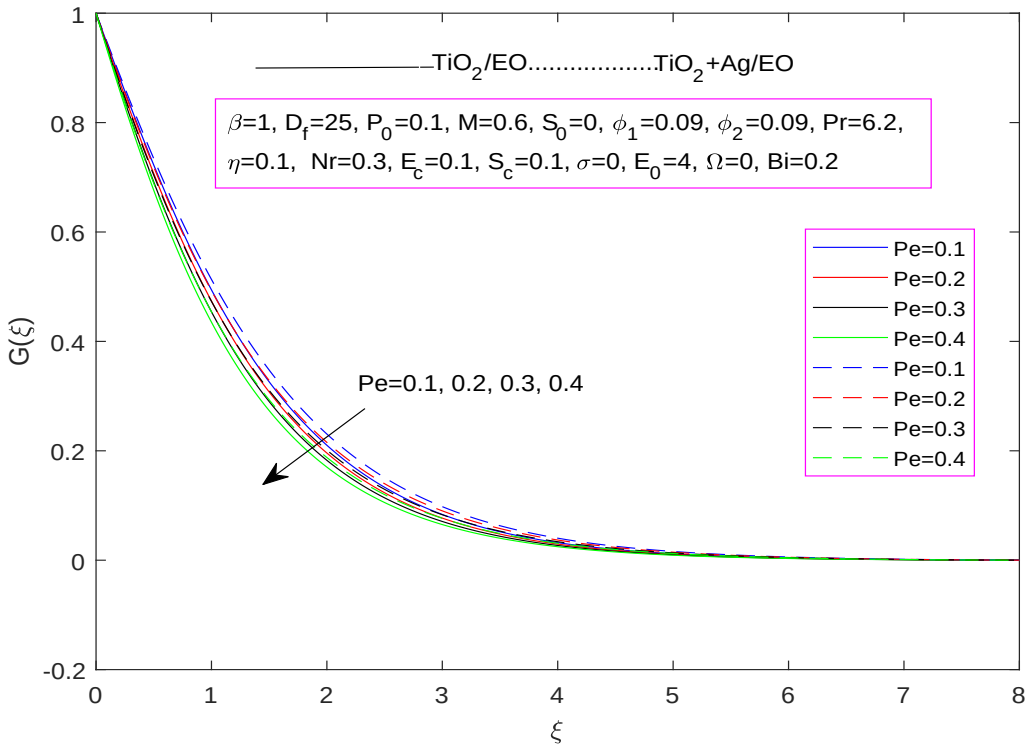

FIGURE 4.36: Impact of Pe on $G(\xi)$

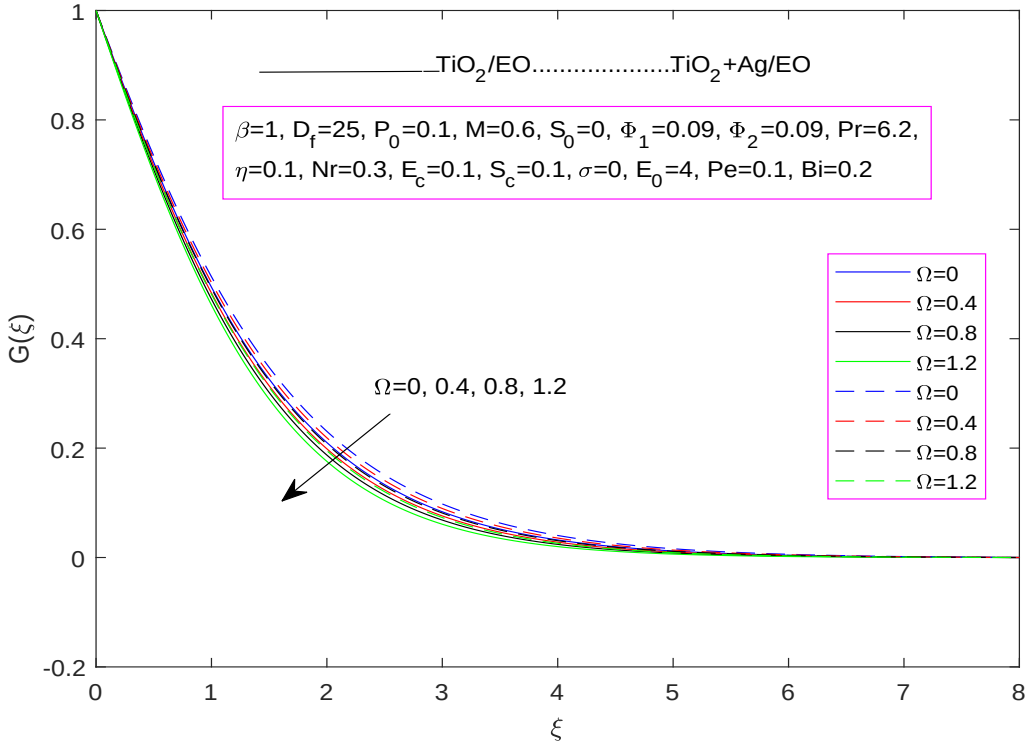

FIGURE 4.37: Impact of Ω on $G(\xi)$

Chapter 5

Conclusion

The main goal of the current research was to analyze the boundary layer flow of a specific hybrid nanofluid over a stretched sheet incorporating various complex phenomena like bioconvection, magnetic fields, thermal radiation, heat source/sink effects, chemical reactions, and Cattaneo-Christov double diffusion effect. This study involved a computational analysis to understand the interactions and effects of these multiple factors on the flow and associated phenomenaon. The following are some of the crucial outcomes:

- An increment in the Casson parameter β, Darcian parameter D_f, porosity parameter P_0, magnetic parameter M, and suction parameter S_0, leads to a decay in the velocity profile $f'(\xi)$ but opposite trend observed for the rising values of volume fraction Φ_1.

- The positive variation in the Casson parameter β, porosity parameter P_0, magnetic parameter M, volume concentration of nanofluid Φ_1, radiation parameter Nr and Eckert number E_c enhanced the temperature profile.

- The temperature profile falls with the greater vales of suction parameter S_0, Prandtl number Pr and relaxation parameter η.

- For the enhancing values of Casson parameter β, Darcian parameter D_f, porosity parameter P_0 and magnetic parameter M, concentration profile

falls while revers regime observed for increasing values of suction parameter S_0, volume concentration of nanofluid ϕ_1, relaxation parameter η, Schmidt number S_c, and chemical reaction rate constant σ.

- For the positive variation in Casson parameter β, Darcian parameter D_f and porosity parameter P_0 and magnetic parameter M, motile profile rises whereas a declining trend is disclosed for the rising values of suction parameter S_0, volume concentration of nanofluid Φ_1, relaxation parameter η, Schmidt number S_c, chemical reaction rate constant σ, Peclet number Pe and bioconvection parameter Ω.

Bibliography

[1] S. Hussain, S. E. Ahmed, and T. Akbar, "Entropy generation analysis in MHD mixed convection of hybrid nanofluid in an open cavity with a horizontal channel containing an adiabatic obstacle," *International Journal of Heat and Mass Transfer*, vol. 114, pp. 1054–1066, 2017.

[2] M. Mollamahdi, M. Abbaszadeh, and G. A. Sheikhzadeh, "Analytical study of Al_2O_3-Cu/water micropolar hybrid nanofluid in a porous channel with expanding/contracting walls in the presence of magnetic field," *Scientia Iranica*, vol. 25, no. 1, pp. 208–220, 2018.

[3] A. Karabanova, P. Berdiyeva, L. Helfen, A. Tengattini, T. Buecherl, M. G. Makowska, S. Deledda, and D. Blanchard, "Neutron radiography for local modelling of thermochemical heat storage reactors: Case study on $SrCl_2 - NH_3$," *International Journal of Heat and Mass Transfer*, vol. 178, p. 121287, 2021.

[4] M. Nawaz, H. A. Madkhali, M. Haneef, S. O. Alharbi, and M. K. Alaoui, "Numerical study on thermal enhancement in hyperbolic tangent fluid with dust and hybrid nanoparticles," *International Communications in Heat and Mass Transfer*, vol. 127, p. 105535, 2021.

[5] L. M. Jasim, H. Hamzah, C. Canpolat, and B. Sahin, "Mixed convection flow of hybrid nanofluid through a vented enclosure with an inner rotating cylinder," *International Communications in Heat and Mass Transfer*, vol. 121, p. 105086, 2021.

[6] N. Biswas, N. K. Manna, A. J. Chamkha, and D. K. Mandal, "Effect of surface waviness on MHD thermo-gravitational convection of $Cu - Al_2O_3/$ water hybrid nanofluid in a porous oblique enclosure," *Physica Scripta*, vol. 96, no. 10, p. 105002, 2021.

[7] J. Wang, Z. Jia, X. Liu, J. Dou, B. Xu, B. Wang, and G. Wu, "Construction of 1-D heterostructure $NiCo@C/ZnO$ nanorod with enhanced microwave absorption," *Nano-micro Letters*, vol. 13, no. 1, p. 175, 2021.

[8] "The desirable dielectric properties and high thermal conductivity of epoxy composites with the cobweb-structured $SICNW - SiO_2 - NH_2$ hybrids, author=Wang, Z. and Wang, X. and Zhao, N. and He, J. and Wang, S. and Wu, G. and Cheng, Y., journal=Journal of Materials Science: Materials in Electronics, volume=32, pages=20973–20984, year=2021, publisher=Springer,"

[9] S. Ahmad, K. Ali, K. S. Nisar, A. A. Faridi, N. Khan, W. Jamshed, T. Y. Khan, and C. A. Saleel, "Features of Cu and TiO_2 in the flow of engine oil subject to thermal jump conditions," *Scientific Reports*, vol. 11, no. 1, p. 19592, 2021.

[10] S. Nadeem, R. U. Haq, and C. Lee, "MHD flow of a Casson fluid over an exponentially shrinking sheet," *Scientia Iranica*, vol. 19, no. 6, pp. 1550–1553, 2012.

[11] S. Mukhopadhyay, P. R. De, K. Bhattacharyya, and G. Layek, "Casson fluid flow over an unsteady stretching surface," *Ain Shams Engineering Journal*, vol. 4, no. 4, pp. 933–938, 2013.

[12] A. Khalid, I. Khan, A. Khan, and S. Shafie, "Unsteady MHD free convection flow of Casson fluid past over an oscillating vertical plate embedded in a porous medium," *Engineering Science and Technology, an International Journal*, vol. 18, no. 3, pp. 309–317, 2015.

[13] H. R. Kataria and H. R. Patel, "Radiation and chemical reaction effects on MHD Casson fluid flow past an oscillating vertical plate embedded in porous medium," *Alexandria Engineering Journal*, vol. 55, no. 1, pp. 583–595, 2016.

[14] F. Mabood and K. Das, "Outlining the impact of melting on MHD Casson fluid flow past a stretching sheet in a porous medium with radiation," *Heliyon*, vol. 5, no. 2, 2019.

[15] B. S. Goud, P. P. Kumar, and B. S. Malga, "Effect of heat source on an unsteady MHD free convection flow of Casson fluid past a vertical oscillating plate in porous medium using finite element analysis," *Partial Differential Equations in Applied Mathematics*, vol. 2, p. 100015, 2020.

[16] W. Jamshed, M. Goodarzi, M. Prakash, K. S. Nisar, M. Zakarya, A.-H. Abdel-Aty, *et al.*, "Evaluating the unsteady Casson nanofluid over a stretching sheet with solar thermal radiation: An optimal case study," *Case Studies in Thermal Engineering*, vol. 26, p. 101160, 2021.

[17] J. Fourier, "Theórie analytique de la chaleur, chez firmin didot. père et fils. libraires pour les mathématiques. l'arquitecture hydraulique et la marine. rue jacob no. 24," *Francia: Google Digital Books*, 1822.

[18] C. Cattaneo, "Sulla conduzione del calore," *Atti Sem. Mat. Fis. Univ. Modena*, vol. 3, pp. 83–101, 1948.

[19] C. Christov, "On frame indifferent formulation of the Maxwell-Cattaneo model of finite-speed heat conduction," *Mechanics Research Communications*, vol. 36, no. 4, pp. 481–486, 2009.

[20] M. Mustafa, "Cattaneo-Christov heat flux model for rotating flow and heat transfer of upper-convected Maxwell fluid," *AIP Advances*, vol. 5, no. 4, 2015.

[21] W. Jamshed and A. Aziz, "Cattaneo-Christov based study of TiO_2-CuO/EG Casson hybrid nanofluid flow over a stretching surface with entropy generation," *Applied Nanoscience*, vol. 8, no. 4, pp. 685–698, 2018.

[22] U. Farooq, M. Imran, N. Fatima, S. Noreen, M. Tahir, A. Akgül, M. De la Sen, and A. M. Galal, "Cattaneo-Christov heat flux model in radiative flow

of ($Fe_3O_4 - TiO_2$/transformer oil) and ($Cu - TiO_2$/transformer oil) magnetized hybrid nanofluids past through double rotating disks," *Case Studies in Thermal Engineering*, vol. 45, p. 102905, 2023.

[23] A. Alsaedi, A. Razaq, T. Hayat, and S. A. Khan, "Modeling and simulation of Cattaneo-Christov fluxes in entropy induced flow through Reiner-Rivlin fluid conveying tiny particles," *Alexandria Engineering Journal*, vol. 74, pp. 1–19, 2023.

[24] M. B. Ashraf, A. Tanveer, S. Ulhaq, *et al.*, "Effects of Cattaneo-Christov heat flux on MHD Jeffery nano fluid flow past a stretching cylinder," *Journal of Magnetism and Magnetic Materials*, vol. 565, p. 170154, 2023.

[25] K. Muhammad, T. Hayat, S. Momani, and S. Asghar, "Fdm analysis for squeezed flow of hybrid nanofluid in presence of Cattaneo-Christov (CC) heat flux and convective boundary condition," *Alexandria Engineering Journal*, vol. 61, no. 6, pp. 4719–4727, 2022.

[26] K. B. S. Latha, M. G. Reddy, D. Tripathi, O. A. Bég, S. Kuharat, H. Ahmad, D. U. Ozsahin, and S. Askar, "Computation of stagnation coating flow of electro-conductive ternary Williamson hybrid $GO - AU - Co_3O_4/EO$ nanofluid with a Cattaneo-Christov heat flux model and magnetic induction," *Scientific Reports*, vol. 13, no. 1, p. 10972, 2023.

[27] K. Jabeen, M. Mushtaq, T. Mushtaq, and R. M. A. Muntazir, "A numerical study of boundary layer flow of Williamson nanofluid in the presence of viscous dissipation, bioconvection, and activation energy," *Numerical Heat Transfer, Part A: Applications*, pp. 1–22, 2023.

[28] N. Acharya, R. Bag, and P. K. Kundu, "Influence of hall current on radiative nanofluid flow over a spinning disk: a hybrid approach," *Physica E: Low-dimensional Systems and Nanostructures*, vol. 111, pp. 103–112, 2019.

[29] M. M. Maskeen, A. Zeeshan, O. U. Mehmood, and M. Hassan, "Heat transfer enhancement in hydromagnetic alumina-copper/water hybrid nanofluid flow

over a stretching cylinder," *Journal of Thermal Analysis and Calorimetry*, vol. 138, pp. 1127–1136, 2019.

[30] K. U. Rehman, A. A. Malik, M. Malik, and N. U. Saba, "Mutual effects of thermal radiations and thermal stratification on tangent hyperbolic fluid flow yields by both cylindrical and flat surfaces," *Case Studies in Thermal Engineering*, vol. 10, pp. 244–254, 2017.

[31] M. Bilal, A. Saeed, T. Gul, W. Kumam, S. Mukhtar, and P. Kumam, "Parametric simulation of micropolar fluid with thermal radiation across a porous stretching surface," *Scientific Reports*, vol. 12, no. 1, p. 2542, 2022.

[32] W. Li, U. Farooq, H. Waqas, A. M. Alharthi, N. Fatima, A. M. Hassan, T. Muhammad, and A. Akgül, "Numerical simulations of Darcy-Forchheimer flow of radiative hybrid nanofluid with Lobatto-iiia scheme configured by a stretching surface," *Case Studies in Thermal Engineering*, vol. 49, p. 103364, 2023.

[33] B. Ali, Y. Nie, S. A. Khan, M. T. Sadiq, and M. Tariq, "Finite element simulation of multiple slip effects on MHD unsteady Maxwell nanofluid flow over a permeable stretching sheet with radiation and thermo-diffusion in the presence of chemical reaction," *Processes*, vol. 7, no. 9, p. 628, 2019.

[34] A. U. Yahya, N. Salamat, W.-H. Huang, I. Siddique, S. Abdal, and S. Hussain, "Thermal charactristics for the flow of Williamson hybrid nanofluid ($MoS_2 + ZnO$) based with engine oil over a streched sheet," *Case Studies in Thermal Engineering*, vol. 26, p. 101196, 2021.

[35] B. Shankaralingappa, B. Gireesha, B. Prasannakumara, and B. Nagaraja, "Darcy-Forchheimer flow of dusty tangent hyperbolic fluid over a stretching sheet with Cattaneo-Christov heat flux," *Waves in Random and Complex Media*, vol. 33, no. 3, pp. 742–761, 2023.

[36] M. Nayak, S. Shaw, M. I. Khan, V. Pandey, and M. Nazeer, "Flow and thermal analysis on Darcy-Forchheimer flow of copper-water nanofluid due

to a rotating disk: a static and dynamic approach," *Journal of Materials Research and Technology*, vol. 9, no. 4, pp. 7387–7408, 2020.

[37] T. Hayat, F. Haider, T. Muhammad, and A. Alsaedi, "Darcy-Forchheimer flow by rotating disk with partial slip," *Applied Mathematics and Mechanics*, vol. 41, pp. 741–752, 2020.

[38] S. Riasat, M. Ramzan, S. Kadry, and Y.-M. Chu, "Significance of magnetic Reynolds number in a three-dimensional squeezing Darcy-Forchheimer hydromagnetic nanofluid thin-film flow between two rotating disks," *Scientific Reports*, vol. 10, no. 1, p. 17208, 2020.

[39] A. Saeed, W. Alghamdi, S. Mukhtar, S. I. A. Shah, P. Kumam, T. Gul, S. Nasir, and W. Kumam, "Darcy-Forchheimer hybrid nanofluid flow over a stretching curved surface with heat and mass transfer," *PLoS One*, vol. 16, no. 5, p. e0249434, 2021.

[40] W.-F. Xia, M. I. Khan, S. Qayyum, M. I. Khan, and S. Farooq, "Aspects of constructive/destructive chemical reaction with activation energy for Darcy-Forchheimer hybrid nanofluid flow due to semi-infinite asymmetric channel with absorption and generation features," *Ain Shams Engineering Journal*, vol. 12, no. 3, pp. 2981–2989, 2021.

[41] S. Ahmad, M. Ashraf, and K. Ali, "Heat and mass transfer flow of gyrotactic microorganisms and nanoparticles through a porous medium," *International Journal Heat Technology*, vol. 38, no. 2, pp. 395–402, 2020.

[42] S. Ahmad, M. Ashraf, and K. Ali, "Bioconvection due to gyrotactic microbes in a nanofluid flow through a porous medium," *Heliyon*, vol. 6, no. 12, 2020.

[43] S. Ahmad, M. Ashraf, and K. Ali, "Nanofluid flow comprising gyrotactic microorganisms through a porous medium," *Journal of Applied Fluid Mechanics*, vol. 13, no. 5, pp. 1539–1549, 2020.

[44] A. Harfash, "Magnetic effect on instability and nonlinear stability of double-diffusive convection in a reacting fluid," *Continuum Mechanics and Thermodynamics*, vol. 25, no. 1, pp. 89–106, 2013.

[45] S. Bilal, M. Malik, M. Awais, A. Hussain, and I. Khan, "Numerical investigation on 2d viscoelastic fluid due to exponentially stretching surface with magnetic effects: an application of non-Fourier flux theory," *Neural Computing and Applications*, vol. 30, pp. 2749–2758, 2018.

[46] S. Ahmad, S. Akhter, M. I. Shahid, K. Ali, M. Akhtar, and M. Ashraf, "Novel thermal aspects of hybrid nanofluid flow comprising of manganese zinc ferrite $MnZnFe_2O_4$, nickel zinc ferrite $NiZnFe_2O_4$ and motile microorganisms," *Ain Shams Engineering Journal*, vol. 13, no. 5, p. 101668, 2022.

[47] K. Ali, S. Ahmad, T. Tayebi, M. Ashraf, W. Jamshed, A. Abd-Elmonem, and S. M. El Din, "Thermal attributes of hybrid $(MWCNT - NiZnFe_2O_4)$ nanofluid flow having motile microbes and activation energy: A computational approach," *Case Studies in Thermal Engineering*, vol. 47, p. 103088, 2023.

[48] Y. Cengel and J. Cimbala, *Ebook: Fluid Mechanics Fundamentals and Applications (SI units)*. McGraw Hill, 2013.

[49] R. Bansal, *A Textbook of Fluid Mechanics and Hydraulic Machines:(in SI units)*. LAXMI Publications, Ltd., 2005.

[50] S. K. Das, S. U. Choi, W. Yu, and T. Pradeep, *Nanofluids: Science and Technology*. John Wiley & Sons, 2007.

[51] H. M. Ali, *Hybrid Nanofluids for Convection Heat Transfer*. Academic Press, 2020.

[52] S. S. Molokov, R. Moreau, and H. K. Moffatt, *Magnetohydrodynamics: Historical Evolution and Trends*, vol. 80. Springer Science & Business Media, 2007.

[53] C. Kothandaraman, *Fundamentals of Heat and Mass Transfer*. New Age International, 2006.

[54] J. N. Reddy and D. K. Gartling, *The Finite Element Method in Heat Transfer and Fluid Dynamics*. CRC press, 2010.

[55] J. Kunes, *Dimensionless Physical Quantities in Science and Engineering*. Elsevier, 2012.

[56] B. Lautrup, *Physics of Continuous Matter: Exotic and Everyday Phenomena in the Macroscopic World*. CRC press, 2011.